ISSN: 2630-533X

JOURNAL OF PHARMACEUTICAL AND BIOPHARMACEUTICAL RESEARCH

VOLUME 1
ISSUE 1
January 2019

Editor-In-Chief: Prof. Pal Perjesi

SyncSci PUBLISHING

Editorial Board

Editor-in-Chief

Editorial Board Members

Editorial Board Members

January 2019 | Volum 1 | Issue 1 | Page 1-47
http://www.syncsci.com/journal/index.php/JPBR

Journal of Pharmaceutical and Biopharmaceutical Research

Contents

RESEARCH ARTICLE

REVIEW

J Pharm Biopharm Res, 2019, 1(1): 1−14
DOI: 10.25082/JPBR.2019.01.001

RESEARCH ARTICLE

Functionalization of carbopol with NVP for designing antibiotic drug loaded hydrogel dressings for better wound management

Baljit Singh* Abhishek Dhiman

Abstract: In the present work an attempt has been made to design the antibiotic drug loaded carbopol-poly(NVP) based hydrogel wound dressings for better wound care. The polymer films were characterized by SEM-EDX, AFM, FTIR, ^{13}CNMR, TGA/DTA/DTG, DSC, and swelling studies. Besides drug release, various biomedical properties (*viz.* blood compatibility, mucoadhesion, oxygen permeability, water vapour transmission rate, microbial penetration, tensile strength, bursting strength, resilience, stress relaxation, and folding endurance) have also been studied. The polymer films have been observed to be biocompatible, permeable to oxygen and water vapour and have absorbed simulated wound fluid 11.37±0.31g/g of polymer film. The drug release profile followed the Case-II diffusion mechanism and release profile best fitted in Hixson-Crowell's kinetic models. Mechanical properties results showed that the polymer film had 0.65±0.12 Nmm^{-2} tensile strength, 119.38±14.26% elongationand 25.49±0.72% resilience.

Keywords: drug delivery, 1-Vinyl-2-pyrollidone, hydrogel, wound dressing

1 Introduction

The concept of wound treatment always focuses on reducing the risk caused by wound itself, minimizing potential environmental complications and enhancing proper regeneration and reestablishment of the wounded skin tissue.[1] Infected skin that is left untreated may delay healing and even lead to death.[1,2]Recently, a wide range of wound dressings are available in market, but hydrogel is a material of choice for designing dressings for better wound management.Hydrogel dressings are more successful in clinical results as compared to the conventional wound dressings. Hydrogel wound dressings containing antibiotic drugs have been used against wound infections.[3]In order to maximise the effectiveness of antibiotics for longer periods, slow and sustained release of antibiotics is very important. These drug loaded hydrogel dressings have been found to be instrumental in achieving successful and long lasting healing effects from antibiotic loaded wound dressings.[4]

Hydrogels are three-dimensional, hydrophilic, polymeric networks capable of absorbing large amounts of biological fluids. These are closely related to the natural living tissue, more than any other class of synthetic biomaterials due to their high water content, porosity and soft consistency.[5]They can be made from a wide range of biocompatible materials. They can provide moist healing environment, and slow drug delivery at wound site.[6] Hydrogels are capable of promoting the autolytic debridement of necrotic tissues and are usually more efficient at drying wounds with few exudates.[7] A great advantage of hydrogel dressings is that they are usually applied and removed without interfering with the wound bed. In addition, these dressings are flexible, non-antigenic, and permeable to water, oxygen and metabolites.[8]

In view of the above, it is reasonable to assume that a antibiotic drug (moxifloxacin) loaded hydrogel dressings composed of carbopol-poly(NVP) would provide the slow release of antibiotic drug locally in a controlled manner besideproviding moistwound for improving wound healing. Poly(NVP) is a water solublehydrophilic biocompatiblepolymer.[9,10] Its hydrogel films have been applied as local dressings.[11] These hydrogel dressings can act as a barrier against bacterial penetration.[12] It is one of the most frequently used material in biomedical applications due to their biocompatibility with living tissues and extremely low cytotoxicity.[13,14]Inclusion of poly(NVP) in the composite hydrogels can improve swelling and other biomedical proper-

Received: January 7, 2019 **Accepted:** January 21, 2019 **Published:** January 25, 2019

***Correspondence to**: Baljit Singh, Department of Chemistry, Himachal Pradesh University, Shimla, 171005, India; Email: baljitsinghhpu@yahoo.com

Citation: Singh B and Dhiman A. Functionalization of carbopol with NVP for designing antibiotic drug loaded hydrogel dressings for better wound management. *J Pharm Biopharm Res*, 2019, **1**(1):1−14

ties.[9,15] On the other hand, carbopol is a hydrophilic, non-toxic, biocompatible, bioadhesive and non-irritant polymer.[16,17]It has been used in drug delivery systems for buccal, transdermal,[18] ocular, rectal, vaginal,[19] nasal[20] and wound dressing applications.[21]

2 Experimental

2.1 Materials used

1-Vinyl-2-pyrollidone (NVP) [MerckSpecialities Pvt. Ltd. Mumbai-India], carbopol (CP) [Loba Chemie Pvt. Ltd., Mumbai-India], N,N-methylenebisacrylamide (NN-MBA) [Acros organics, New Jersey-USA], ammonium persulphate (APS) [Qualigens Fine Chemicals, Mumbai-India], glycerol, [S.D. Fine Chemical Ltd., Mumbai, India], and moxifloxacin HCl [Lifestar Pharma Pvt. Ltd.], New Delhi, India] were used as received.

2.2 Synthesis of CP-cl-poly(NVP) polymers

Synthesis of the polymers was carried out by chemically induced free radical copolymerization method using APS as initiator and NN-MBA as cross-linker. Polymer reaction was carried out with solution of definite concentration of CP [2.0% (w/v)], taken in beaker. This solution was prepared by stirring at 100 rpm for definite time after 12 hours hydration. To this homogenous content, solutions of a definite concentration of [NVP] = 28.15×10^2 mol/L, [NN-MBA] = 8.10×10^3 mol/L, glycerol = 0.27 mol/L and [APS] = 5.48×10^3 mol/L were added, and the reaction mixture was again stirred. The reaction content was stirred for total 12 hours at 25 °C. The reaction mixture was then transferred to the petri dish which was placed in hot air oven maintained at 55 °C to get the cross-linked polymer. The polymer films were formed by solution casting method. The cross-linked polymer formed was washed with distilled water and ethanol to remove the soluble fractions left in the polymer. Then it was dried in an oven maintained at 40 °C till constant weight was obtained. This cross-linked polymer was named as CP-*cl*-poly(NVP) polymer.

2.3 Characterization

The polymers were characterized by scanning electronmicrography (SEMs), energy dispersion X-ray analysis (EDX), atomic force microscopy (AFM), Fourier transform infrared (FTIR) spectroscopy, ^{13}C nuclear magnetic resonance (NMR) spectroscopy, X-ray diffraction study (XRD), thermo gravimetric analysis (TGA), differential scanning calorimetry (DSC) and swelling studies. SEM-EDX analysis was done on FEI Quanta 200 F (The Netherlands). AFM (NTEGRA, NT-MDT, Russia) of polymer film was done in 5 m^2 areas, in semi-contact mode. FTIR of polymer was recorded on Perkin Elmer-Spectrum RX-I (USA). The solid state ^{13}C NMR of polymer was carried out using JEOL RESONANCE ECX 400 solid state NMR spectrometer operating at a magnetic field of 9.3 T and at a frequency of 100 MHz for carbons. X-ray diffractogram were obtained using a Bruker D8 Advance diffractometer (USA), operating at 40 kV with Cu-K radiation.TGA of polymer was done using EXSTAR TG/DTA 6300 thermal analyzer (Japan), at a scan rate of 10 °C/min. DSC thermogram of polymer was recorded with NETZSCH DSC 204 (USA) in temperature range 25-500 °C at a scan rate of 10 °C/min.

2.4 Swelling Studies

Swelling studies of the polymers were carried out in different mediums for 24 hours, by gravimetric method.[22]

2.5 Drug release studies

Initially the drug loading into hydrogels was carried out by the swelling equilibrium method.[22] Release profile of moxifloxacin HCl from drug loaded polymer samples was carried out in simulated wound fluid (SWF) and release was determined from the standard curve made on Cary 100 Bio, Varian, UV visible spectrophotometer at λ_{max} (288nm). Drug release mechanism was evaluated by using power law expression given by Ritger and Peppas.[23,24] Different kinetic models (*i.e.* zero order, first order, Higuchi square root law, Korsmeyer-Peppas and Hixson-Crowell cube root model) were applied to drug release profileto determine the best fit model for the release of drug from the drug loaded polymers.[25,26]

2.6 Blood compatibility

As a preliminary investigation, the in vitro biocompatibility was determined on the basis of thrombogenicity and hemolysis assessment. Thrombogenicity of CP-*cl*-poly(NVP) polymer was carried out using a gravimetric method.[27] The positive and negative control was taken as glass beaker with absence of sample and glass beaker with absence of sample and blood respectively.[28] The thrombose percentage is calculated as follow:

$$\text{Thrombogenicity (\%)} = \frac{\text{Mass of test sample - Mass of negative control}}{\text{Mass of positive control - Mass of negative control}} \times 100 \quad (1)$$

The haemoglobin released by haemolysis was measured by the optical densities (OD) of the supernatants at 540 nm using a UV-visible spectrophotometer. The

percentage of haemolyis (%) was calculated as follows:

$$\text{Haemolysis (\%)} = \frac{\text{OD of sample - OD of negative control}}{\text{OD of positive control - OD of negative control}} \times 100 \quad (2)$$

2.7 Mucoadhesion studies

Mucoadhesive property of the polymer was investigated by using texture analyzer (TA-XT, Stable Micro Systems, UK) equipped with a 5 kg load cell and a mucoadhesive holder. The maximum force required to separate the probe from the goat mucosa (*i.e.* maximum detachment force, F_{max}) and distance travelled by film before detachment could be directly recorded in the instrument.

2.8 Oxygen permeability

Permeability of synthesized polymer towards O_2 has been evaluated by using Winkler's method.[29] The test flasks were placed in an open environment for 24 h.[3] The collected water samples were then analyzed for dissolved oxygen according to Winkler's method.[29]

2.9 Water vapour transmission rate

WVTR of polymer film was determined gravimetrically using desiccant method.[30] All the vials were then placed in desiccator, containing saturated solution of NaCl at 37 °C (Relative humidity ∼75%).[31] These vials were weighed after every 24 hours up to eight days and WVTR (g/m^2/day) was calculated using following equation.[31]

$$WVTR = \left(\frac{\Delta w}{\Delta t}\right) \times \frac{24}{A} \quad (3)$$

In this equation (Δw/Δt) is the slope of the plot 'w' *vs* 't', where 'w' is the weight gain (g) along the specified time period, 't' (h) and A is the effective transfer area (m^2).

2.10 Microbial penetration

In the present study, microbial penetration test was performed for polymer film to check their capacity, to prevent secondary infection. The polymeric film (thickness = 1 mm) was placed on top of the test tubes (test area: 1.3±0.03 cm^2) containing 5ml of sterile nutrient broth (2.5% w/v) (Merck Specilities Pvt. Ltd. Mumbai-India) and was sealed to test microbial penetration through them. Before test, polymeric films, nutrient broth and glass test tubes were sterilized in autoclave at 121 °C, 15l bs pressure for 20 minutes. The negative control was the closed test tube with an airtight cap preventing any kind of microbial penetration, while the positive control was the open test tube having no barrier for microbes. The test tubes were placed in an open environment and observed for 30 days period. Permeability for micro-organisms was evaluated by observing microbial growth (in term of turbidity) in test tubes. Any visual turbidity of the nutrient broth was considered as sign of microbial contamination.

2.11 Mechanical properties

In order to access the mechanical strength of the polymer film, some important mechanical tests such as, tensile strength, burst strength, resilience, relaxation, and folding endurance have been performed.

2.11.1 Tensile Strength

Tensile strength of polymeric film was studied using texture analyzer (TA-XT, Stable Micro Systems, UK) equipped with 50 kg load cell.

2.11.2 Bursting strength

Bursting strength of polymeric film was studied using texture analyzer (TA-XT, Stable Micro Systems, UK) equipped with 50 kg load cell. The force (N) and distance (mm) at break point were recorded.

2.11.3 Resilience

Resilience is measurement of how well a sample recovers from deformation. Resilience of polymeric film was studied using texture analyzer (TA-XT, Stable Micro Systems, UK) equipped with 50 kg load cell. Resilience was calculated by using following equation.

$$\text{Resilience (\%)} = \frac{A_2}{A_1} \times 100 \quad (4)$$

where A_2 is the work returned by the sample as compressive strain is removed (known as recoverable work) andA1 is work required for compression.

2.11.4 Stress relaxation test

Stress relaxation of polymeric film was studied using texture analyzer (TA-XT, Stable Micro Systems, UK) equipped with 50 kg load cell. Stress relaxation was evaluated in terms of retained force (%) which was calculated by the following equation.

$$\text{Retained force (\%)} = \frac{\text{Relaxed force}}{\text{Force at targate distance}} \times 100 \quad (5)$$

2.11.5 Folding endurance

The flexibility of the film was accessed from the determination of the folding endurance of film. During folding endurance test, polymer film of thickness 1 mm, length 30 mm and breath 30 mm was repeatedly folded

and de-folded at the same place until it breaks. The number of repeated folding and de-folding at the same place without breaking or cracking gives the value of folding endurance.[32]

3 Result and discussion

3.1 Characterization

A photograph of CP-*cl*-poly(NVP) polymer film was showed transparent nature of the wound dressing (Figure 1(a)) which helps in monitoring of the wound healing progress wound exudates accumulation without removal of wound dressing.[33] Generally transparent wound dressings are preferred for partial-thickness wounds with moderate exudation. SEM image ofCP-*cl*-poly(NVP)polymer film is given in Figure 1(b). This image showed less degree of heterogeneity in the polymer surface which indicating the high degree of miscibility of polymeric contents. Further, the average surface roughness (S_a) was 14.26 nm and root mean square roughness (S_q) was 18.59 nm from the AFM image of CP-cl-poly(NVP) polymer film (Figure 1(c)). Recently, AFM has been implemented as a surface characterization technique in biomaterial research and it is very helpful for the determination and verification of morphological features of polymer film. AFM particularly permits non-destructive imaging of surfaces on a molecular scale.[34] Being more hydrophilic poly(NVP) is more miscible in CP and it increases surface hydrophilicity of the crosslinked polymer. A more hydrophilic surface and high water content in the hydrogel leads to less surface roughness.[35] It has also been reported that grafting of NVP on polymers can make the surface smoother.[36,37] In another research Kennedy and co-workers (2009) have reported that polymer grafted with NVP give smooth surface in comparison to acrylic acid grafted polymers.

Results of EDX analysis of CP and CP-*cl*-poly(NVP) polymers indicating the incorporation of poly(NVP) in the crosslinked polymer in the form of additional peak of nitrogen which is correlated to the presence of poly(NVP) and cross linker NNMBA in the polymer film (Figure 2).

FTIR spectra of CP and CP-*cl*-poly(NVP) polymer are presented in Figure 3. In case of CP, a broad band at 3116.4 cm^{-1} (due to O-H stretching), a band at 2961.4 cm^{-1} (due to C-H stretching), a sharp intense band at 1714.1 cm^{-1} (due to C=O stretching), at 1454.4 cm^{-1} (due to C-H bending), at 1413.5 cm^{-1} (due to O-H in plane bending), and at 1247.4 (due to C-O stretching) have been observed. Beside, absorption band at 1171.4 cm^{-1} due to C-O-C stretching was observed which has proved ethereal crosslonking in CP. Some less intense

(a)

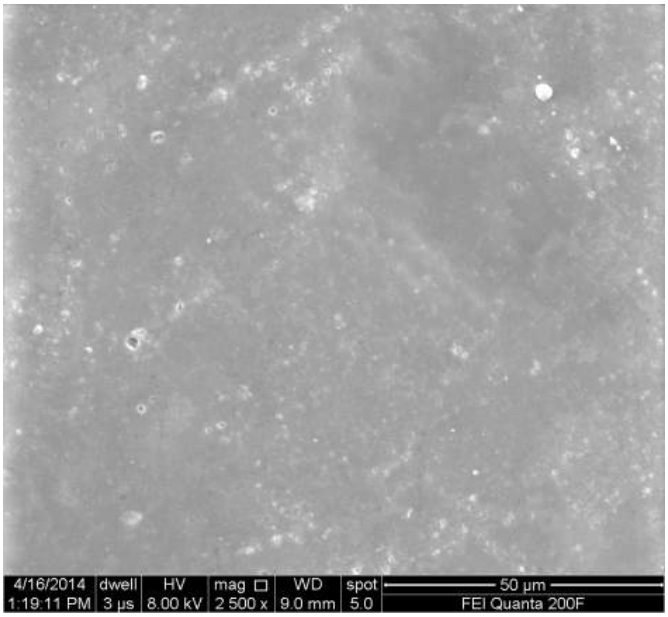

(b)

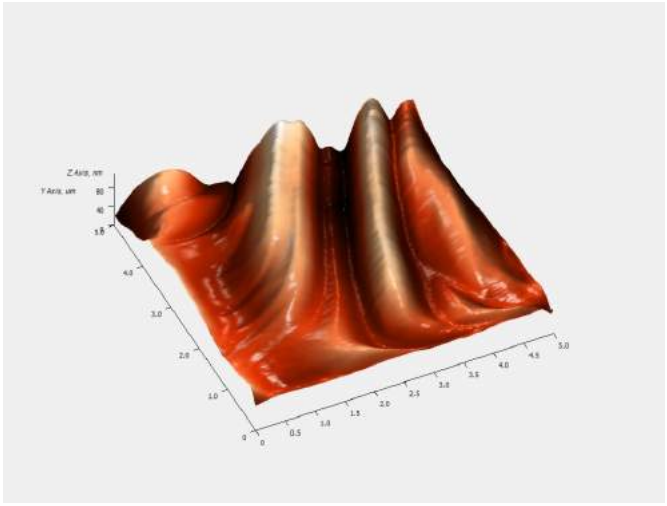

(c)

Figure 1. (a) Photograph, (b) SEM image, and (c) AFM image of CP-*cl*-poly(NVP) polymer film

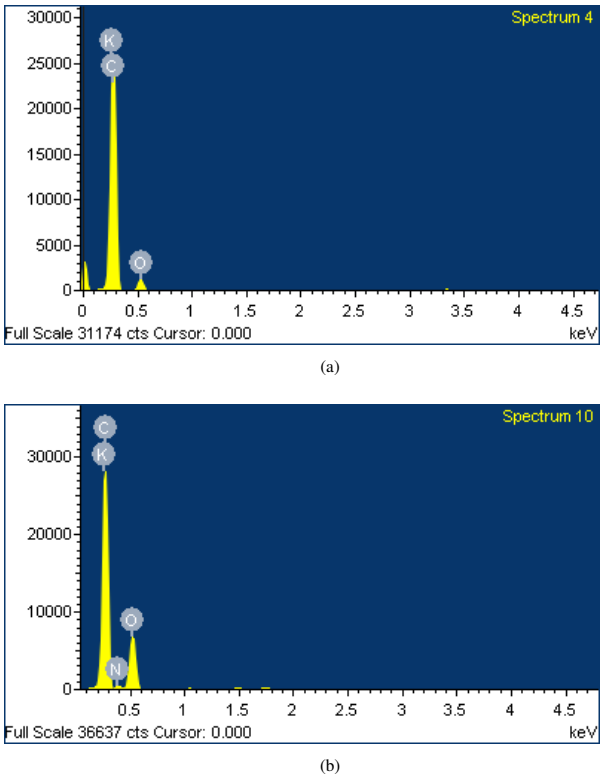

Figure 2. Elemental analysis results of (a) CP and (b) CP-*cl*-poly(NVP) polymer

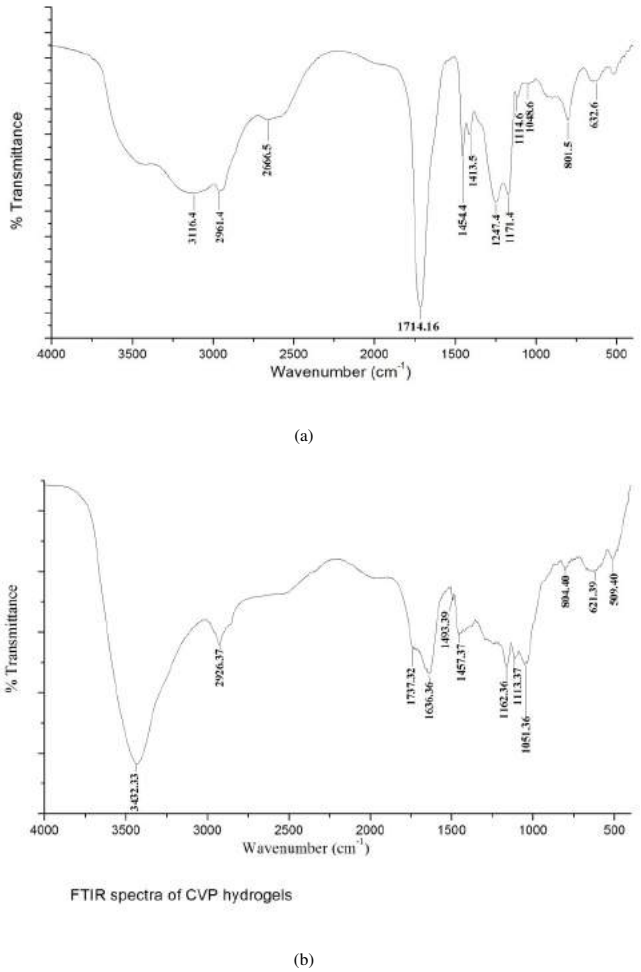

Figure 3. FTIR spectra of (a) CP and (b) CP-*cl*-poly(NVP) polymer

bands at 1114.6 and 1048.6 cm^{-1} (due to O-H deformations), along with a sharp band at 801.5 cm^{-1} due to =C-H out of plane bending vibrations have been observed. This band at 801.5 cm^{-1} is characteristic of CP 940, which appears due to the presence of crosslinker (allyl ether of pentaerythrol) in carpool 940.[38–40] In case of CP-*cl*-poly(NVP) polymera broad band around 3432.33 cm^{-1} (due to O-H), a band at 2926.37 cm^{-1} (due to C-H stretching), at 1737.32 cm^{-1} (C=O stretching of CP), at 1636.36 cm^{-1} (C=O stretching of polyNVP), at 1457.37 cm^{-1} (ring CH_2 wagging, ring C-N stretching of polyNVP), at 1162.36 (C-O-C stretching in CP and ring CH_2 twist of polyNVP). Some less intense bands at 1113.37 and 1051.36 cm^{-1} (due to O-H deformations) have been observed.[39–41]

^{13}C NMR spectra of CP and CP-*cl*-poly(NVP) polymer are presented in Figure 4. In case of CPan intense splitted peak at 183.49, 179.90 ppm [due to carbon ofcarbonyl groups] and another intense but broad peak at 42.57 ppm [due to methylene (-$\underline{C}H_2$-CH-) and methine (-CH_2-$\underline{C}H$-) groups of acrylic chains] has been observed.[38,42] The signal due to methylene and methine carbons overlapped to give a single broad peak at 42.57 ppm. In case of CP-*cl*-poly(NVP) polymer, the chemical shift peak at 178.44 ppm [due to carbonyl (C=O) carbons of poly(NVP) and CP] was observed. Broad peak along with some adjacent smaller peaks was observed, due to different environments of carbonyl carbon in the major constituents. Some peaks at 43.43 ppm [due to CP main chain carbons (-$\underline{C}$H-), vinylic carbons (-$\underline{C}$H-N<) and ring carbons (-$\underline{C}H_2$-N) of poly (NVP)]. This peak represents the polymerization of N-vinyl 2-pyrrolidone to poly (N-vinyl 2-pyrrolidone). The absence of characteristic peak of NVP around δ=94.0 and 129.0 ppm for sp^2 hybridized carbon atoms (CH_2=CH-) indicate the involvement of double bond in grafting and cross-linking during polymerization reaction. Chemical shift peaks at 31.97 ppm [due to ring carbons of NVP (O=C-$\underline{C}H_2$-CH_2-) and18.90 ppm [due to ring carbons of NVP -CH_2-$\underline{C}H_2$-CH_2)] were also observed.[38,43,44] Besides, sharp peaks at 73.50 ppm and 63.94 ppm can be attributed to formation of some new cross links during polymerization reaction.

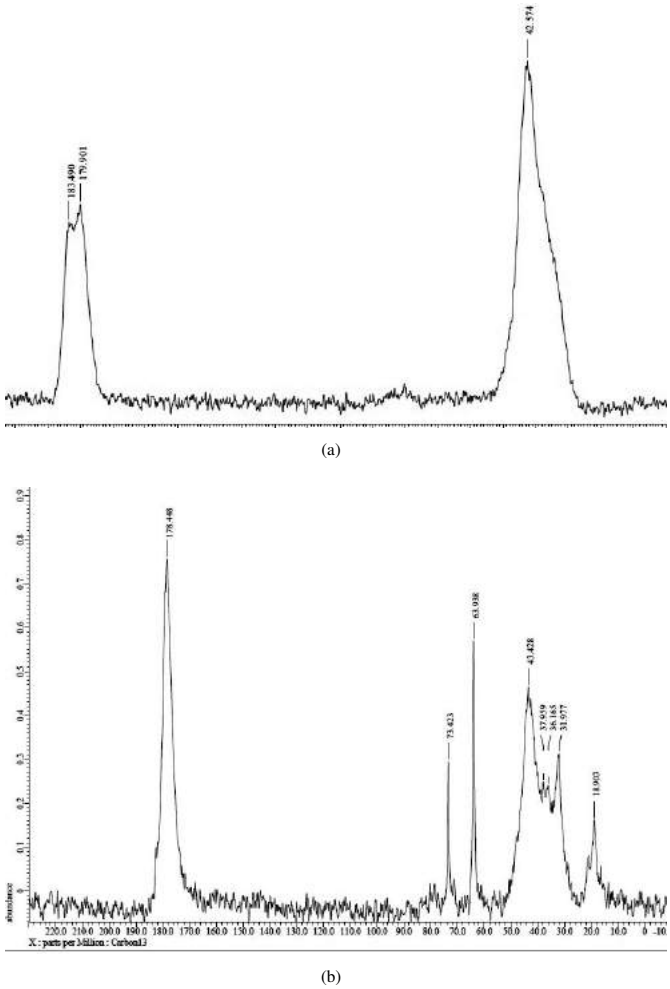

Figure 4. ^{13}CNMR spectra of (a) CP and (b) CP-*cl*-poly(NVP) polymer

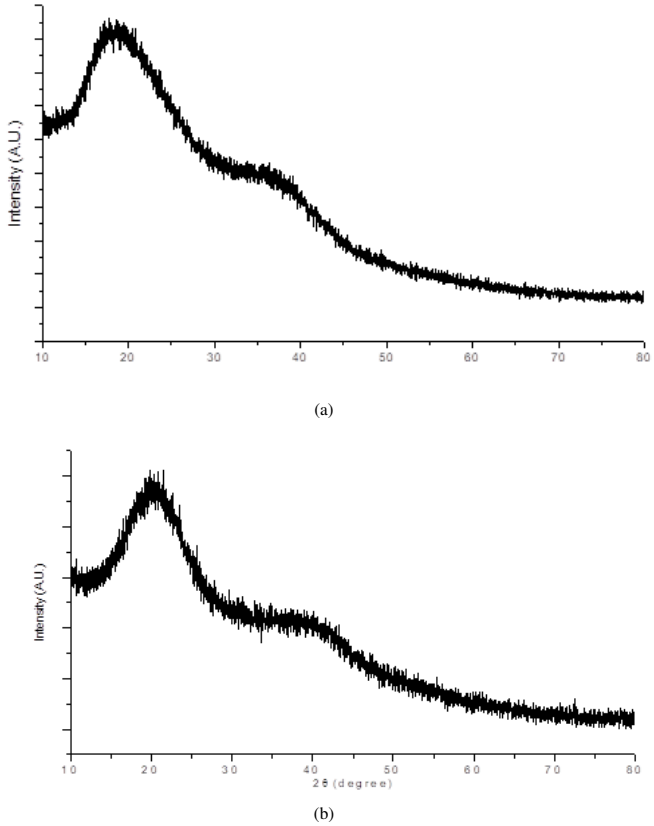

Figure 5. XRD of (a) CP and (b) CP-*cl*-poly(NVP) polymer

XRD spectra of CP and CP-*cl*-poly(NVP) polymer are presented in Figure 5. In case of CP there is no crystalline region in its X-ray diffractogram, indicating completely amorphous nature of CP.[45] XRD spectra of CP-*cl*-poly(NVP) polymer also showed no crystalline region in its polymer sample. Process of cross-linking and grafting may have hindered formation of any regular pattern in polymeric samples.

TGA, DTA and DTG of CP and CP-*cl*-poly(NVP) polymer are presented in Figure 6. In each case weight loss due to entrapped moisture has been ignored and initial decomposition temperature (IDT) has been taken as the temperature where actual degradation of material started. In case of CP, initial 7.59% weight loss occurred up to 100 °C, which indicates that CP has 7.59% bounded water. Kanis and co-workers (2000) have observed about 5% weight loss upto 150 °C due to bounded water. Ignoring the initial weight loss due to free and bounded water, two stages decomposition was observed in CP. In the present case, first stage started at 198.99 °C (residue left = 88.78%) and second stage started at 396.86 °C (residue left = 31.92%). IDT and final decomposition temperature (FDT) have been observed 199 °C and 462 °C (residue left = 5.29%) respectively. Early degradation after 199 °C can be attributed to the formation of formation of cyclic structures (anhydrides) associated with loss of water loss of water. Final decomposition of CP after 396.86 °C onwards occuredat a very high rate, due to decarboxylation, formation of unsaturated structures, depolymerisation of the residual polymer and and complete degradation of polymer forming gaseous products.[46–48]In case of CP-*cl*-poly(NVP)initial 4.30% weight loss occurred upto 100 °C, which indicates that CP-*cl*-poly (NVP) polymer has 4.30% bounded water. Three stage decomposition observed in the case of crosslinked polymer. In the present case, first stage started at 152.95 °C (residue left = 91.25%), second stage started at 315.64 °C (residue left = 71.29%) and third stage started at 439.24 °C (residue left = 26.17%). IDT and FDT have been observed 157 °C and 527 °C (residue left = 0.05%) respectively.

TGA curves show that thermal degradation of cross-

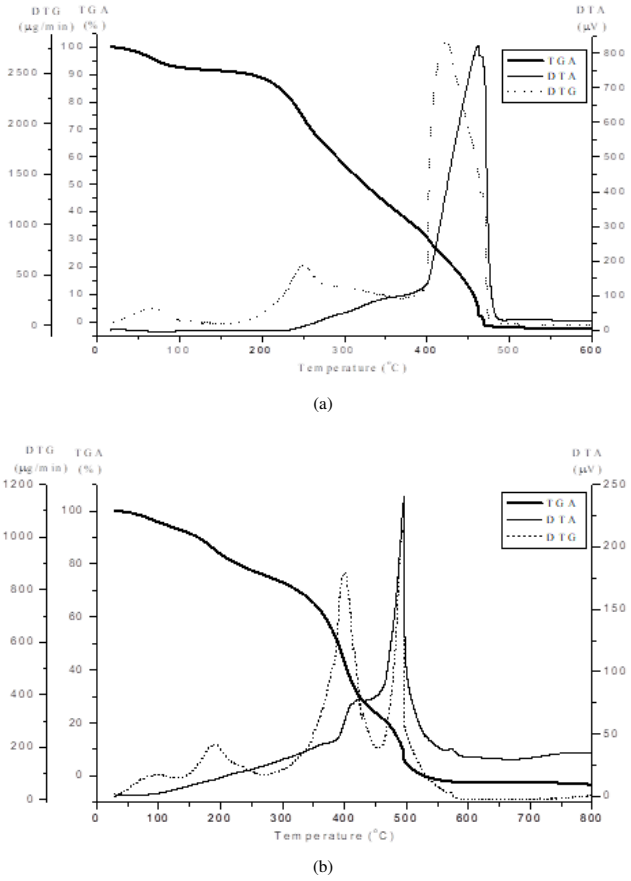

Figure 6. TGA/DTA/DTG curves of (a) CP and (b) CP-*cl*-poly(NVP) polymer

linked hydrogel was slow in comparison to CP, indicating more interactions in cross-linked polymer. 50% weight loss occurred at 325 °C and 390 °C for CP and CP-*cl*-poly(NVP) polymer respectively, indicating that crosslinked polymeric filmsto be more thermally stable than CP. Thermal degradation of the hydrogels was slow and gradual in comparison to CP, as no sudden weight loss has been observed. Increase in thermal stability of cross-linked hydrogels can be attributed to crosslinking and grafting reactions.[49] Besides the strong interaction between carboxyl of CP and carbonyl group of polyNVP may be one factor for enhanced thermal stability.[50]

DTG analysis was studied as a function of rate of weight loss (μg/min) with increase in temperature. In case of CP, two peaks at 251 °C (590 μg/min) and 424 °C (2810 μg/min) have been observed. In case of CP-*cl*-poly(NVP) polymer three stage degradation has been observed, where first stage is associated with very slow degradation rate with a peak at 190 °C (211 μg/min), second stage degradation showed DTG peak at 400 °C (870 μg/min), third peak at 493 °C (1030 μg/min). Results of DTG support the TGA, as relatively slow degradation rate was observed in cross-linked polymer matrices in comparison to CP. It is important to mention here that temperature at which maximum degradation rate was observed shifted from 424 °C to 493 °C on going from CP to cross-linked polymer. The results of thermal degradation thus confirm the conclusion that cross linking and grafting has occurred which has improved thermal stability of CP-*cl*-poly(NVP) polymer in comparison to CP.

DSC curves of CP and CP-*cl*-poly(NVP) polymer are presented in Figure 7. In case of CP two endothermic peaks, at 61.0 and 228.7 °C, were observed, with a heat of fusion 122.6 and 248.7 J/g respectively. The initial endotherm can be due to the evaporation of unbound water in the polymer and the latter can be attributed to the loss of water due to formation of anhydrides in CP.[51] Glass transition temperature (T_g) for CP has been observed in the temperature range 128.5-135.1 °C (ΔCp = 0.574 J/g K). Gómez-Carracedo *et al.* (2004) have reported that various grades of CPs show T_g in the range 130-140 °C. CP-*cl*-poly(NVP) polymer showed quite different DSC thermo gram in comparison to CP. Two endothermic peaks have been observed at 89.3 °C and 221.9 °C. The first endotherm with a heat of fusion 89.74 J/g, can be attributed to the evaporation of unbound water in the cross-linked polymer and second endotherm (108.6 J/g) can be due to anhydride formation in the polymer.[52]

3.2 Swelling studies

The swelling polymers was determined in simulated wound fluid (pH = 8), phosphate buffer saline and pH 2.2 buffer to evaluate the effect of nature of swelling medium on network structure of hydrogels (Table 1). Swelling was observed more in SWF (1137.35±31.21%) as compared to swelling in pH 2.2 buffer (287.49±23.47%) and PBS (1100.04±12.25%). pH sensitivity of the hydrogel can be attributed to the presence of CP in the polymer matrix and in alkaline solution, partially ionization of carboxylic groups develop internal ion osmotic pressure due to electrostatic repulsion and swelling of hydrogels.[53] On the other hand, at lower pH solution, the hydrogen-bonding interactions leading to generation of additional physical crosslinking. So, the electrostatic repulsion due to COO- groups is restricted, and the polymeric network tends to shrink.[54]The swelling of polymers was observed less in 0.9% NaCl solution (355.04±5.88%) as compared to distilled water (1198.78±34.30%).Increase in salt concentration shielded the electrostatic repulsion between charged groups, causing decrease of hydrogel swelling.[45] Swelling of hydrogels increased with increase in temperature of swelling medium. At higher

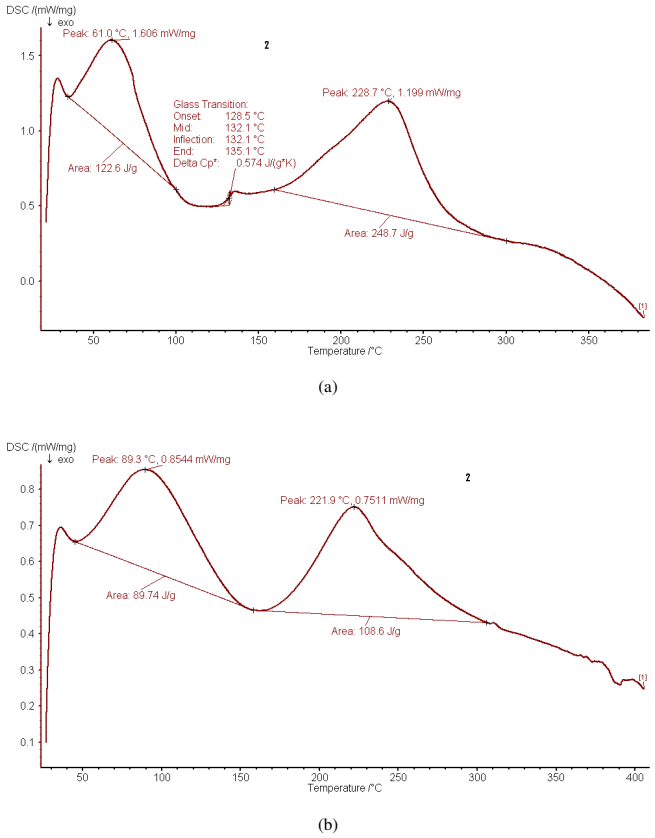

Figure 7. DSC curves of (a) CP and (b) CP-*cl*-poly(NVP) polymer

temperature the chain mobility increases which facilitates the network expansion and leads to increase in swelling of hydrogel[55](Table 1).

Overall, these hydrogel wound dressing showed high wound fluid absorption capacity and one gram of hydrogel film has taken 11.37±0.31 g of simulated wound fluid. Moist wound bed has been widely accepted as the most ideal environment for effective wound healing.[56] The accumulation of wound exudates often causes maceration and bacterial overgrowth in the wound site.

Table 1. Results of swelling for CP-*cl*-poly(NVP) hydrogels

Sr. No.	Parameter	Swelling after 24 hrs (%)
	Effect of swelling medium	
1.	pH 2.2 buffer	287.49±23.47
2.	Phosphate buffered saline (pH 7.4)	1100.04±12.25
3.	Simulated wound fluid (pH 8.0)	1137.35±31.21
4.	Distilled water	1198.78±34.30
5.	0.9% Sodium chloride solution	355.04±5.88
	Effect of temperature	
6.	27°C	1127.93±52.65
7.	37°C	1198.78±34.30
8.	47°C	1264.31±54.51

3.3 Drug release profile

Release profile of moxifloxacin from drug loaded CP-*cl*-poly(NVP) hydrogels was evaluated in simulated wound fluid (SWF) and results are shown in Figure 8 and Table 2. The release profile of entrapped drug showed slow and sustained release in SWF. No significant burst release was observed and considerable amount of drug release was observed after every half an hour, which can help in maintaining constant drug concentration at the wound site for a long time. The high surface area and porous structure of the hydrogels enabled the drugs to diffuse into the aqueous medium. Penetration of solvent led to formation of micro-cavities which cause the drug migration into solvent.[57] Diffusion exponent and various diffusion coefficients for the release of drug from the drug loaded polymers have been calculated and results have been presented in Table 2. The release of moxifloxacin from hydrogels occurred through Case-II diffusion mechanism. Case II diffusion mechanism occurs when rate of diffusion is very rapid as compared to the rate of relaxation of polymeric chains (relaxation controlled transport).The values of initial and late time diffusion coefficients were found comparable. The *in vitro* drug release data from CP-*cl*-poly(NVP) hydrogels in different releasing mediums were evaluated kinetically using various important mathematical models like zero order, first order, Higuchi, KorsmeyerPeppas, and Hixson-Crowell models. When the respective R^2 were compared, it was found that it followed best by Hixson-Crowell's model with highest values of regression coefficient. Hixson-Crowell's model applies to such pharmaceutical dosages, where the dissolution occurs in planes that are parallel to the drug surface if the dosage dimensions diminish proportionally, in such a manner that the initial geometrical form keeps constant all the time.[58]

3.4 Blood compatibility

Hemolysis, defined as the release of hemoglobin into plasma due to damage of erythrocytes membranes, is directly related to blood compatibility of material. Direct contact hemolytic assay is considered to be reliable method for measuring blood biocompatibility of biomaterials. Results of hemolysis test for CP-*cl*-poly(NVP) polymer have shown (3.97±0.72)% haemolysis classifying it as non-haemolytic material. These hydrogels can be regarded as safe for wound applications. Li *et al.* have reported increase in blood compatibility on grafting with NVP.[59] Moreover, Blood compatibility of these crosslinked polymer can be attributed to its constituting materials poly(NVP) and CP, which are highly hydrophilic and biocompatible in nature.[13,60] These re-

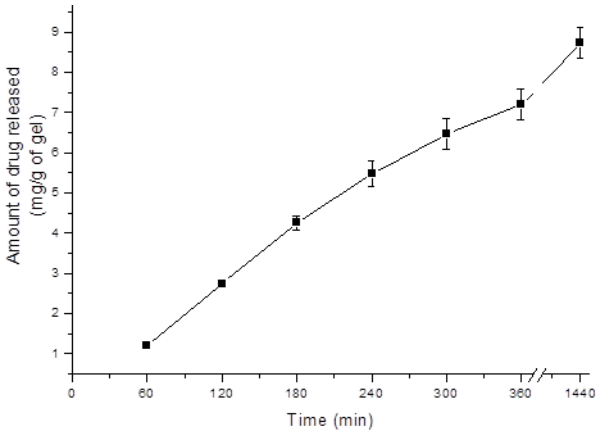

Figure 8. Release profile of moxifloxacin hydrochloride from drug loaded CP-*cl*-poly(NVP) hydrogels, in simulated wound fluid at 37 °C

sults revealed the hemocompatibility of hydrogel dressings, which indicates material will not alter the integrity of the blood during *in-vivo* application.During thrombogenicity test, weight of the clot formed with hydrogels was slightly less (0.31±0.02 g) in comparison to blood without hydrogels (0.34±0.05 g). These results indicate that 91.39±7.44% thrombogenicity was observed in the presence of CP-*cl*-poly(NVP) polymer, classifying the material as non-thrombogenic (Table 3).

3.5 Mucoadhesion studies

The results of mucoadhesion studies for CP-*cl*-poly(NVP) polymer are presented in Table 3. Maximum detachment force (F_{max}) required for detachment of hydrogels from mucosal surface was 79.98±8.16 mN. Bioadhesive properties in the present case can be attributed to synergistic mucoadhesive effect of poly(NVP) and CP. CP and poly (NVP) are known to improve mucoadhesive properties of the biomaterials.[61,62] Carboxylic groups of CP are capable of forming strong hydrogen bonds with oligosaccharide chains present in mucins leading to adhesion.[62] Mucoadhesion is desirable for a topical wound dressing as it will help the dressing to retain its position with less chances of dislocation from the wound site. Mucoadhesive polymers are widely explored for developing novel drug delivery systems. The close contact between a delivery system and the absorbing cell layer will improve both efficiency and effectiveness of the mucoadhesive system. Interaction of a polymeric system with these mucus glycoproteins is the major reason for the mucoadhesion phenomenon. Inter-penetration and inter-diffusion of polymeric chains with the mucus lining is one among the important steps in determining the bioadhesive interactions. Specific non-covalent interactions between the functional groups in the polymers and the mucus glycoproteins further reinforce these interactions.[63]

Table 2. Results of diffusion exponent 'n', gel characteristic constant 'k', various diffusion coefficients, and correlation coefficients of different models for release profile of moxifloxacin hydrochloride from drug loaded CP-*cl*-poly(NVP) hydrogels, in simulated wound fluid at 37 °C

Diffusion exponent 'n'		1.013
Gel characteristic constant 'k'×10^2		0.233
Correlation coefficient (R^2)		0.985
Diffusion coefficients (cm^2/min):	Initial D_i×10^6	7.73
	Average D_A×10^6	2.41
	Late Time D_L×10^6	5.4
Zero Order Model:	R^2	0.977
	k_0 ×10^2 (min^{-1})	0.23
First Order Model:	R^2	0.99
	k_1×10^2 (min^{-1})	0.533
Higuchian Model:	R^2	0.997
	k_H ×10^2 ($min^{-1/2}$)	6.28
Korsmeyer-Peppas Model:	R^2	0.985
	k_{KP}×10^2(min^{-n})	0.233
Hixson–Crowell's Model:	R^2	0.999
	k_{HC} ×10^2 ($min^{-1/3}$)	0.132

3.6 Oxygen permeability

The results of oxygen permeability are presented in Table 3. In the present case, the airtight flask (negative control) and opened flask (positive control) had dissolved oxygen values of 4.95±0.07 mg/L and 7.4±0.0 mg/L, respectively, whereas flasks covered CP-*cl*-poly(NVP)polymer film had dissolved oxygen values of 6.43±0.05 mg/L. The results show that CP-*cl*-poly(NVP) polymer film has shown considerable permeability to oxygen. Similar results have been reported in literature.[64] These results can be attributed to hydrophilicity of hydrogel films as observed in swelling studies. Hydrophilicity of the material results in water plasticization effect that will lead to polymer chain relaxation, increase in pore size and hence improved gaseous permeability.[65,66] Gaseous permeability especially for oxygen is a crucial factor for proper wound healing. On one side oxygen is necessary for regeneration of damaged tissue, while on the other side wound hypoxia leads to impaired wound healing. All result suggested that sufficient oxygen was able to penetrate through the polymeric network of crosslinked films. Oxygen availability is suitable for tissue homoeostasis, energy production, cell membrane maintenance, mitochondrial function, and cellular repair.[64]

Table 3. Results of biomedical properties of ofCP-*cl*-poly(NVP) hydrogels

Thrombogenicity	**Weight of blood clot (g)**	**Thrombose (%)**	**Inference**
	0.31±0.02	91.39±7.44	Non-thrombogenic
Haemolysis	OD at λ_{max} = 540 nm	Haemolytic Index (%)	Inference
	0.23±0.03	3.97±0.72	Non-haemolytic
Mucoadhesion[a]	Maximum detachment force F_{max} (mN)	Work of adhesion, W_{ad} (mN.mm)	Detachment distance (mm)
	79.98±8.16	32.40±4.34	5.19±0.55
Tensile strength[b]	Breaking force (N)	Tensile strength ($N.mm^{-2}$)	Elongation at break (%)
	13.19±2.41	0.65±0.12	119.38±14.26
Burst strength[c]	Dimension of film (cm^2)	Bursting strength (N)	Distance at burst (mm)
	3×3	8.25±0.31	15.30±1.65
Resilience[d]	Dimension of film (cm^2)	Force at target distance (g)	Resilience (%)
	3×3	154.70±29.89	25.49±0.72
Relaxation[e]	Force at target distance (N)	Relaxed force (N)	Retained force (%)
	0.54±0.09	0.23±0.02	43.56±2.69
O_2 permeability	Thickness of polymer(mm)	O_2 in test flask (mg/L)	Inference
	1.0	6.43±0.05	Permeable
Water vapour	Thickness of polymer (mm)	WVTR ($g/m^2/day$)	Inference
permeability	1.0	400.00±13.90	Permeable
Microbial penetration	Time (days)	Positive control (turbidity)	Polymeric films and negative control (turbidity)
	1	No	No
	2	Light	No
	14	Clear	No
	30	Complete	No

[a] (Contact time = 60 s, Return distance =15.0 mm, Applied force = 0.10 N, Trigger force = 0.029 N, Test speed = 0.10 mm/s, Pre test speed = 0.50 mm/s, Post test speed = 0.10 mm/s)

[b] (Trigger force = 0.029N, Test speed = 2.00 mm/s, Pre test speed = 0.20 mm/s, Post test speed = 10 mm/s)

[c] (Distance = 15.0 mm, Trigger force = 0.049 N, Test speed = 1.0 mm/s, Pre test speed = 2.0 mm/s, Post test speed = 10 mm/s)

[d] (Distance = 2.0 mm, Trigger force = 0.049 N, Test speed = 0.5 mm/s, Pre test speed = 1.0 mm/s, Post test speed = 0.5 mm/s)

[e] (Distance = 2.0 mm, Trigger force = 0.049 N, Test speed = 0.5 mm/s, Pre test speed = 1.0 mm/s, Post test speed = 10 mm/s)

3.7 Water vapour transmission rate

Parallel to oxygen permeability, evaluation of water vapour transmittance through the films is also necessary. WVTR for CP-*cl*-poly(NVP) films was 400.00±13.90 $g/m^2/day$, and for open vial it was 4192.38±106.29 $g/m^2/day$. However in case of sealed vial no water vapor transmittance was observed indicating CP-*cl*-poly(NVP) films were permeable to water vapors, but to a very less extent in comparison to open vial. Excess evaporation from the wound leads to wound dehydration and complete sealing leads to collection of wound exudates, both results in delayed wound healing. Intermediate WVTR for CP-*cl*-poly(NVP) hydrogels will help to maintain moist wound healing environment without collection of wound exudates.

3.8 Microbial penetration

Microbial penetration test was carried out for a month period and it was found that no microbial contamination occurred in open environment in case of nutrient broth sealed with CP-*cl*-poly(NVP) hydrogel films, while high turbidity in the open test tube was observed as a result of microbial contamination (Table 3). This test highlights that these hydrogel films could be considered as a good barrier against the microbes to prevent any secondary infection during wound healing. Similar results have been reported in literature.[56] The goal of wound therapy is to keep the wound microorganism content as low as possible in order to prevent infection and accordingly to stimulate the repair process. The hydrogel has the potential to mimic the extracellular matrix, which may lead to the tissue regeneration necessary for wound healing. In designing a matrix which promotes wound healing, it is important to provide an adequate antimicrobial protection. Hydrogel dressings are considered as a good barrier against microbes and this is important, especially for protecting the wound from further infection and accelerating the healing of the wound.[56]

3.9 Mechanical Properties

The results of mechanical properties (viz. tensile strength, burst strength, resilience, stress relaxation and folding endurance) of the CP-*cl*-poly(NVP) polymer film are given in Table 3. The polymers showed tensile strength (0.65±0.12 Nmm^{-2}) and elongation at break (119.38±14.26%). Tensile strength represented to the maximum tension that a material can withstand without tearing, while elongation at break was used to evaluate the malleability of materials. A crosslinked network im-

parts greater tensile strength and a more malleability to the hydrogels.[3] The considerable tensile strength are the results of long polymeric chains and interpenetrating network present in the polymeric film. Results of burst strength test revealed that 8.25±0.31 N force was required to burst the polymer film with a ball probe (P/5s) and distance at burst (15.30±1.65 mm) was shown by the polymer, indicating high mechanical strength. In stress relaxation test, when a constant strain (2 mm) was applied for 30 second (F_{max}=0.54±0.09 N) on 1 mm thick polymeric films, 0.23±0.02 N force was relaxed/retained by the polymer.

So, stress relaxation test shows 43.56±2.69% force was retained by the polymer sample indicting viscoelastic behaviour of the polymer film. The folding endurance was determined by repeatedly folding one film at the same place till it broke or folded up to 300 times manually, which was considered satisfactory to reveal good film properties. These polymer films did not show any cracks even after folding for more than 300 times. Folding Endurance test results reveal that these hydrogels were flexible and suitable for wound dressing applications. High flexibility can be attributed to high hydrophilicity of the hydrogels and glycerol, the biocompatible plasticizer.[65] Resilience is evaluated from of work returned by the sample when it is strained upto a distance (2 mm in present case). 25.49±0.72% resilience of the polymers was observed, indicating slight elastic character of the polymer film. Resilience and elongation values are measure for elasticity of a material, and in the present case the polymer film has shown high values for elongation and was resilient upto an extent, displaying elastic nature of the material.[66] Hence, the mechanical parameters obtained for the CP-*cl*-poly(NVP) polymer film indicate that it meets the requirements for a potential wound dressing material. Compromised mechanical properties of hydrogels often limit the scope of their applications.

4 Conclusion

From the forgone discussion it can be concluded that modification of CP with poly(NVP) was successfully carried out by free radical polymerization. The polymer was obtained in the form of a transparent flexible film. SEM and AFM studies demonstrate small degree of heterogeneity of the surface of the polymer film. The hydrogels showed high simulated wound fluid absorption and hydrogel dressings were found non-hemolytic, non-thrombogenic, oxygen permeable and water vapour permeable. In addition these hydrogels were transparent which will allow monitoring wound healing progress. Moxifloxacin released was observed in controlled manner from drug loaded hydrogels. Drug release from hydrogels occurred through Case-II diffusion mechanism and best fitted in Hixson-Crowell's model. Since the polymers were transparent, real time monitoring of wound healing is possible. These polymer films displayed high mechanical strength and flexibility. Overall the preliminary investigation suggested that CP-*cl*-poly(NVP) hydrogel films can act as potential candidate for wound dressing applications.

References

[1] Chandika P, Ko SC, Jung WK. Marine-derived biological macromolecule-based biomaterials for wound healing and skin tissue regeneration. Int J Biolog Macromol, 2015, **77**: 24-35. https://doi.org/10.1016/j.ijbiomac.2015.02.050

[2] Percival SL, Emanuel C, Cutting KF, *et al*. Microbiology of the skin and the role of biofilms in infection. Int Wound J, 2012, **9**: 14-32. https://doi.org/10.1111/j.1742-481X.2011.00836.x

[3] Jiang Q, Wang J, Tang R, *et al*. Hypromellose succinate-crosslinked chitosan hydrogel films for potential wound dressing.Int J Biolog Macromo, 2016, **l91**: 85-91. https://doi.org/10.1016/j.ijbiomac.2016.05.077

[4] Tavakoli J, Tang Y. Honey/PVA hybrid wound dressings with controlled release of antibiotics: Structuralphysico-mechanical and *in vitro* biomedical studies. Materials Science and Engineering, 2017, **C77**: 318-325. https://doi.org/10.1016/j.msec.2017.03.272

[5] Caló E, Khutoryanskiy VV. Biomedicalapplications of hydrogels: A review of patents and commercial products Eur Polym J, 2015, **65**:252-267. https://doi.org/10.1016/j.eurpolymj.2014.11.024

[6] Slaughter BV, Khurshid SS, Fisher OZ, *et al*. Hydrogels in regenerative medicine. Adv Mater, 2009, **21**: 3307-3329. https://doi.org/10.1002/adma.200802106

[7] Moura LI, Dias AM, Carvalho E, *et al*.Recent advances on the development of wound dressings for diabetic foot ulcer treatment-a review. Acta biomaterialia, 2013, **9**: 7093-7114. https://doi.org/10.1016/j.actbio.2013.03.033

[8] Lloyd LL, Kennedy JF, Methacanon P, *et al*. Carbohydrate polymers as wound management aids. Carbohydr Polym, 1998, **37**: 315-322. https://doi.org/10.1016/S0144-8617(98)00077-0

[9] Song J, Yu R, Wang L, *et al*. Poly (N-vinylpyrrolidone)-grafted poly (N-isopropylacrylamide) copolymers: synthesis characterization and rapid deswelling and reswelling behavior of hydrogels. Polymer, 2011, **52**: 2340-2350. https://doi.org/10.1016/j.polymer.2011.03.038

[10] Telford AM, James M, Meagher L, *et al*. Thermally crosslinked PNVP films as antifouling coatings for biomedical applications. ACS Appl Mater Interfaces, 2010, **2**: 2399-2408. https://doi.org/10.1021/am100406j

[11] Shahbuddin M, Bullock AJ, MacNeil S, *et al*. Glucomannan-poly (N-vinyl pyrrolidinone) bicomponent hydrogels for wound healing. J Mater Chem, 2014, **B2**: 727-738. https://doi.org/10.1039/C3TB21640C

[12] Zheng A, Xue Y, Wei D, *et al*. Synthesis and characterization of antimicrobial polyvinyl pyrrolidone hydrogel as wound dressing. Soft Mater, 2014, **12**: 179-187. https://doi.org/10.1080/1539445X.2013.831357

[13] Smith LE, Rimmer S, MacNeil S. Examination of the effects of poly (N-vinylpyrrolidinone) hydrogels in direct and indirect contact with cells. Biomaterials, 2006, **27**: 2806-2812. https://doi.org/10.1016/j.biomaterials.2005.12.018

[14] Wan LS, Xu ZK, Huang XJ, *et al*. Hemocompatibility of Poly (acrylonitrilecoNvinyl2pyrrolidone): Swelling Behavior and Water States. Macromol Biosci, 2005, **5**: 229-236. https://doi.org/10.1002/mabi.200400157

[15] Bajpai SK, Pathak V, Soni B, et al. CNWs loaded poly (SA) hydrogels: effect of high concentration of CNWs on water uptake and mechanical properties. Carbohydr Polym, 2014, **106**: 351-358. https://doi.org/10.1016/j.carbpol.2014.02.069

[16] Islam MT, Rodriguez-Hornedo N, Ciotti S, *et al*. Rheological characterization of topical carbomer gels neutralized to different pH. Pharma Res, 2004, **21**: 1192-1199.

[17] Sahoo S, Pani NR, Sahoo SK. Microemulsion based topical hydrogel of sertaconazole: Formulationcharacterization and evaluation.Colloids SurfB Biointerfaces, 2014, **120**: 193-199. https://doi.org/10.1016/j.colsurfb.2014.05.022

[18] Jana S, Manna S, Nayak AK, *et al*. CP gel containing chitosan-egg albumin nanoparticles for transdermal aceclofenac delivery. Colloids Surf B Biointerfaces, 2014, **114**: 36-44. https://doi.org/10.1016/j.colsurfb.2013.09.045

[19] Wang Y, Lee CH. Characterization of a female controlled drug delivery system for microbicides. Contraception, 2002, **66**(4): 281-287. https://doi.org/10.1016/S0010-7824(02)00354-2

[20] Jaiswal M, Kumar A, Sharma S. Nanoemulsions loaded CP? 934 based gel for intranasal delivery of neuroprotective Centella asiatica extract: invitro and exvivo permeation study. J Pharma Invest, 2016, **46**: 79-89. https://doi.org/10.1007/s40005-016-0228-1

[21] Silva JP ,Dhall S, Garcia M, *et al*. Improved burn wound healing by the antimicrobial peptide LLKKK18 released from conjugates with dextrin embedded in a CP gel. Acta Biomater, 2015, **26**: 249-262. https://doi.org/10.1016/j.actbio.2015.07.043

[22] Singh B, Sharma N. Mechanistic implication for cross-linking in sterculia-based hydrogels and their use in GIT drug delivery.Biomacromolecules, 2009, **10**: 2515-2532. https://doi.org/10.1021/bm9004645

[23] Ritger PL, Peppas NA. A simple equation for description of solute release I, Fickian and non-Fickian release from non-swellable devices in the form of slabsspherescylinders or discs. J Control Rel, 1987, **5**:23-36. https://doi.org/10.1016/0168-3659(87)90034-4

[24] Ritger PL, Peppas NA. A simple equation for description of solute release II, Fickian and anomalous release from swellable devices. J Control Release, 1987, **5**: 37-42. https://doi.org/10.1016/0168-3659(87)90035-6

[25] Dash S, Murthy PN, Nath L, *et al*. Kinetic modeling on drug release from controlled drug delivery systems. Acta Pol Pharm, 2010, **67**: 217-223.

[26] Sullad AG, Manjeshwar LS, Aminabhavi TM. Novel pH-sensitive hydrogels prepared from the blends of poly (vinyl alcohol) with acrylic acid-graft-guar gum matrixes for isoniazid delivery. Ind Eng Chem Res, 2010, **49**: 7323-7329. https://doi.org/10.1021/ie100389v

[27] Imai Y, Nose Y. A new method for evalution of antithrombogenicity of materials. J Biomed Mater Res, 1972, **6**: 165-172. https://doi.org/10.1002/jbm.820060305

[28] Ferreira P, Pereira R, Coelho JFJ, *et al*. Modification of the biopolymer castor oil with free isocyanate groups to be applied as bioadhesive. Int J Biolog Macromol, 2007, **40**: 144-152. https://doi.org/10.1016/j.ijbiomac.2006.06.023

[29] Winkler LW. Die bestimmung des im wasser gel?sten sauerstoffes,Berichte der deutschen chemischen Gesellschaft, 1888, **21**: 2843-2854. https://doi.org/10.1002/cber.188802102122

[30] Chamb iHNM, Grosso CRF. Mechanical and water vapor permeability properties of biodegradables films based on methylcelluloseglucomannanpectin and gelatin. Food Sci Technol, 2011, **31**: 739-746. https://doi.org/10.1590/S0101-20612011000300029

[31] Greenspan L. Humidity fixed points of binary saturated aqueous solutions. J Res Natl Bur Stand, 1977, *81*: 89-96. https://doi.org/10.6028/jres.081A.011

[32] Wu P, Fisher AC, Foo PP, *et al*. In vitro assessment of water vapour transmission of synthetic wound dressings. Biomaterials, 1995, **16**: 171-175. https://doi.org/10.1016/0142-9612(95)92114-L

[33] Bajpai SK, Saggu SS. Insulin release behaviour of Poly(methacrylamideco Nvinyl2pyrrolidonecoitaconic acid) Hydrogel: An Interesting Probe, Part II. J Macromol Sci A, 2007, **44**: 153-157. https://doi.org/10.1080/10601320601030707

[34] Pal K, Banthia AK, Majumdar DK. Preparation of transparent starch based hydrogel membrane with potential application as wound dressing. Trends Biomater Artif Organs, 2006, **20**: 59-67.

[35] Wei Y, Xie R ,Lin Y, *et al*. Structure formation in pH-sensitive hydrogels composed of sodium caseinate and NO-carboxymethyl chitosan. Int JBiolog Macromol, 2016, **89**: 353-359. https://doi.org/10.1016/j.ijbiomac.2016.04.081

[36] Pramanick AK, Gupta S, Mishra T, *et al*. Topographical heterogeneity in transparent PVA hydrogels studied by AFM,Mater Sci Eng C, 2012, **32**: 222-227. https://doi.org/10.1016/j.msec.2011.10.022

[37] Ahuja M, Thakur K, Kumar A. Amylopectin-g-poly (N-vinyl-2-pyrrolidone): Synthesischaracterization and in vitro release behaviour.Carbohydr Polym, 2014, **108**: 127-134. https://doi.org/10.1016/j.carbpol.2014.03.007

[38] Du J, Liu X, Liu W, *et al*. One-step preparation of vinyl-functionalized material surfaces: a versatile platform for surface modification. Sci China Chem, 2014, **57**: 654-660. https://doi.org/10.1007/s11426-014-5067-1

[39] Patel MM, Smart JD, Nevell TG, *et al*. Mucin/poly (acrylic acid) interactions: a spectroscopic investigation of mucoadhesion. Biomacromolecules, 2003, **4**: 1184-1190. https://doi.org/10.1021/bm034028p

[40] Capra RH, Baruzzi AM, Quinzani LM, *et al*. Rheologicaldielectric and diffusion analysis of mucin/CP matrices used in amperometric biosensors Sens Actuators B Chem, 2007, **124**: 466-476. https://doi.org/10.1016/j.snb.2007.01.022

[41] Szakonyi G, Zelkó R. CP?-crospovidone interpolymer complex for pH-dependent desloratadine release. J Pharma Biomed Anal, 2016, **123**: 141-146. https://doi.org/10.1016/j.jpba.2016.02.012

[42] Zhu X, Lu P, Chen W, *et al*. Studies of UV crosslinked poly (N-vinylpyrrolidone) hydrogels by FTIRRaman and solid-state NMR spectroscopies.Polymer, 2010, **51**: 3054-3063.

[43] Tanodekaew S, Prasitsilp M, Swasdison S, *et al*. Preparation of acrylic grafted chitin for wound dressing application. Biomaterials, 2004, **25**: 1453-1460. https://doi.org/10.1016/j.biomaterials.2003.08.020

[44] Jin S, Gu J, Shi Y, *et al*. Preparation and electrical sensitive behavior of poly (N-vinylpyrrolidone-co-acrylic acid) hydrogel with flexible chain nature. Eur Polym J, 2013, **49**: 1871-1880. https://doi.org/10.1016/j.eurpolymj.2013.04.022

[45] Liu S, Luo W, Huang H. Characterization and behavior of composite hydrogel prepared from bamboo shoot cellulose and -cyclodextrin. IntJBiolog Macromol, 2016, **89**: 527-534. https://doi.org/10.1016/j.ijbiomac.2016.05.023

[46] Loh GOK, Tan YTF, Pe KK. Hydrophilic polymer solubilization on norfloxacin solubility in preparation of solid dispersion.Powder Technol, 2014, **256**: 462-469. https://doi.org/10.1016/j.powtec.2014.01.089

[47] Bentez-Guerrero M, López-Beceiro J, Sánchez-Jimnez PE, *et al*. Comparison of thermal behavior of natural and hot-washed sisal fibers based on their main components: Cellulosexylan and lignin, TG-FTIR analysis of volatile products. Thermochimica Acta, 2014, **581**: 70-86. https://doi.org/10.1016/j.tca.2014.02.013

[48] Verma SK, Pandey VS, Behari MYK. Gellan gum-g-N-vinyl-2-pyrrolidone: Synthesisswellingmetal ion uptake and flocculation behavior. Int J Biolog Macromol, 2015, **72**: 1292-1300. https://doi.org/10.1016/j.ijbiomac.2014.10.036

[49] Chun MK, Bhusal P, Choi HK. Application of CP/PVP interpolymer complex to prepare mucoadhesive floating granule.Arch Pharmacal Res, 2013, **36**: 745-751.

[50] Lin SY ,Yu HL. Thermal stability of methacrylic acid copolymers of Eudragits LSand L30D and the acrylic acid polymer of CP. J Polym Sci A, 1999, **37**: 2061-2067. https://doi.org/10.1002/(SICI)1099-0518(19990701)37:13⟨2061::AID-POLA20⟩3.0.CO;2-Y

[51] Lee WF, Chiang WH. Swelling and drugrelease behaviour of the poly (AAcoNvinyl pyrrolidone)/chitosan interpenetrating polymer network hydrogels. J Appl Polym Sci, 2004, **91**: 2135-2142. https://doi.org/10.1002/app.13353

[52] Shah R, Saha N, Saha P. Influence of temperaturepH and simulated biological solutions on swelling and structural properties of biomineralized (CaCO3) PVPCMC hydrogel. Prog Biomater, 2015, **4**: 123-136. https://doi.org/10.1007/s40204-015-0043-1

[53] Singh R, Singh D. Radiation synthesis of PVP/alginate hydrogel containing nanosilver as wound dressing. J Mater Sci Mater Med, 2012, **23**: 2649-2658. https://doi.org/10.1007/s10856-012-4730-3

[54] Jain GK, Pathan SA, Akhter S, *et al*. Mechanistic study of hydrolytic erosion and drug release behaviour of PLGA nanoparticles: Influence of chitosan. Polym Degrad Stab, 2010, **95**: 2360-2366.

[55] Tally M, Atassi Y. Synthesis and characterization of pH-sensitive superabsorbent hydrogels based on sodium alginate-g-poly (acrylic acid-co-acrylamide) obtained via an anionic surfactant micelle templating under microwave irradiation. Polym, Bulletin, 2016, **1**: 26. https://doi.org/10.1007/s00289-016-1649-8

[56] Costa P, Lobo JMS. Modeling and comparison of dissolution profiles. Eur J Pharma Sci1, 2001, **3**: 123-133. https://doi.org/10.1016/S0928-0987(01)00095-1

[57] Tang C, Yin L, Yu J, *et al*. Swelling behavior and biocompatibility of CPcontaining superporous hydrogel composites.J Appl Polym Sci, 2007, **104**: 2785-2791. https://doi.org/10.1002/app.25930

[58] Malik S, Kumar A, Ahuja M. Synthesis of gum kondagogug-poly (N-vinyl-2-pyrrolidone) and its evaluation as a mucoadhesive polymer.Int J Biolog Macromol, 2012, **51**: 756-762. https://doi.org/10.1016/j.ijbiomac.2012.07.009

[59] L R, Wang H, Wang W, *et al*. Simultaneous radiation induced graft polymerization of N-vinyl-2-pyrrolidone onto polypropylene non-woven fabric for improvement of blood compatibility. Rad Phys Chem,2013, **88**: 65-69. https://doi.org/10.1016/j.radphyschem.2013.03.013

[60] Hall DJ, Khutoryanskaya OV, Khutoryanskiy VV. Developing synthetic mucosa-mimetic hydrogels to replace animal experimentation in characterisation of mucoadhesive drug delivery systems. Soft Matter, 2011, **7**: 9620-9623. https://doi.org/10.1039/c1sm05929g

[61] Sajeesh S, Sharma CP. Mucoadhesive hydrogel microparticles based on poly (methacrylic acid-vinyl pyrrolidone)-chitosan for oral drug delivery. Drug Deliv, 2011, **18**:227-235. https://doi.org/10.3109/10717544.2010.528067

[62] Zhang D, Zhou W, Wei B, *et al*. Carboxyl-modified poly(vinyl alcohol)-crosslinked chitosan hydrogel films for potential wound dressing. Carbohydr Polym, 2015, **125**: 189-199. https://doi.org/10.1016/j.carbpol.2015.02.034

[63] Dias AMA, Rey-Rico A, Oliveira RA, *et al*. Wound dressings loaded with an anti-inflammatory juca (Libidibia ferrea) extract using supercritical carbon dioxide technology. J Supercrit Fluids, 2013, **74**: 34-45. https://doi.org/10.1016/j.supflu.2012.12.007

[64] Wittaya-areekul S, Prahsarn C. Development and in vitro evaluation of chitosanpolysaccharides composite wound dressings. Int JPharma, 2006, **313**: 123-128. https://doi.org/10.1016/j.ijpharm.2006.01.027

[65] Chen Q, Liang S, Thouas GA. Elastomeric biomaterials for tissue engineering. Prog Polym Sci, 2013, **38**: 584-671. https://doi.org/10.1016/j.progpolymsci.2012.05.003

[66] Borde A, Larsson M, Odelberg Y, *et al*. Increased water transport in PDMS silicone films by addition of excipients. Acta Biomater, 2012, **8**: 579-588. https://doi.org/10.1016/j.actbio.2011.09.022

J Pharm Biopharm Res, 2019, 1(1): 15-20
DOI: 10.25082/JPBR.2019.01.002

RESEARCH ARTICLE

The preparation of Garcinia Glycosides solid dispersion and intestinal absorption by rat in situ single pass intestinal perfusion

Shengnan Li[1] Jingchao Ji[1] Yinghui Chen[1] Ye Chen[1*] Ju Liu[1] Yang Wang[1] Hongsheng Liu[2]

Abstract: Garcinia Glycosides is a candidate drug obtained by structural modification of Gambogic Acid (GA), which was acquired through High Throughput Screening(HTS). As Garcinia Glycosides is an effective but insoluble anti-tumor drug, the aim of this study was to obtain a solid dispersion form Garcinia Glycosides by using solvent-melt method so that improve the solubility and dissolution rate. The solid dispersion was characterized by High Performance Liquid Chromatography (HPLC), infrared spectroscopy and evaluated the intestinal absorption of the drug by rat in situ single pass intestinal perfusion. The results showed the increase of solubility, dissolution velocity and absorption compared to other forms. This indicated that solid dispersion could greatly improve the relative bioavailability of Garcinia Glycosides *in vivo*.

Keywords: Garcinia Glycosides, solid dispersion, intestinal perfusion, in situ single-pass perfusion method

1 Introduction

Garcinia Glycosides is synthesized by structural modification of gambogic acid, which is a natural product found in gamboges. As a highly effective and low toxicity anticancer drug, the effect of anti-tumor is accomplished through different mechanisms, including induction of cell cycle arrest and cell apoptosis, inhibition of telomerase and topoisomerase activity, inversion of multidrug resistance and so on.[1] Animal experimental studies show that the half-life is 2.2 h following oral administration, the metabolic rate is rapid, multiple continuous administration is not conducive to clinical treatment of patients, while produces lots of toxicity.[2,3]

Drug release is a crucial and limiting step for oral drug bioavailability, particularly for drugs with low gastrointestinal solubility and high permeability.[4] Given Garcinia Glycosides's poor solubility in water and short half-life, Garcinia Glycosides is prepared into solid dispersion to increase the solubility and the dissolution rate of the drug, thereby increasing the relative bioavailability, so that solid dispersion can not only retain the immediate release of onset, but also extend the delivery time, while reduce the toxic and side effects.

The term solid dispersion (SD) is used to describe a solid system in which the drug is dispersed in a biologically innocuous hydrophilic carrier. These systems are generally centered on the conversion of a candidate pharmaceutical carrier mix from liquid to solid state.[5] The solid dispersion technology has been used extensively to enhance the solubility, dissolution and bioavailability of poorly water soluble drugs by water soluble carriers.[6] As we known, solid dispersion preparations using hydrosoluble carriers lead to significantly enhanced dissolution rates of poorly water-soluble drugs.[7–9] So in the present study, we choose water-soluble carrier material Polyethylene Glycol for Garcinia Glycosides solid dispersion, based on drug release and production many other aspects adventages of SD. Then we established HPLC to examine the basic properties of Garcinia Glycosides, to determine the drug release and the content. And studied the kinetic characteristic of Garcinia Glycosides solid dispersion in the rats in vivo intestinal absorption through single-pass perfusion technology. The paper provided biopharmaceutical basis for the research of Garcinia Glycosides.

Intestinal absorption characteristics of drugs are very important for oral drug delivery system. In situ perfusion experiment is under the condition of not cutting animal blood vessels and nerves, the drugs will be transported

Received: December 25, 2018 **Accepted:** January 25, 2019 **Published:** January 30, 2019

***Correspondence to**: Liaoning University, No. 66, Chongshan Middle Road, Huanggu District , Shenyang 110036, China; Email: sy-chenye@163.com

[1] Research Center for Computer Simulating and Information Processing of Biomacromolecules of Liaoning Province; School of Pharmacy, Liaoning University, Shenyang City, Liaoning Province, 110036, China.

[2] School of Life Sciences, Liaoning University, Shenyang City, Liaoning Province, 110036, China.

Citation: Li S, Ji J, Chen Y, *et al*. The preparation of Garcinia Glycosides solid dispersion and intestinal absorption by rat in situ single pass intestinal perfusion. *J Pharm Biopharm Res*, 2019, **1**(1):15—20

in blood after penetrating the intestinal epithelial cells to avoid the effect of gastric emptying and digestive tract inherent movement and other factors on the experimental results. The drug concentration of the circulating fluid in absorbing parts is so low that sink conditions can be formed, and can be excluded liver first-pass effect.[10–12]

2 Materials and methods

2.1 Materials

Garcinia Glycosides (Lot#: 0404901) was made by School of pharmacy, Liaoning Unversity. (Shenyang, China). Hydroxy propyl methyl cellulose (HPMC) and ethyl cellulose(RT-N-10) were obtained from Ruitai Chemical Group Co., Ltd. (Shandong, China). Lauryl sodium sulfate was purchased from Sinopharm Chemical Reagent Co., Ltd (Beijing, China). Methanol of HPLC grade was provided from Yuwang Chemical Co. (Shandong, China). Polyethylene Glycol (4000,6000) of Chinese Pharmacopoeia grade was purchased from Shanghai Chineway Pharmaceutical Tech.Co., Ltd. (Shanghai, China). All other chemicals and solvents used were of AR grade.

2.2 Preparation of Solid Dispersion

As a result of solvent-melt method using less solvent, simple process, requiring short time and remaining less residue, the solid dispersion was prepared by solvent-melt method.

2.2.1 Effect of carrier species on drug dissolution

Prepared different solid dispersions with different molecular weights PEG as carrier material, investigated the effects of glycosides in the case of the solid dispersion of drug dissolution. Determined drug-carrier mass ratio of 1:8, prepared different solid dispersions with PEG4000, PEG6000 and PEG4000-EG6000(1:1w/w) as carrier material separately. Then the cumulative release percentage of the three batches solid dispersions were measured, and drawed the release curve in Figure 1.

2.2.2 Effect of drug / carrier ratio on drug dissolution

PEG4000-PEG6000 (3:10, w/w) was used as the carrier material to prepare the solid dispersion as the drug/carrier ratio was 1:8, 1:13 and 1:18 separately. The cumulative release percentage of these three batches of solid dispersion was determined, and the release curve was plotted in Figure 2.

2.2.3 Effect of solvent ratio on drug dissolution

Respectively of Garcinia glycosides dissolved in anhydrous ethanol as the proportion was 1:10, 1:20 and 1:30, (w/V), fixed drug/carrier ratio was 1:8, water bath temperature of 80 °C, stirring time was 2h of the preparation of solid dispersion. Observed the effects of both ratio of drug dissolution. The cumulative release percentage of these three batches of solid dispersion was determined, and the release curve was plotted in Figure 3.

2.2.4 Effect of agitation time on drug dissolution

Mixing makes the carrier materials with the molten state of the drug fully exposed, so that the solid dispersion can be uniformly and stably. The ratio of the fixed drug/carrier was 1:8, the stirring time was 0.5h, 1h, 2h and 3h respectively. Prepared solid dispersion respectively, and the cumulative release percentage of these four batches of solid dispersion is determined, and the release curve chart was drawn in Figure 4.

2.2.5 Effect of bath temperature on drug dissolution

The melting point of PEG4000 and PEG6000 were about 60 °C, to ensure the carrier's completely molten and organic solvent volatilization, stirring time was 2h, fixed drug/carrier ratio was 1:8, with anhydrous ethanol (1:10, w/v) as solvent, respectively in 60 °C, 70 °C, 80 °C and 90 °C water bath temperature of four batches of solid dispersions were obtained, and the cumulative release percentage of these four batches of solid dispersion was determined, and the drug release curve was plotted in Figure 5.

2.2.6 Effect of cooling rate on drug dissolution

Fixed drug /carrier ratio 1:8, anhydrous ethanol (1:10, w/v) as solvent, stirring time was 2h, the water bath temperature of 80 °C. The two batches of solid dispersion were prepared, and a batch of the method of rapid cooling was used, while the other group was cooled at room temperature. The cumulative release percentage of these two batches of solid dispersion was determined, and the drug release curve was plotted in Figure 6.

2.2.7 The process of preparation

Weighed medicament and carrier in a 1:8 proportion, while the relative proportions of the carrier material PEG4000:PEG6000 was 3:10. Garcinia Glycosides was dissolved in bit anhydrous ethanol (1:10, w/v) with heat, then placed the carrier material in 80 °C water bath heated to molten state, added Garcinia Glycosides solution into the carrier material until completely melted. The mixing time was 2h under mechanical agitation and evaporated the solvent, the resultant rapidly poured onto -20 °C steel plates and severely stirred to make it cool.

2.3 Characterization of Garcinia Glycosides solid dispersion

2.3.1 High-Performance Liquid Chromatography

The exact content of the compounds was determined using Waters 1525 Brnary HPLC Pump, and a Waters 2487 Dual λ Absorbance Detector (Waters, Amer-

ica). A C18 reversed-phase chromatographic column (150mm3.9 mm; 5m particle size) was used. The column was kept at 30 °C throughout the elution process, which used a mobile phase consisting of 5% Phosphoric acid solution and Methanol at a total flow rate of 1.0 mL/min and the detection wavelength set to 360 nm; injection volume: 20μL.

The method was fully validated for specificity, lower limit of quantification (LLOQ), accuracy, precision and linearity Control samples were assessed by the procedure as described above to evaluate specificity of the method.

2.3.2 Phase identification of the preparation

There are plenty of dispersion states of drugs in solid dispersion, like the molecular state, no fixed patterns, colloidal microcrystalline or micronized state, *etc*. Therefore, identification of drug dispersion state is primary to analysis solid dispersion. The experiment used infrared spectroscopy to identify the present state in Garcinia Glycosides of solid dispersion.

2.3.3 Evaluation of solubility

The SD of Garcinia Glycosides were dispersed in a distilled water solution, 0.5% Sodium dodecyl sulfate; maintained horizontally with agitation at a temperature of 37±0.5 °C. Sampling 5ml per predetermined time interval, and promptly supplemented with an equal volume of fresh medium. After this stage, the samples were first filtered with qualitative paper filters and subsequently passed through a filter with 0.45 mm pores. The quantity of Garcinia Glycosides dissolved was determined by spectrometry. Substituting the corresponding standard curve equation to calculate the concentration, obtained the drug cumulative release percentage Q:

$$Q(100\%) = \frac{C \times V \times D}{W \times F \times 1000} \times 100\%$$

where the drug cumulative release percentage Q is determined by C, the concentration of the dissolution liquid g/ml; V, the volume of the dissolution medium ml; D, dilution ratio; W, the weight of solids; F, the percentage of the drug in the formulation. Then, plot a graph showing the dissolution calculated by time as X-axis and drug cumulative release percentage as Y-axis.

2.4 Evaluation of intestinal absorption

Adopt in situ single-pass perfusion method to evaluate the SD of Garcinia Glycosides in intestinal absorption. This experiment was conducted using male adult rats and the animals were deprived of solid food for 12 hours (Free access to water) before the start of the experiment. Then intraperitoneal injection of 10% chloral hydrate(3.4 ml/kg), fixed and maintained them body temperature. A midline abdominal incision was made and the small intestine was exposed. The intestine was rinsed by physiological saline at 37 °C until the washing appeared clear and ligated after cannulated into intestine. Then kept it thermal insulated under infrared lamps.

After that, cannulated to the constant flow pump, Garcinia Glycosides solution of 100ml at 37 °C was perfused as 1ml/min flow rate for 2 hours. Sampling 1ml to 10ml volumetric flasks at times 0, 10, 30, 60, 90 and 120 minutes and immediately filtered through membranes with 0.45 mm pores. The perfusate was diluted to 10 ml and was detected by HPLC. The volume of the dissolution medium was maintained constant by the addition of 1ml of Garcinia Glycosides solution. Then took gambogic acide 0.5% CMC-Na suspension as a control, operated the same method.(Table 1, Table 2)

Table 1. Gambogic acid reference substance

Time (min)	Area (Microvolt * s)	Concentration (mg/ml)	Percent Absorption (%)
0	137389	0.005279	0.00
10	137310	0.005276	0.0568
30	132432	0.005084	3.646
60	112486	0.004322	18.13
90	96982	0.003726	29.42
120	90137	0.003463	34.40

Table 2. Garcinia Glycosides SD

Time (min)	Area (Microvolt * s)	Concentration (mg/ml)	Percent Absorption (%)
0	175119	0.0132	0.00
10	165800	0.0125	5.383
30	91946	0.006932	47.47
60	75561	0.005696	56.85
90	63131	0.004764	63.95
120	42420	0.003198	75.77

3 Results

3.1 Effect of carrier species on drug dissolution

The figure showed the type of carriers was a significant factor. Drug release rate increased with the increase of polyethylene glycol (PEG) molecular weight. Its order was PEG6000>PEG4000-PEG6000>PEG4000. However, the solid dispersion prepared by PEG6000 was used as the carrier to make the preparation process difficult. Therefore, PEG4000-PEG6000 was used and adjusted the proportion of the PEG6000. Determined PEG4000-PEG6000 (3:10, w/w) as the carrier.

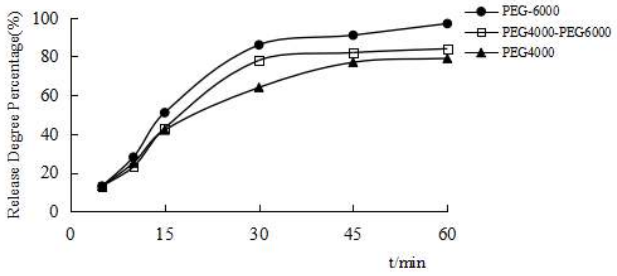

Figure 1. The release curve of different carrier types of the Garcinia Glycosides solid dispersion and the carriers were PEG4000, PEG4000-6000 and PEG6000 respectively

3.2 Effect of drug /carrier ratio on drug dissolution

By the graph, the proportion of the drug carriers could be increased, but the effect was small. Considering the amount of solid dispersion containing the amount of the solid dispersion, the initial determination of the drug / carrier ratio was 1:8.

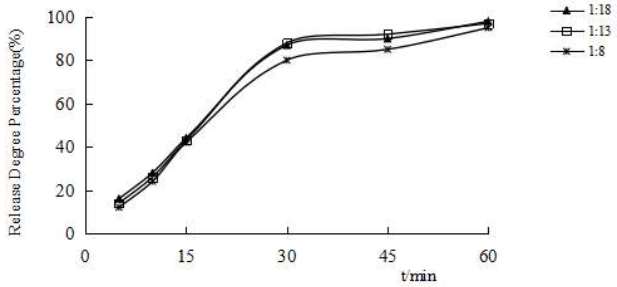

Figure 2. The release curve of the proportion of different carrier of the solid dispersion and the ratio of drug and carrier were 1:8, 1:13and 1:18 respectively

3.3 Effect of solvent ratio on drug dissolution

The figure showed the dissolution rate of the solid dispersions increased with the increase of absolute ethanol ratio, but the difference was not obvious. In the case of the full dissolution of the drug, the proportion of the solvent was not the main factor affecting the drug dissolution. So determination of solvent ratio of drug / ethanol (1:10, w/v).

3.4 Effect of agitation time on drug dissolution

As shown in Figure 4, the time of stirring had a great influence on the drug dissolution. However the increase of the mixing time after 2h had little effect on the drug dissolution. Therefore, in order to ensure the uniform and stable dispersion of solid dispersion and the organic solvent, the stirring time should be 2h.

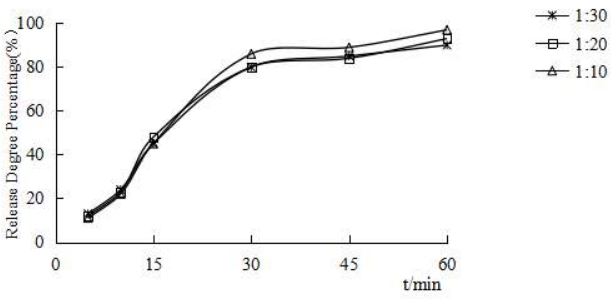

Figure 3. The release curve of the solid dispersion of the proportion of the different solvents and the solvent ratio of drug and ethanol were 1:10, 1:20 and 1:30 respectively

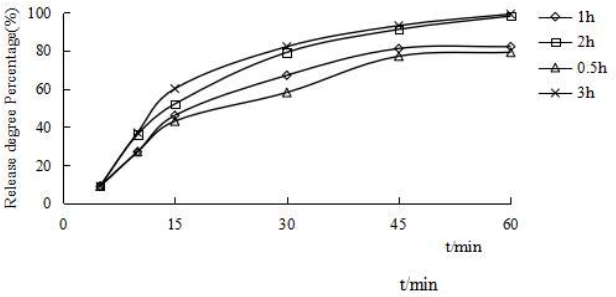

Figure 4. The release curve of the solid dispersion of different stirring time and the stirring time were 0.5 h, 1 h and 2 h respectively

3.5 Effect of bath temperature on drug dissolution

The diagram showed with the increase of the water bath temperature, the drug dissolution rate increased, but after temperature more than 80 °C, drug dissolution rate decreased. Probably because of the high temperature accelerated solvent evaporation speed, so the solvent evaporate uneven, bring about shell encapsulated drug, the drug release rate decreased. So the bath temperature was 80 °C.

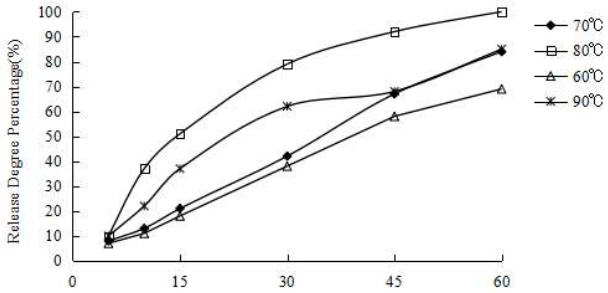

Figure 5. The release curve of Garcinia glycosides solid dispersions in different water bath temperature and the bath temperature were 70 °C, 80 °C and 90 °C respectively

3.6 Effect of cooling rate on drug dissolution

It was found that the cooling rate had a great effect on the dissolution of the drug, which may be due to the dissolution of the solid dispersion, which was caused crystallization by the slow cooling of the drug. In this experiment, the solid dispersion was prepared by rapid cooling method.

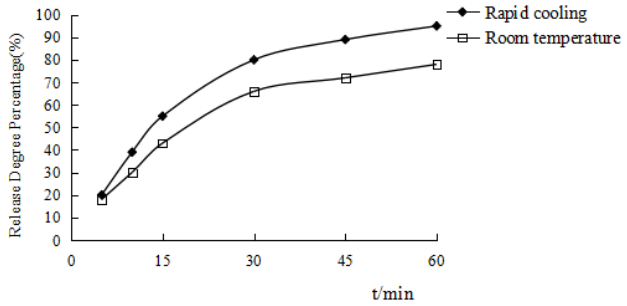

Figure 6. The release curve of the solid dispersion with different cooling methods and the cooling methods were rapid cooling and cooling with room temperature

3.7 Phase identification of the solid dispersion

If Garcinia Glycosides existed in complex molecular, forming hydrogen bond, the absorption peak of some drugs and carriers disappeared or displaced between 2800-3200. IR spectra shown in Figure 7 did not show the absorption peak change, so the solid dispersion may not be in the form of complex molecule, it may exist in microcrystallines or nano-particles.

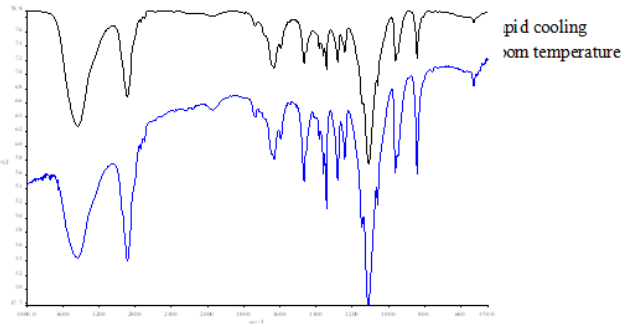

Figure 7. The infrared spectroscopy of the THS SD and physical mixtures of PEG4000 and PEG6000 with THS

3.8 Evaluation of solubility

The result showed that the release rate of the sample reached the standard and the release rate was good.

3.9 Evaluation of intestinal absorption

The Figure 9 showed the intestinal absorbability of Garcinia Glycosides SD apparently higher than gambogic acid. Probably due to the Garcinia Glycosides made into solid dispersion, the drug highly dispersed in the carriers as microcrystalline or amorphous, so that greatly improved the dissolution and absorption of the drug.

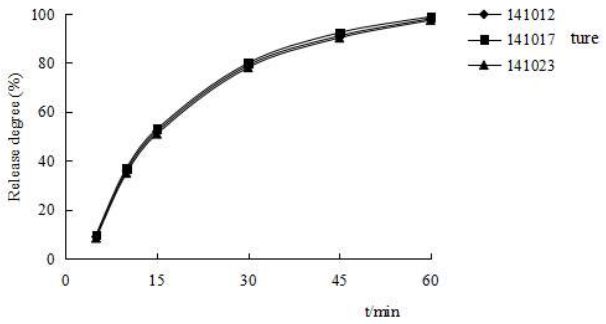

Figure 8. The drug release curves of 3 batches solid dispersion

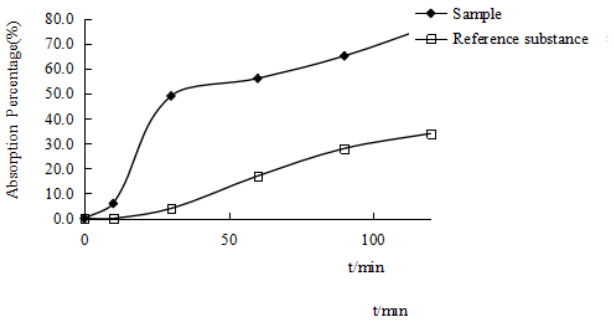

Figure 9. The intestinal absorption of solid dispersion and reference substance

4 Discussion

The properties of the solid dispersion carrier directly affect the properties of the solid dispersion, so the carrier should have the following conditions: physiological inertia, no carcinogenic, no toxic, no opposite effect with drug treatment purposes; no chemical reaction with the drug, do not affect the chemical stability of the main drug; can get the best dispersion state; get the source easily and cheap price, *etc.*. PEG is a crystalline polymer with stable properties and heat resistance, which can be compatible with many drugs, and the melting point is low (60 °C). Also solid dispersion can be crushed and stored easily. Therefore, PEG polymer was used as the carrier material.

In the present study, the characterization results indicated that Garcinia Glycosides was prepared into solid dispersions with the carrier of PEG. The dissolution rate of the drug was not determined by the change of the molecular weight of PEG, instead depended on the drug

specific. With the increase of the PEG molecular weight, the dissolution rate increased slightly; with the increase of the proportion of the carrier, the dissolution rate was significantly improved. PEG6000 was used alone as the carrier, which makes the preparation process complex and difficult. So the experiment selects PEG4000 and PEG6000 as the joint carrier.

In this paper, the method of single-pass perfusion was used in the study of intestinal absorption. Compared with the circulation method, the experimental conditions of this method were close to the intestinal circumstances after the drug delivery, so that avoided the measurement error caused by the high flow rate of the Injury of intestinal mucous membrane.

5 Conclusions

Oral drug delivery is the simplest and commonest way of administering drugs. Actually, most drugs are poorly water soluble drugs, not well absorbed after oral administration.[13] So Garcinia Glycosides was prepared into solid dispersion. By improving the drug release profile of these drugs, it is possible to enhance their bioavailability and reduce side effects.[14, 15] This series of results show that SD is a useful strategy for increasing the bioavailability of Garcinia Glycosides and have conducive to intestinal absorption.The single-pass intestinal perfusion studies in rats also confirmed that Garcinia Glycosides solid dispersion displayed a good absorption in intestinal.

6 Acknowledgements

This study was supported by grants from the Drug Discovery Initiative of the National 11th Five Year Plan (2009ZX09103-030) and Innovation Team Project (No: LT2015011) from the Education Department of Liaoning Province. Gareinia glycosides was provided by College of Pharmacy of Liaoning University, New Drug R&D Key Laboratory of Liaoning Province.

References

[1] Wang Y, Zhang Q, Liu J, *et al*. Synthesis and antitumor activities of Gareinia glycosides. Chin J New Drugs, 2013, **22**:2739-2744.

[2] Li WJ, Chen Y, Li TW, *et al*. Formulation optimization and the release mechanism of Gareinia glycosides sustained-release tablets. Chin J Modern Appl Pharm, 2013, **10**:1081-1085.

[3] Fu YP, Wang R, Li TW, *et al*. Pharmacokinetics and tissue distribution of TJXG nano emulsion in rats. Chin Medical Herald, 2013, **11**:19-22.

[4] Liu C, Zhu S, Zhou Y, *et al*. In Situ Intestinal Absorption of Cyclosporine A Solid Dispersion in Rats. Drug Dev Ind Pharm, 2008, **34**(6):627-631. https://dx.doi.org10.1080/03639040701833948

[5] Chaud MV, Tamascia P, Lima AC, *et al*. Solid dispersions with hydrogenated castor oil increase solubility, dissolution rate and intestinal absorption of praziquantel. Braz J Pharm Sci, 2010, **46** (3): 473-481. https://dx.doi.org/10.1590/S1984-82502010000300010

[6] Liu C, Zhu SJ, Zhou Y, *et al*. Enhancement of dissolution of cyclosporine A using solid dispersions with polyoxyethylene (40) stearate. Pharmazie Die Pharmazie-An Int J Pharm Sci, 2006, **61**(8):681-684.

[7] Chaud MV, Paula FC, Moraes LC, *et al*. Assessment of Solubility and Intestinal Absorption In Vitro of Praziquantel in Solid Dispersions of Polyethylene Glycol 6000. Lat Am J Pharm, 2011, **30** (10): 1910-1915.

[8] Yang M, He S, Fan Y, *et al*. Microenvironmental pH-modified solid dispersions to enhance the dissolution and bioavailability of poorly water-soluble weakly basic GT0918, a developing anti-prostate cancer drug: Preparation, characterization and evaluation *in vivo*. Int J Pharm Sci, 2014, **475** (1-2): 97-109. https://doi.org/10.1016/j.ijpharm.2014.08.047

[9] Surampalli G, Nanjwade B, Patil PA. Corroboration of naringin effects on the intestinal absorption and pharmacokinetic behavior of candesartan cilexetil solid dispersions using in-situ rat models. Drug Dev Ind Pharm, 2015, **41** (7):1057-1065. https://dx.doi.org/10.3109/03639045.2014.925918

[10] Zhou, W, Di LQ, Bi XL, *et al*. Intestinal absorption of forsythoside A byrat circulation in situ. Acta Pharmaceutica Sinica, 2010, **45** (11):1373-1378.

[11] Dang YJ, Feng HZ, Zhang L, *et al*. In Situ Absorption in Rat Intestinal Tract of Solid Dispersion of Annonaceous Acetogenins. Gastroenterology Res Pract, 2012, **10**:81-89.

[12] Shi CY, Tong Q, Fang J, *et al*. Preparation, characterization and in vivo studies of amorphous solid dispersion of berberine with hydrogenated phosphatidylcholine. Eur J Pharm Sci, 2015, **74**:11-47. https://doi.org/10.1016/j.ejps.2015.04.001

[13] Streubel A, Siepmann J, Bodmeier R. Drug delivery to the upper small intestine window using gastroretentive technologies. Curr Opin Phar, 2006, **6** (5): 501-508. https://doi.org/10.1016/j.coph.2006.04.007

[14] Tanaka N, Imai K, Okimoto K, *et al*. Development of novel sustained-release system, disintegration-controlled matrix tablet (DCMT) with solid dispersion granules of nilvadipine (II): in vivo evaluation. J Controlled Release, 2006, **112**(1):52-56. https://doi.org/10.1016/j.jconrel.2006.01.020

[15] Szts A, Láng P, Ambrus R, *et al*. Applicability of sucrose laurate as surfactant in solid dispersions prepared by melt technology. Int J Pharm Sci, 2011, **410**(1-2):107-110. https://doi.org/10.1016/j.ijpharm.2011.03.033

J Pharm Biopharm Res, 2019, 1(1): 21-27
DOI: 10.25082/JPBR.2019.01.003

RESEARCH ARTICLE

Binding studies of trans-resveratrol with superoxide dismutase (SOD1): Docking assessment and Thermoanalysis

Janhvi Dureja[1] Renu Chadha[1*] Maninder Karan[1] Akshita Jindal[1] Kunal Chadha[1]

Abstract: The binding pursuits of trans-resveratrol (t-RSV), an amazing health supplement are investigated with an antioxidant enzyme, superoxide dismutase (SOD1). The aim of the study is to dock t-RSV on the adrenaline binding site on SOD1 in order to explore its potential to act as a safety net against amyotrophic lateral sclerosis (ALS), a fatal neurodegenerative disorder that affects motor neurons. In *silico* GLIDE docking methodology and in vitro microcalorimetry technique is utilized for the investigation of binding parameters of t-RSV with SOD1. The study provides useful and distinct information about the amino acids involved in the interactions at molecular level along with the nature of forces involved in binding of t-RSV with SOD1. The docking analysis using the scoring functions of Schrodinger's Glide package depicts that GLU100, PRO28, LYS23, TRP32 residues of the peptide backbone on SOD1 interact with phenolic groups of t-RSV. The information on thermodynamic parameters, *i.e.* binding constant (K_b), free energy (ΔG) and enthalpy (ΔH) generated through calorimetric titrations suggests that the reaction between t-RSV and SOD1 is spontaneous and exothermic. Both the studies are found to be in close agreement with each other based as far as the magnitude of binding constant ($K_b = 9.9 \times 10^4$) is concerned.

Keywords: trans-Resveratrol, superoxide dismutase, docking, microcalorimetry, binding constant, free energy

1 Introduction

Trans-resveratrol (3,5,4′-trihydroxy-trans-stilbene), widely regarded as a powerful dietary supplement with a multitude of health benefits, slows down the ageing process and helps keeping the body's cells, inside and out, looking young and healthy.[1] It is already reported that various species treated with resveratrol has shown lifespan extensions.[2,3] This nutraceutical helps in preventing age-related diseases such as atherosclerosis, cancer, Parkinson's disease, and Alzheimer's disease. It mainly exerts its action due to its intrinsic antioxidant property that attenuates oxidative damage to biological systems.[4–8] It works against ageing by protecting the body cells from free radicals generated during normal metabolism and damage caused by oxidative stress. Trans-resveratrol (t-RSV) either directly scavenges reactive oxygen species (ROS) or modulates the expression and activity of antioxidant enzymes such as superoxide dismutase (SOD).[9]

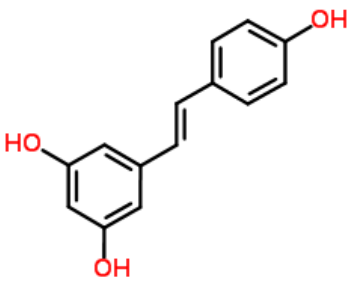

Figure 1. Molecular structure of trans-resveratrol

SOD acts as one of the essential biomarkers of ageing,[10–12] the parameters that change qualitatively or quantitatively during ageing or age related diseases.[13] These are regarded as potential key targets for studying anti-ageing effect of the drug molecules. Thus one of the ways to contribute towards quest of youth is to study the interaction of these intrinsic key targets with drug molecules having anti-ageing potential. The metalloenzyme, SOD plays a pivotal role in metabolism of

Received: December 30, 2018 **Accepted:** February 19, 2019 **Published:** February 22, 2019

*Correspondence to: Renu Chadha, University Institute of Pharmaceutical Sciences, Panjab University, Chandigarh 160014, India; Email: renukchadha@rediffmail.com
[1] University Institute of Pharmaceutical Sciences, Panjab University, Chandigarh 160 014, India

Citation: Dureja J, Chadha R, Karan M, *et al*. Binding studies of trans-resveratrol with superoxide dismutase (SOD1): Docking assessment and Thermoanalysis. *J Pharm Biopharm Res*, 2019, **1**(1):21-27.

deleterious ROS and free radicals. It removes superoxide O^{2-} radical, repairs cells and reduces the damage done to them by superoxide and oxygen free radicals. SOD catalyzes the reduction of superoxide anions to hydrogen peroxide (Figure 1). It also promotes the activity of nitric oxide (NO) by scavenging the superoxide anions and thus prevents the conversion (inactivation) of NO to peroxynitrite.[14]

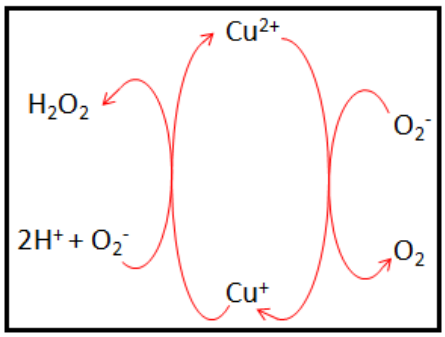

Figure 2. Catalytic cycle of SOD-1 ('ping-pong' mechanism)

The x-ray crystal structure (Figure 2) of the oxidized form of Cu, Zn-SOD from bovine erythrocytes shows a protein consisting of two identical subunits (a dimer composed of 2 chains (A and F)) held together almost entirely by hydrophobic interactions.[15]

Intervention to stabilize SOD1 dimer and inhibit aggregation is regarded as a potential therapeutic strategy in control of ageing. This approach can be successfully applied in treatment of major age-related disorders characterized primarily by selective neurodegeneration of the motor neurons leading to muscle atrophy and paralysis (fatal human neuropathy).[16] It is well established that binding of adrenaline with SOD1 dimer maintains its integrity by circumventing the dimer aggregation and thus controls amyotrophic lateral sclerosis (ALS).[17] Literature reports show that amyotrophic lateral sclerosis (ALS) is one of the rapidly progressive ageing disorders in which mutations in the gene encoding Cu/Zn SOD1 decrease protein stability. This further promotes misfolding or aggregation leading to toxicity due to oxidative damage stemming from aberrant SOD1 redox chemistry. However, this malfunctioning of superoxide dismutase (SOD1) can be prevented by binding SOD1 with ligands at the site where adrenaline is bound. The drugs or ligands binding at this site are found to be mainly useful in treatment of ALS by acting as SOD1 stabilizers as proposed in literature.[17–22] This binding site is different from well studied hydrophobic cavity created by Val7-Gly147-Val148 in the dimerization region and active site on SOD1.[23,24]

Many group of workers have successfully investigated the interactions between SOD1 and some important molecules.[13,25–28] However, the binding aspects of SOD1 with t-RSV, an innovative anti-ageing molecule, have not yet been taken into consideration. With this background in mind, it was envisaged to study the binding of t-RSV with SOD1 at a key region identified in chain A of SOD1(Figure 2) with the aim to stabilize SOD1 dimer which is useful for treatment of ALS. In this manuscript, it is tried to explore the interaction of t-RSV with SOD through in silico docking and in vitro microcalorimetry technique. The molecular docking provides useful information on the binding mode and microcalorimetry is a direct tool to generate the thermodynamic data pertaining to binding of t-RSV with SOD1.[29–31]

2 Materials and Methods

2.1 Datasets

The crystal structure of SOD1(PDB entry code 4A7U) was downloaded from the RSCB Protein Data Bank (http://www.rscb.org), and ligand structures (SDF 3D format) were obtained from the PubChem database (http://pubchem.ncbi.nlm.nih.gov).

2.2 Chemicals

Trans-resveratrol (99% purity) and Superoxide dismutase (SOD) (bovine) were procured from Alfa Aesar (Thermo Fisher Scientific). They were properly stored at cool and dry place as per their recommendations.

Phosphate buffer (pH= 7.4, 0.1 M): It was prepared as per IP' 1996 recommendations.

2.3 In silico binding study using molecular docking methodology

A robust, high- speed and accurate computational strategy was employed to predict binding mode of a t-RSV on SOD1. The Schodinger's GLIDE (grid-based ligand docking with energetics)[32–36] docking methodology, supported by Maestro 10.5 was used to locate the appropriate binding orientations and ligand conformations with respect to SOD1.

The study involves the preparation of SOD1 (4A7U) structure. It was done by cleaning up the X ray structure using the protein preparation wizard in the Schrodinger software graphical user interface Maestro. This was attained by adding protons, fixing bond orders, optimizing protonation states and hydrogen bond networks and performing a minimization under restraints. Here chain A of SOD dimer was retained and chain F was deleted for further simplification of structure. This was followed by

the generation of energy grid using the GLIDE protocol previously described.[35,36] A grid representing the properties of SOD 1(4A7U) PDB structure, *i.e.* electrostatic potential generated on each grid points, van der Waals forces *etc* was generated from the prepared structure. Further the ligand (t-RSV) was also prepared using Ligprep from the Schrdinger suite. All possible protomers (protonation states) and ionization states were enumerated generating various potential tautomers which are themselves minimized. The prepared ligand was then screened using the grid that was previously generated. During this step, the ligand poses generated pass through a series of hierarchical filters that evaluate the ligand's interaction with the protein (SOD). The ligand orientations (poses) were assigned scores, related to the intermolecular interaction energy, and ranked relatively. The best 10 poses and corresponding scores were evaluated using Glide in Standard precision mode (Glide SP) of Glide algorithm. The protocol of Prime/MM-GBSA module of Schrdinger software 2016 was applied on the minimum energy conformation state of ligand bound protein complex obtained from the Glide SP to estimate the binding free energy (ΔG_{bind}). Energy minimization for the complex using OPLS3 force field within Macro Model was performed. The results of Glide docking were incorporated in the project table as a pose viewer file which was further explored for various types of bonding and non-bonding interactions. The theoretical calculations were done as follows:

$GScore = 0.05\,vdW + 0.15\,Coul + Lipo + H_{bond} + Metal + Rewards + RotB + Site$

vdW- Van der Waals energy

Coul- Coulomb energy

Lipo- lipophilic term

H_{bond}- hydrogen- bonding term

Metal- Metal-binding term

Rewards- term including rewards and penalties for buried polar groups, hydrophobic enclosure, *etc*.

RotB- penalty for freezing rotatable bonds Site- Polar interactions in binding site.

2.4 *In vitro* binding study using micro calorimetry

Calorimetric titrations were performed on Micro reaction calorimeter-μRCSYS-001 (Thermal Hazard Technology, UK) in isothermal mode at 25^{o}C. The stock solutions of SOD (3μM) and trans-resveratrol (150 μM) were prepared in phosphate buffer, pH= 7.4. The temperature difference between the sample cell (1.5 ml capacity) containing SOD1 and reference cell (1.5 ml capacity) containing buffer was measured as heat change signal. The titration was done by adding equal volumes of (10 aliquots of 25 μl) t-RSV solution taken in 250μl syringe to the sample and reference cells. Prior to start of titration, all solutions were degassed properly and the system was properly calibrated to get a stable base line. The dilution effect and machine effects were nullified by running the control experiments. It was achieved by first titrating the t-RSV taken in the syringe with phosphate buffer taken in sample cell and then titrating the buffer taken in syringe and SOD in the sample cell. The contents of the sample cell were stirred throughout the experiment at 200 rpm to ensure thorough mixing.

3 Results

3.1 Molecular docking analysis using site marker adrenaline

The t-RSV was made to dock at adrenaline (site marker) binding site in chain A of SOD 1(figure 1). This particular site was chosen in the study as discussed earlier[9] based on the established hypothesis of stabilization of SOD1 dimer by adrenaline as a means of preventing ALS, an age-related disorder.

The GlideScore values of the 10 best energy minimized docked ligand poses were used for qualitative assessment of the binding of t-RSV to SOD1. Visual inspection of those in silico poses clearly demonstrates the existence of both hydrogen bonding and hydrophobic interactions. It is quite apparent from the docking observations that the phenolic functional groups present in t-RSV facilitates hydrogen bonding interactions with the carboxyl functional groups of glutamic acid and proline residues of the peptide backbone present in the selected cavity of SOD1 *i.e.* 3-O-H (t-RSV)--- O-C=O (GLU 100) and 5-O-H (t-RSV)---O=C (PRO 28). Besides this one of the phenolic group of t-RSV forms hydrogen bond with amino group of lysine residue at the considered site *i.e.* (LYS 23) N-H---O-H (5) (t-RSV). Figure 2 also displays the hydrophobic interaction in form of pi-pi stacking between phenyl rings of t-RSV and tryptophan residue present in the cavity on SOD1 *i.e.* 4' Hydroxyphenyl ring---TRP 32. Furthermore the relevant amino acid residues lying within within 2 A^o around the docked t-RSV are also portrayed. The docking results are represented in Figure 2 and Table 1.

The minimum energy conformation state of ligand bound protein complex with least GlideScore was further considered out of ten generated binding poses. The hydrogen bonding and hydrophobic interactions between ligands and SOD1 were observed using pose viewer file.

The binding free energy (ΔG_{bind}) was calculated using Prime-MM-GBSA module of Maestro 10.5 as fol-

lows (Equation 1) and was found out to be -40.05.

$$\Delta G_{bind} = G_{complex} - (G_{protein} + G_{ligand}) \quad (1)$$

The binding constant (K_b) for SOD- t-RSV interactions was calculated by using the following equation (Equation 2) and was found out to be 9.9×10^4 kJmol^{-1}.

$$\Delta G = -2.303RTlogK_b \quad (2)$$

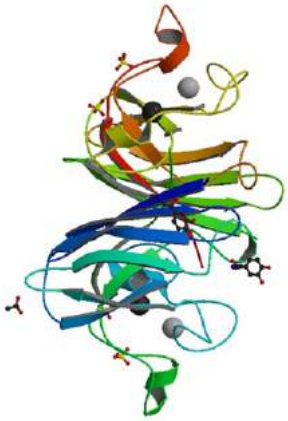

Figure 3. Crystal structure of SOD1 bound with adrenaline

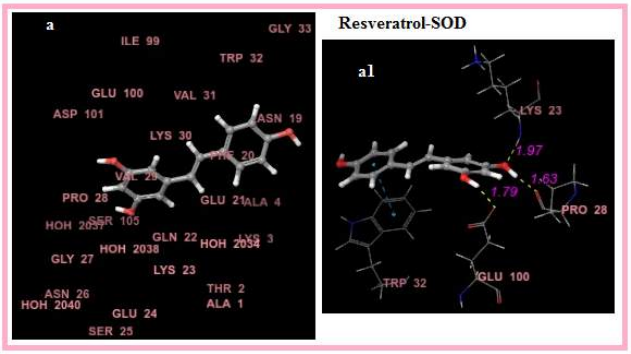

Figure 4. The Docking results. (a) represents best docked poses depicting relevant amino acid residues at SOD binding site within 2 A^o around the docked ligand (t-RSV); (a1) represents type of interaction (hydrogen bonds and stacking) between t-RSV and SOD.

3.2 Thermodynamics of t-RSV- SOD 1 interaction using microcalorimetry

This ultrasensitive technique analyses the thermal parameters associated with binding process of t-RSV with SOD 1. The hydrogen bonds and van der Waals forces are the major driving forces behind these binding events.

At each injection of ligand into the sample having 1:1 stochiometry, an equilibrium of free and bound ligand is established, and heat is released (exothermic) as a binding event. At the end of the titration, all the binding sites in the sample are occupied and heat evolved become negligible.

Interaction of t-RSV and SOD1 at equilibrium is represented as:

$$SOD + t-RSV \leftrightarrow SOD : t-RSV \quad (3)$$

The enthalpy of binding per mole of drug (ΔH^o) can be calculated using the molar concentration of SOD1–t-RSV complex (c) in solution at equilibrium and experimentally observed enthalpy of interaction (ΔH_{exp}), by using Equation 4.

$$\Delta H_{exp} = \Delta H^o x\, c \quad (4)$$

Equilibrium constant for Equation 3 is calculated as

$$K = \frac{c}{(a-c)\ (b-c)} \quad (5)$$

where 'c' is the concentration of SOD–t-RSV complex; a and b corresponds to the concentrations of reactants, *i.e.*, SOD and t-RSV, respectively.

$$c = \frac{\left[A - \sqrt{(A^2 - 4ab)}\right]}{2} \quad (6)$$

where $A = a + b + \frac{1}{K}$

$$\Delta H_{cal} = \Delta H^o \times \frac{\left[A - \sqrt{(A^2 - 4ab)}\right]}{2} \quad (7)$$

The data assessment was executed with an assumption of one-site binding model. The binding constant (K_b)[1] and ΔH were calculated using a self-consistent iterative nonlinear least-square regression program to minimize the values of (ΔH_{exp}- ΔH_{cal}).[2]

Binding parameters such as enthalpy of binding (ΔH) and binding constant (K_b) were calculated (Table 2) and binding isotherm was thus generated from the computer program prepared by us as discussed under experimental section (Figure 3). Since temperature[1] is held constant throughout, the free energy (ΔG) of the binding reaction is determined following the Equation 2 and entropy is determined as follows:

$$\Delta G = \Delta H - T\Delta S \quad (8)$$

4 Discussion and Conclusions

Molecular docking g1ives us an insight of the preferred orientation and interaction paradigm of the drug molecule to the macromolecule. Microcalorimetry is an explicit technique to elucidate the thermodynamics of binding of a ligand to macromolecules. Both these

Table 1. Molecular docking parameters of t-RSV with SOD 1 using adrenaline as site

Docking Score	Type of interaction	Corresponding Bond length (A^o)
-5.966	(i)3O-H---O-C=O (GLU 100)	1.79
	(ii) 5O-H---O=C (PRO 28)	1.63
	(iii) (LYS 23)N-H---O-H (5)	1.97
	(iv) 4'Hydroxyphenyl ring---TRP 32 (pi-pi stacking)	-

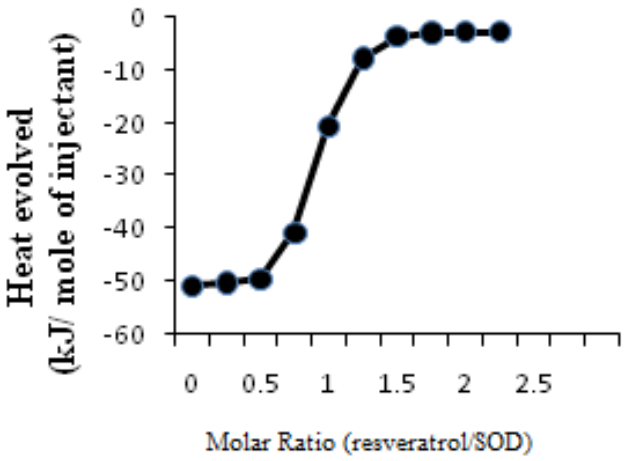

Figure 5. Binding isotherm of trans-resveratrol with SOD obtained from calorimetric measurements

methodologies work complementary to each other defining the binding criteria of t-RSV with SOD1 in the present study. Both the above mentioned results were found to complement each other with respect to binding affinity data as compiled in Table 2. The small variations in computational and experimental values may be attributed to the fact that docking was based upon the static and fixed X-ray crystal structure of protein where significant protein structural freedom is not allowed to acquire different conformations upon ligand binding.

Unlikely, the calorimetric results are based upon full freedom in the structural flexibility of the protein in phosphate buffer (pH 7.4).[37,38] Thus, structural rearrangements observed in the SOD that occurred upon ligand binding in solution, may be the plausible cause of this difference.

The negative values of free energy (ΔG) and enthalpy (ΔH) support that the binding of t-RSV to SOD is spontaneous and exothermic. The fairly good value of binding constant indicates good stability of t-RSV-SOD 1 complex. Thus binding strategy of t-RSV to SOD1 further supports the hypothesis of stabilization of SOD dimer and thus acts as an effective measure to prevent the occurrence of ALS.

Table 2. Binding parameters of t-RSV with SOD 1 obtained from docking analysis and calorimetric titrations

Binding parameter	Docking analysis (in silico study)	Calorimeteric titrations (in vitro study)
K_b (M^{-1})	9.9 x10 ^{4}	7.3x 10^4
ΔH ($kJmol^{-1}$)	-	-47.8
ΔG($kJmol^{-1}$)	-40.05	-39.17
ΔS($kJmol^{-1}K^{-1}$)	-	0.29

It has been concluded that the virtual and experimental aspects are working hand in glove with each other to figure out the binding events between the nutraceutical, t-RSV and the natural antioxidant, SOD1. The docking analysis and calorimetric results were found to complement each other in the present study. The significant magnitude of binding constant summarized in Table 2 revealed the strong binding affinity of t-RSV with ageing biomarker, SOD1. The present study is a beneficial step towards exploring the potential of ligands in stabilization of the antioxidant enzyme, SOD1 leading to control of the neurodegenerative disorders such as ALS. This information about the binding affinity and the interactions involved during complex formation of SOD1 with t-RSV would embolden future studies to postulate the various mechanisms of ageing and its control at molecular and cellular level. The knowledge generated from this study would be a favorable underpinning in the promising field of anti-ageing therapy and proteomics.

References

[1] Harikumar KB and Aggarwal BB. Resveratrol: a multitargeted agent for age-associated chronic diseases. Cell cycle, 2008, **7**(8): 1020-1035. https://doi.org/10.4161/cc.7.8.5740

[2] Valenzano DR, Terzibasi E, Genade T, *et al*. Resveratrol prolongs lifespan and retards the onset of age-related markers in a short-lived vertebrate. Current Biology, 2006, **16**(3): 296-300. https://doi.org/10.1016/j.cub.2005.12.038

[3] Baur JA, Pearson KJ, Price NL, *et al*. Resveratrol improves health and survival of mice on a high-calorie diet. Nature, 2006, **44**(7117): 337. https://doi.org/10.1038/nature05354

[4] Berrougui H, Grenier G, Loued S, *et al*. A new insight into resveratrol as an atheroprotective compound: inhibition of lipid peroxidation and enhancement of cholesterol efflux. Atherosclerosis, 2009, **207**(2): 420-427. https://doi.org/10.1016/j.atherosclerosis.2009.05.017

[5] Frankel EN, German JB, Kinsella JE, *et al*. Inhibition of oxidation of human low-density lipoprotein by phenolic substances in red wine. The Lancet, 1993, **341**(8843): 454-457. https://doi.org/10.1016/0140-6736(93)90206-V

[6] Kaindl U, Eyberg I, Rohr-Udilova N, *et al*. The dietary antioxidants resveratrol and quercetin protect cells from exogenous pro-oxidative damage. Food and chemical toxicology, 2008, **46**(4): 1320-1326. https://doi.org/10.1016/j.fct.2007.09.002

[7] Ndiaye M, Philippe C, Mukhtar H, *et al*. The grape antioxidant resveratrol for skin disorders: promise, prospects, and challenges. Archives of biochemistry and biophysics, 2011, 508(2): 164-170. https://doi.org/10.1016/j.abb.2010.12.030

[8] Udenigwe CC, Ramprasath VR, Aluko RE, *et al*. Potential of resveratrol in anticancer and anti-inflammatory therapy. Nutrition reviews, 2008, **66**(8): 445-454. https://doi.org/10.1111/j.1753-4887.2008.00076.x

[9] Robb EL, Winkelmolen L, Visanji N, *et al*. Dietary resveratrol administration increases MnSOD expression and activity in mouse brain. Biochemical and biophysical research communications, 2008, **372**(1): 254-259. https://doi.org/10.1016/j.bbrc.2008.05.028

[10] Flanagan SW, Anderson RD, Ross MA, *et al*. Overexpression of manganese superoxide dismutase attenuates neuronal death in human cells expressing mutant (G37R) Cu/Zn-superoxide dismutase. Journal of neurochemistry, 2002, **81**(1): 170-177. https://doi.org/10.1046/j.1471-4159.2002.00812.x

[11] Alscher RG, Erturk N and Heath LS. Role of superoxide dismutases (SODs) in controlling oxidative stress in plants. Journal of experimental botany, 2002, **53**(372): 1331-1341. https://doi.org/10.1093/jxb/53.372.1331

[12] Raychaudhuri SS and Deng XW. The role of superoxide dismutase in combating oxidative stress in higher plants. The Botanical Review, 2000, **66**(1): 89-98. https://doi.org/10.1007/BF02857783

[13] Simm A, Nass N, Bartling B, *et al*. Potential biomarkers of ageing. Biological chemistry, 2008, **389**(3): 257-265. https://doi.org/10.1515/BC.2008.034

[14] Krishna Sree V and Das S. Oxidative Stress and Antioxidant-The Link to Cancer Celebrating 60 years of excellence, **2014**: 38.

[15] Richardson J, Thomas KA, Rubin BH, *et al*. Crystal structure of bovine Cu, Zn superoxide dismutase at 3 A resolution: chain tracing and metal ligands. Proceedings of the National Academy of Sciences, 1975, **72**(4): 1349-1353. https://doi.org/10.1073/pnas.72.4.1349

[16] Forbes RB, Colville S and Swingler RJ. The epidemiology of amyotrophic lateral sclerosis (ALS/MND) in people aged 80 or over. Age and ageing, 2004, **33**(2): 131-134. https://doi.org/10.1093/ageing/afh013

[17] Wright GSA, Antonyuk SV, Kershaw NM, *et al*. Ligand binding and aggregation of pathogenic SOD1. Nature communications, 2013, **4**: 1758. https://doi.org/10.1038/ncomms2750

[18] Mitchell JD and Borasio GD. Amyotrophic lateral sclerosis. The Lancet, 2007, **369**(9578): 2031-2041. https://doi.org/10.1016/S0140-6736(07)60944-1

[19] Traynor BJ, Codd MB, Corr B, *et al*. Clinical features of amyotrophic lateral sclerosis according to the El Escorial and Airlie House diagnostic criteria: A population-based study. Archives of neurology, 2000, **57**(8): 1171-1176. https://doi.org/10.1001/archneur.57.8.1171

[20] Rosen DR, Siddique T, Patterson D, *et al*. Mutations in Cu/Zn superoxide dismutase gene are associated with familial amyotrophic lateral sclerosis. Nature, 1993, **362**(6415): 59. https://doi.org/10.1038/362059a0

[21] Logroscino G, Tortelli R, Rizzo G, *et al*. Amyotrophic lateral sclerosis: an aging-related disease. Current Geriatrics Reports, 2015, **4**(2): 142-153. https://doi.org/10.1007/s13670-015-0127-8

[22] Ganesalingam J and Bowser R. The application of biomarkers in clinical trials for motor neuron disease. Biomarkers in medicine, 2010, **4**(2): 281-297. https://doi.org/10.2217/bmm.09.71

[23] Ray SS, Nowak RJ, Brown RH, *et al*. Small-molecule-mediated stabilization of familial amyotrophic lateral sclerosis-linked superoxide dismutase mutants against unfolding and aggregation. Proceedings of the National Academy of Sciences, 2005, **102**(10): 3639-3644. https://doi.org/10.1073/pnas.0408277102

[24] Nowak RJ, Cuny GD, Choi S, *et al*. Improving binding specificity of pharmacological chaperones that target mutant superoxide dismutase-1 linked to familial amyotrophic lateral sclerosis using computational methods. Journal of medicinal chemistry, 2010, **5**3(7): 2709-2718. https://doi.org/10.1021/jm901062p

[25] Kelly GS. A review of the sirtuin system, its clinical implications, and the potential role of dietary activators like resveratrol: part 2. Alternative medicine review, 2010, **15**(3): 245-264.

[26] Feoktistov IA, Baldenkov GN, Barannik IV, *et al*. Interaction of calcium agonists and antagonists with Ca-binding proteins and their effect on cyclic nucleotide phosphodiesterase. Biokhimiia (Moscow, Russia), 1990, **55**(4): 754-759.

[27] Gertz M, Nguyen GTT, Fischer F, *et al*. A molecular mechanism for direct sirtuin activation by resveratrol. PloS one, 2012, **7**(11): e49761. https://doi.org/10.1371/journal.pone.0049761

[28] Agarwal B and Baur JA. Resveratrol and life extension. Annals of the New York Academy of Sciences, 2012, **1215**(1): 138-143. https://doi.org/10.1111/j.1749-6632.2010.05850.x

[29] Leavitt S and Freire E. Direct measurement of protein binding energetics by isothermal titration calorimetry. Current opinion in structural biology, 2001, **11**(5): 560-566. https://doi.org/10.1016/S0959-440X(00)00248-7

[30] Ghai R, Falconer RJ and Collins BM. Applications of isothermal titration calorimetry in pure and applied research-survey of the literature from 2010. Journal of Molecular Recognition, 2012, **25**(1): 32-52. https://doi.org/10.1002/jmr.1167

[31] Nunez S, Venhorst J and Kruse CG. Target-drug interactions: first principles and their application to drug discovery. Drug discovery today, 2012, **17**(1-2): 10-22. https://doi.org/10.1016/j.drudis.2011.06.013

[32] Release, Schrdinger. "2: Maestro, version 9.8; Schrdinger, LLC: New York, NY, USA, 2014. 36. Lew, JM; Kapopoulou, A.; Jones, LM; Cole, ST TubercuList10 years after" Tuberculosis (Edinb), 2011, **91**: 17.

[33] Yamali C, Gul HI, Ece A, *et al*. Synthesis, molecular modeling, and biological evaluation of 4-[5-aryl-3-(thiophen-2-yl)-4,5-dihydro-1H-pyrazol-1-yl] benzenesulfonamides toward acetylcholinesterase, carbonic anhydrase I and II enzymes. Chemical biology and drug design, 2017, **91**(4): 854-866. https://doi.org/10.1111/cbdd.13149

[34] Friesner RA, Murphy RB, Repasky MP, *et al*. Extra precision glide: Docking and scoring incorporating a model of hydrophobic enclosure for protein ligand complexes. Journal of medicinal chemistry, 2006, **49**(21): 6177-6196. https://doi.org/10.1021/jm051256o

[35] Halgren TA, Murphy RB, Friesner RA, *et al*. Glide: a new approach for rapid, accurate docking and scoring. 2. Enrichment factors in database screening. Journal of medicinal chemistry, 2004, **47**(7): 1750-1759. https://doi.org/10.1021/jm030644s

[36] Friesner RA, Banks JL, Murphy RB, *et al*. Glide: a new approach for rapid, accurate docking and scoring. 1. Method and assessment of docking accuracy. Journal of medicinal chemistry, 2004, **47**(7): 1739-1749. https://doi.org/10.1021/jm0306430

[37] Ahmad E, Rabbani G, Zaidi N, *et al*. Stereo-selectivity of human serum albumin to enantiomeric and isoelectronic pollutants dissected by spectroscopy, calorimetry and bioinformatics. PloS one, 2011, **6**(11): e26186. https://doi.org/10.1371/journal.pone.0026186

[38] Neelam S, Gokara M, Sudhamalla B, *et al*. Interaction studies of coumaroyltyramine with human serum albumin and its biological importance. The Journal of Physical Chemistry B,2010, **114**(8): 3005-3012. https://doi.org/10.1021/jp910156k

J Pharm Biopharm Res, 2019, 1(1): 28-35
DOI: 10.25082/JPBR.2019.01.004

RESEARCH ARTICLE

Spectroscopic study on the mechanism of meloxicam and α-amylase

Xu Cheng[1] Baosheng Liu[1*] Hongcai Zhang[1]

Abstract: In order to explore the mechanism of action of meloxicam and α-amylase. The interaction between the rheumatoid arthritis drug meloxicam and α-amylase was studied by fluorescence spectroscopy, synchronous fluorescence spectroscopy and molecular docking under the experimental conditions of pH=6.80. The results showed that meloxicam was able to effectively quench the endogenous fluorescence of α-amylase in a static quenching form a 1:1 complex and change the conformation of α-amylase. Thermodynamic results indicated that the main type of meloxicam and α-amylase system was hydrophobic interaction. Molecular docking indicated that the binding system had hydrogen bonds in addition to hydrophobic interaction and meloxicam was surrounded by the active amino acid residues Trp13 and Trp263 of α-amylase, which changed the microenvironment of amino acid residues at the active center of α-amylase. By establishing the binding model, it can be seen that the protein binding rate *W(B)* of meloxicam to -amylase was 2.76%-41.79% under the experimental conditions. The results showed that the binding of meloxicam to -amylase had an effect on the number of free -amylase. The drug binding rate *W(Q)* of the system was 2.76%-1.67%, which indicated that the combination of α-amylase and meloxicam would not affect the efficacy of meloxicam.

Keywords: drug, protein, fluorescence analysis, conformation, molecular docking, binding rate

1 Introduction

Non-steroidal anti-inflammatory drugs can relieve pain and edema to play a role in the treatment of inflammation, however, patients taking non-steroidal anti-inflammatory drugs often cause gastritis, gastric ulcer, kidney and liver damage and other adverse symptoms[1] . Meloxicam (MEL) is one of the non-steroidal anti-inflammatory drugs[2] whose molecular structure is shown in Figure 1. the toxic and side effects of MEL are much less than those of some other non-steroidal anti-inflammatory drugs (such as dotaline, ibuprofen, *etc*.). therefore. The adverse effect of MEL on gastrointestinal function was much smaller[3] . This drug is widely used in daily life and it is a very common drug for the treatment of rheumatoid arthritis. in addition to the treatment of inflammatory diseases, MEL also has a good effect on relieving physical pain in patients[4] .

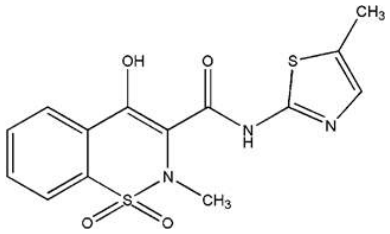

Figure 1. Chemical structure of MEL

α-Amylase (AMS) belongs to a famous group of enzymes, which hydrolyze starch molecules to give diverse products including dextrin and progressively smaller polymers composed of glucose units[5] . They can be found in the body of microorganisms, plants and all of the higher body organisms that use carbohydrates in their metabolism process. Thus, the amylases can be derived from several sources, including plants, animals and microorganisms; microbial enzymes generally meet industrial demands. Today a large number of microbial amylases are available commercially and they have almost completely replaced chemical hydrolysis of starch in starch processing industry[6] . Over the past few decades, considerable research has been under- taken with the extracellular AMS being produced by a wide variety of microorganisms[7] .

In recent years, fluorescence spectroscopy has become an important means to study the mechanism of ligand-

Received: April 2, 2019 **Accepted:** April 15, 2019 **Published:** April 17, 2019

*Correspondence to: Baosheng Liu, College of Chemistry & Environmental Science, Key Laboratory of Analytical Science and Technology of Hebei Province, National Chemistry Experimental Teaching Demonstration Center, Hebei University, Baoding 071002, China; Email: lbs@hbu.edu.cn

[1] College of Chemistry & Environmental Science, Key Laboratory of Analytical Science and Technology of Hebei Province, National Chemistry Experimental Teaching Demonstration Center, Hebei University, Baoding 071002, China.

Citation: Chen X, Liu B and Zhang H. Spectroscopic study on the mechanism of meloxicam and α-amylase. *J Pharm Biopharm Res*, 2019, **1**(1): 28-35.

protein system. So far, R. Omidyan[8] has studied the interaction between AMS and cetyltrimethylammonium bromide by spectroscopy, and He Qiang[9] has studied the interaction between AMS and tannic acid, a hypoglycemic drug, by spectroscopy. There are many reports on the interaction between small molecular drugs and AMS by spectroscopy. Most of the studies only focus on the binding mechanism of ligands and AMS. However, there are relatively few studies on the binding of AMS to drug molecules by spectroscopy, and then infer the effect of MEL on the efficacy and properties of AMS. In this paper, a series of experimental data were obtained by fluorescence experiments and molecular docking, which revealed the binding mechanism of the system and predicted the drug efficacy and enzyme properties of MEL combined with AMS in human body. The qualitative effect provides a useful reference for the rapid prediction of the interaction between drugs and proteins *in vivo*.

2 Experimental

2.1 Apparatus

RF-5301PC fluorometer (Shimadzu, Japan); UV-3600 UV-vis spectrophotometer (Shimadzu, Japan); SYC-15_Bsuper constant temperature water bath (Nanjing Sanli Electronic equipment Factory); SZ-93 automatic double Pure Water Distiller (Shanghai Yarong biochemical instrument Factory).

2.2 Materials

AMS (purity grade inferior 99%, Sigma), reserve solution (1.0×10^{-5} mol/L); MEL (CAS#,71125-28-7), reserve solution(4.0×10^{-4} mol/L), phosphate buffer solution of pH=6.80 was prepared. The water used in the experiment was secondary quartz distilled water, and the above storage solution was kept away from light at 277 K. The fluorescence signal measured in the experiment was corrected by the "internal filter effect" Equation 1 .[10]

$$F_{cor} = F_{obs} \times e^{(A_{ex}+A_{em})/2} \quad (1)$$

Where F_{cor} and F_{obs} are the corrected and observed fluorescence signals, respectively, and A_{ex} and A_{em} are the absorbance values of MEL-AMS system at excitation and emission wavelengths, respectively. The fluorescence signal used in this article was corrected.

2.3 Experiment procedure

2.3.1 Fluorescence experiment

At 298 K, 310 K and 318 K, 1.0 mL phosphate buffer solution, 2.0 mL AMS solution and different volume of MEL solution were added to the 10.0 mL colorimetric tube at constant volume and constant temperature of 30 min. The slit width was 5 nm, λ_{ex} and the scanning fluorescence spectra were 280, 295 nm, respectively. When $\Delta\lambda$=15 nm or 60 nm, scanning synchronous fluorescence spectroscopy.

2.3.2 UV-Vis measurements

At 298 K, 1.0 mL phosphate buffer solution, 2.0 mL AMS solution and different volume MEL solution was added to the 10.0 mL colorimetric tube at constant volume and constant temperature of 30 min. The absorbance of the system was determined by using the corresponding concentration of MEL solution as the blank reference, and the UV absorption spectrum of the system was drawn.

2.3.3 Molecular docking

The crystal structure (PDB ID: 1BLI of AMS comes from the protein database (Protein Data Bank). The ChemDraw Pro 14.0 and ChemBio 3D Ultra 14.0 are used to draw the MEL structure, and the energy minimization of the three-dimensional structure is carried out. AutoDock 4.2.6 was used to study the molecular docking of MEL and AMS, and genetic algorithm was used to calculate the binding conformation of MEL and AMS[11] .

3 Results and discussion

3.1 Fluorescence quenching mechanism studies of MEL-AMS system

The fluorescence effect of protein is produced by the chromophore of Trp, Tyr and Phe residues. The Trp and Tyr residues in protein are excited together at 280 nm wavelength, while at 295 nm wavelength, only Trp residue is excited[12] . Figure 2 showed the fluorescence spectra of the interaction between MEL and AMS (at λ_{ex}=295 nm, the fluorescence spectra of MEL and AMS are similar, but the fluorescence intensity is low). Figure 2 showed that the fluorescence peak of AMS at 343 nm quenched and the emission peak shifts blue with the increase of MEL concentration, indicating that the MEL-AMS system interacted and formed a stable complex.[13]

The Stern-Volmer[14] equation was shown below, through which the quenching constant K_{sv} and the quenching rate constant kq: can be calculated by using the fluorescence signal data obtained from the experiment:

$$F_0/F = 1 + k_q\tau_0[L] = 1 + K_{SV}[L] \quad (2)$$

Where F_0 and F represent the fluorescence signals in the absence and presence of quencher, respectively. τ_0 is the average lifetime of fluorescence without quencher,

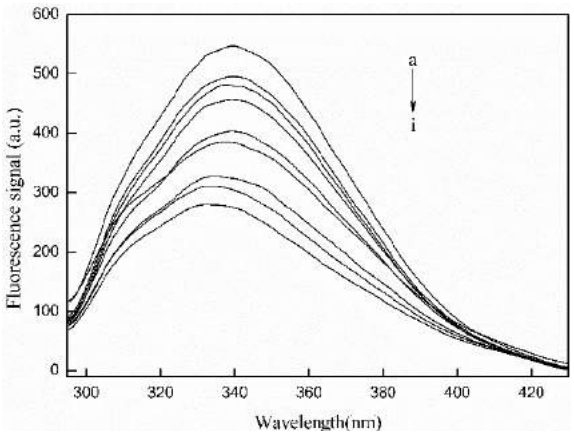

Figure 2. Fluorescence emission spectra of MEL-AMS system (T=310 K, λ_{ex}=280 nm), C_{AMS}=2.0×10^{-6} mol/L, a-i C_{MEL}=(0, 0.2, 0.5, 1.0, 1.5, 2.0, 3.0, 4.0, 5.0)×10^{-5}mol/L

which is about 10^{-8} s. K_{sv} is the Stern-Volmer quenching constant. k_q is the bimolecular quenching constant, and [L] is the concentration of meloxicam. The results were shown in Table 1. The results showed that the k_q values at different temperatures are larger than the maximum diffusion collision quenching constant of 2 × 10^{10} L/mol·s[15] for biomolecules by various quenching agents. at the same time, it can be seen from the data in Table 1 that with the increase of temperature, k_q of MEL-AMS system and K_{sv}'s. The results showed that the quenching mode of MEL-AMS system is static quenching.

For static quenching, the Equation 3[16] is generally used to calculate the binding constant K_a and the number of binding sites n:

$$\lg\left(\frac{F_0-F}{F}\right)=n\lg K_a+n\lg\left\{[L]-n\frac{F_0-F}{F_0}[B_t]\right\} \quad (3)$$

[B$_t$] represents the concentration of AMS, and the results were shown in Table 1. From Table 1, n ≈ 1 at the experimental temperature indicates that there is only one high affinity binding site[17] for MEL to bind to AMS, that is, MEL forms a 1:1 complex with AMS. The binding constant K_a of MEL to AMS decreased with the increased of temperature, which further proved that the fluorescence quenching type of MEL-AMS system was static quenching. Figure 3 showed the participation of Tyr residues and Trp residues of AMS in MEL-AMS system. The results showed that when λ_{ex}=280 nm and λ_{ex}=295 nm, the quenching curve of MEL-AMS system was separated. This indicated that both Tyr residues and Trp residues in AMS participated in the reaction. However, the slope of the quenching curve of MEL-AMS system at λ_{ex}=295 nm was obviously smaller than that of the binding system at λ_{ex}=280 nm, which indicated that the fluorescence quenching degree of AMS was stronger at λ_{ex}=280 nm.

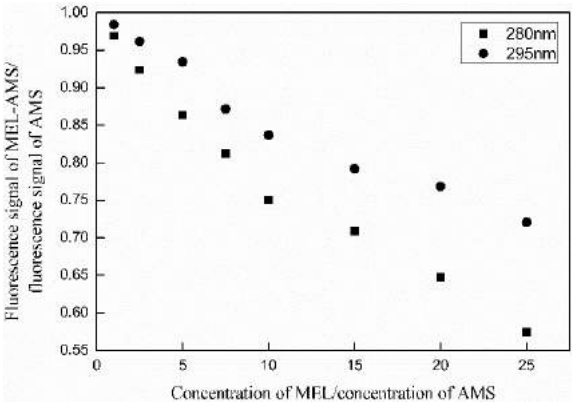

Figure 3. Relative fluorescence curves of the interaction between MEL and AMS (T = 310 K); C_{AMS}=2.0×10^{-6} mol/L, C_{MEL}=(0.2, 0.5, 1.0, 1.5, 2.0, 3.0, 4.0, 5.0)×10^{-5}mol/L

3.2 Type of interaction force of MEL-AMS system

The thermodynamic parameters of MEL-AMS system are calculated according to van't Hoff equation[18] , and the calculated results were shown in Table 2.

$$R\ln K=\Delta S-\Delta H/T \quad (4)$$

$$\Delta G=-RT\ln K=\Delta H-T\Delta S \quad (5)$$

Where R is a gas constant (ΔH and ΔS with a value of about 8.314), MEL and AMS could be calculated by a linear relationship between the natural logarithm (lnK_a) of the binding constant and the reciprocal (1/T) of the temperature. The results were shown in Table 2. It could be seen from Table 2 that ΔG<0 indicated that the binding reaction between MEL and AMS was spontaneous, and ΔH<0 indicated that the formation of MEL-AMS complex was exothermic. The arrangement of water molecules creates a more random configuration around drugs and proteins in a more orderly manner. Therefore, $\Delta S > 0$ is usually used as evidence of hydrophobic interaction between drug molecules and protein molecules[19] . Based on this, the hydrophobic interaction between MEL and AMS could be judged.

Ross and Subramanian[20] believed that when $\Delta H\approx$ 0, ΔS>0, there was electrostatic attraction between drug molecules and biomolecules, but now some reports thought that when ΔH<0, ΔS>0 could directly judge that the main type of force between the binding systems is electrostatic interaction[21] . In order to further verify whether the main force between MEL and AMS is elec-

Table 1. Quenching reactive parameters of MEL-AMS system at different temperatures

λ_{ex} (nm)	T/(K)	K_{sv} (L/mol·s)	k_q (L/mol)	r_1	K_a (L/mol)	n	r_2
	298	1.70×10^4	1.70×10^{12}	0.9932	1.81×10^4	1.03	0.9922
$\lambda_{ex=}$ 280	310	1.38×10^4	1.38×10^{12}	0.9939	1.46×10^4	0.96	0.9969
	318	1.13×10^4	1.13×10^{12}	0.9957	1.17×10^4	0.98	0.9956
	298	1.36×10^4	1.36×10^{12}	0.9938	1.43×10^4	1.06	0.9942
$\lambda_{ex=}$ 295	310	1.12×10^4	1.12×10^{12}	0.9965	1.08×10^4	0.99	0.9969
	318	0.91×10^4	0.91×10^{12}	0.9974	0.88×10^4	1.02	0.9915

Note: r_1 is the linear relative coefficient of F0/F~[L];

r_2 is the linear relative coefficient of lg[(F0-F)/]~lg{[L]-n[Bt](F0-F)/F0}

trostatic force, the effect of ionic strength on MEL-AMS interaction is discussed in this paper.

Fix the concentration of MEL and AMS, add different concentrations of NaCl, to F/F_0 to map C_{NaCl}, the results were shown in Figure 4. The experimental results showed that when the concentration of NaCl increased, the ratio of F/F_0 did not change significantly. The results showed that the binding of MEL to AMS was not affected by ionic strength, that was, the electrostatic interaction of MEL-AMS system was not obvious. If the electrostatic interaction played a leading role in the binding of protein to ligands, with the concentration of salt in the system. With the increased of the interaction intensity between protein and ligand, the interaction intensity between protein and ligand decreased gradually[22] . This also indicated that when $\Delta H<0$, $\Delta S>0$ could not directly judge the main force between MEL-AMS system was electrostatic force.

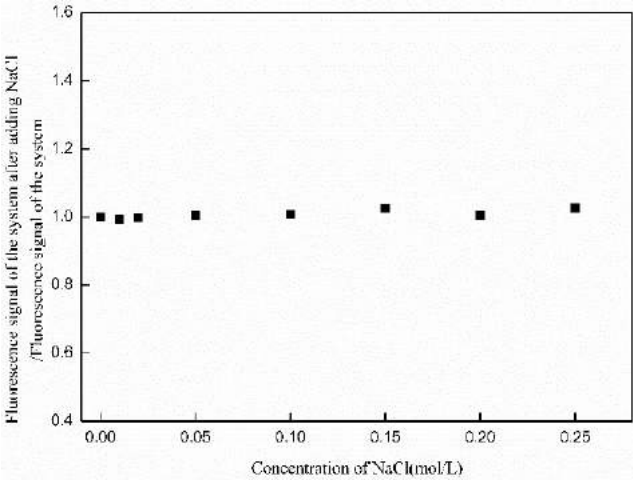

Figure 4. Fluorescence intensity of MEL-AMS system as a function of NaCl concentration (T=298 K); C_{AMS} =2.0×10^{-6} mol/L, C_{MEL}= 2.0×10^{-5}mol/L, C_{Nacl}= (0, 0.1, 0.2, 0.5, 1.0, 1.5, 2.0, 2.5, 3.0) $\times10^{-1}$mol/L

3.3 Conformation studies of MEL-AMS system

3.3.1 Synchronous fluorescence studies of MEL-AMS system

By measuring the shift of the maximum emission wavelength of the synchronous fluorescence spectrum of the binding system, the environmental information of amino acid residues near the fluorescent luminescence group can be explored[23] . As shown in Figure 5, when $\Delta\lambda$=60 nm and $\Delta\lambda$ =15 nm, the intensity of the fluorescence signal of the AMS tended to decrease, and the fluorescence peaks of both the Trp residue and the Tyr residue shifted very slightly, this means that the binding of MEL to AMS changes the microenvironment of amino acid residues in small molecular proteins such as AMS, reducing its hydrophobicity. The extension of peptide chain increased[24] and Tyr and Trp residues were involved in the binding reaction. This result was consistent with conclusion 3.1.

Table 2. The thermodynamic parameters of MEL-AMS at different temperatures

System	T/(K)	K_a /(L/mol)	ΔH/(kJ/mol)	ΔS/(J/mol·K)	ΔG/(kJ/mol)
$\lambda_{ex=}$	298	1.81×10^4		24.49	-24.29
	310	1.46×10^4		24.74	-24.66
280 nm	318	1.17×10^4	-16.99	24.45	-24.77

3.3.2 UV-vis absorption spectra studies of MEL-AMS system

UV-vis absorption spectra can be used to explore the structural changes of proteins and to study the formation of protein-ligand complexes[25] . Figure 6 was an ab-

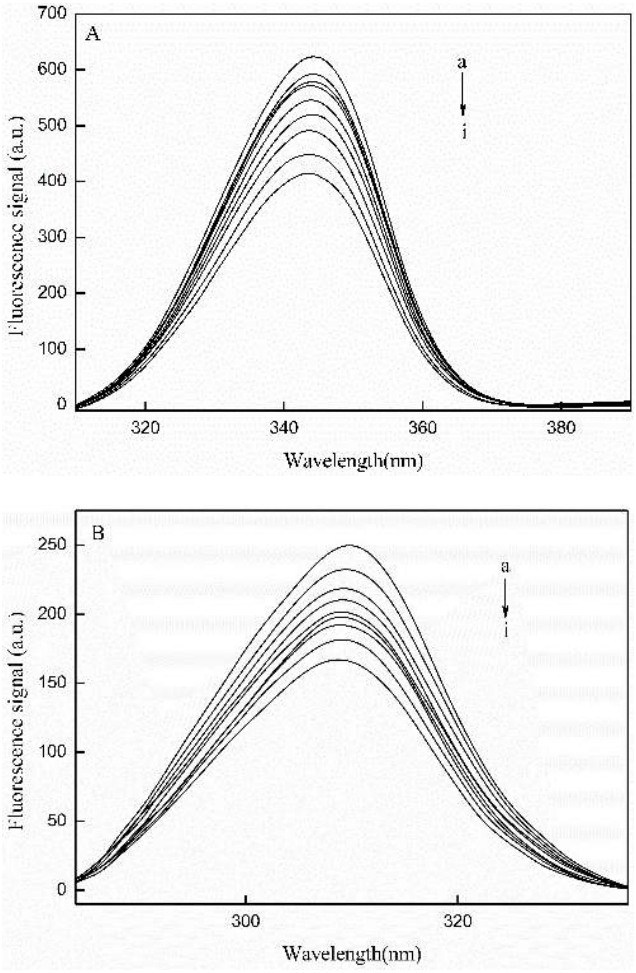

Figure 5. Synchronous fluorescence spectra of MEL-AMS system (T=310 K). (A) $\Delta\lambda$=60 nm; (B) $\Delta\lambda$=15nm; C_{AMS}=2.0×10^{-6} mol/L, a-i C_{MEL}=(0, 0.2, 0.5, 1.0, 1.5, 2.0, 3.0, 4.0, 5.0)×10^{-5}mol/L

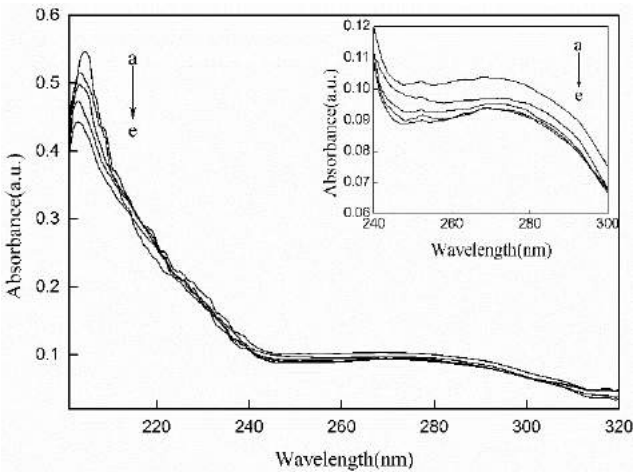

Figure 6. Fluorescence intensity of MEL-AMS system as a function of NaCl concentration (Absorption spectra of MEL-AMS system (T=298 K); C_{AMS}=2.0×10^{-6} mol/L, a-e C_{MEL}= (0, 0.2, 0.5, 1.0, 2.0)×10^{-5}mol/L

sorption spectrum of the MEL-AMS system. from the figure, it could be seen that AMS has two absorption peaks, and its strong absorption peak near 208 nm reflected the frame conformation of the protein. The weak absorption peak at about 280 nm was due to aromatic amino acids (Trp, Tyr and Phe)[26] . With the increased of MEL concentration, Figure 6 showed that the intensity of the absorption peak at 208nm decreased with the blue shifted, and the absorption peak at 280nm also decreased slightly. This result indicated that the interaction between MEL and AMS led to the formation of new complexes, and the AMS molecule tends to fold, the hydrophobicity of AMS microenvironment was enhanced.

3.4 Molecular docking

Molecular docking plays an important role in exploring the interaction between ligands and receptors. In order to further determine the binding position of MEL-AMS system and the effect of MEL binding to AMS on ligands and receptors. In this paper, the binding model of MEL and AMS was established by molecular docking method. By this method, the type of force and the lowest binding energy of MEL and AMS binding system could be obtained. Figure 7(A) showed the optimal binding position after MEL binds to AMS, the Asp328 residue forms two hydrogen bonds with MEL with bond lengths of 2.138 $\mathring{A}$ and 2.144 $\mathring{A}$ respectively, and the His253 residue formed a hydrogen bond with MEL. The bond length is 1.791 $\mathring{A}$, which showed that the hydrogen bond played an important role in the binding of MEL to AMS. Figure 7(B) showed a plurality of hydrophobic amino acid residues such as Ala232, Tyr262, Trp13, Trp263, Leu196, Leu335 and Val233 around MEL, further indicated that there was hydrophobic force in the binding process between MEL and AMS. The amino acid residues such as Tyr262, Trp13 and Trp263 were relatively close to the binding position of MEL and AMS, which led to the binding could effectively quench the endogenous fluorescence of AMS, which was consistent with the conclusion of fluorescence quenching experiment. Trp13 and Trp263 were the key residues of the catalytic active center of AMS[27] . The results of molecular docking also showed that the binding of MEL and AMS could change the microenvironment of the catalytic active center of AMS. In other words, the binding of the system might affect the catalytic activity of AMS.

The binding energy obtained from molecular docking for MEL and AMS interaction was -25.89 kJ/mol. Whereas, the free energy change calculated from fluorescence quenching results was -24.66 kJ/mol at 310 K.

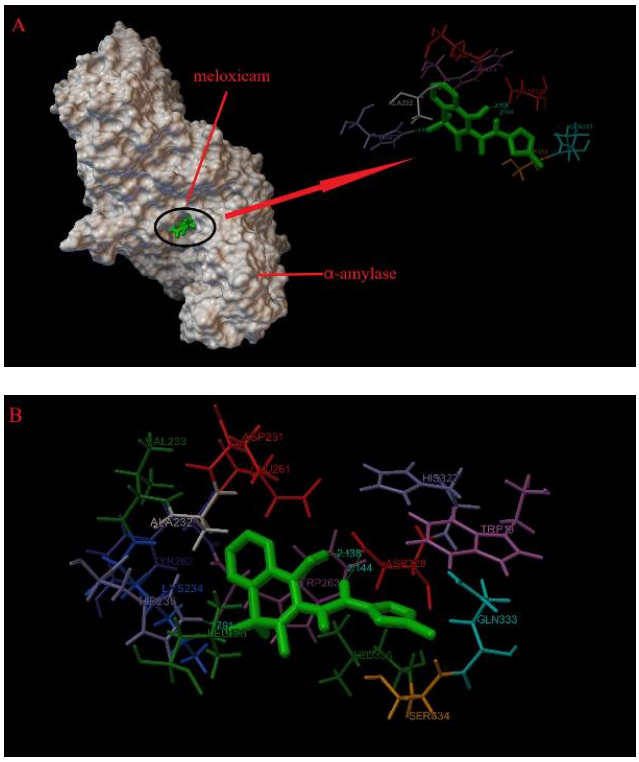

Figure 7. Theoretical Modeling of the Interaction between MEL and AMS; (A) MEL located within the hydrophobic pocket in AMS; (B) Detailed illustration of the amino acid residues lining the binding site in the MEL and AMS cavity

This difference may be due to exclusion of the solvent in docking simulations or rigidity of the receptor other than Trp and Tyr residues[28] . The energy data obtained by docking the molecules were listed in Table 3. From Table 3, it could be also seen that the electrostatic energy was very much lower than the sum of van der Waals energy, hydrogen bonding energy and desolvation free energy in the binding process of MEL with AMS, indicating that the main interaction mode between MEL and AMS was not electrostatic binding mode.Combined with the data of fluorescence experiments and the results of theoretical modeling, it could be seen that hydrophobic interaction and hydrogen bond were the main forces driving the combination of MEL molecules with AMS molecules, which led to the static quenching of AMS.

3.5 MEL-AMS system binding rate

The study of protein binding rate and drug binding rate of drug-protein system is helpful to further study the interaction between drug molecules and protein molecules, so that drug molecules can bind to some proteins in human body. After action, a simple prediction can be made of the efficacy of the drug, the properties and effects of the protein itself, and the effects on the physiological function of the human body. According to the fluorescence experiment of K_a, the drug binding rate and protein binding rate of MEL to AMS can be calculated. When n=1, the binding rate (W) formula of MEL-AMS system was as follows[29] .

Table 3. Docking energy of MEL-AMS system (unit: kJ/mol)

Protein PDB ID	ΔG_0	ΔE_1	ΔE_2	ΔE_3
1BLI	-25.89	-29.65	-28.81	-0.84

ΔG_0 is the binding energy in the binding process.
ΔE_1 denotes intermolecular interaction energy, which is a sum of van der Waals energy, hydrogen bonding energy, desolvation free energy and electrostatic energy.
ΔE_2 is the sum of van der Waals energy, hydrogen bonding energy and desolvation free energy.
ΔE_3 is the electrostatic energy.

Drug binding rate:

$$W(Q) = \frac{x}{Q} \times 100\% = \frac{K_a(Q+B)+1-\sqrt{K_a^2(Q-B)^2+2K_a(Q+B)+1}}{2K_aQ} \times 100\% \quad (6)$$

Protein binding rate:

$$W(B) = \frac{x}{B} \times 100\% = \frac{K_a(Q+B)+1-\sqrt{K_a^2(Q-B)^2+2K_a(Q+B)+1}}{2K_aB} \times 100\% \quad (7)$$

Wherein Q represents the total concentration of MEL and B represents the total concentration of AMS. At the three temperatures of 298K, 310K and 318K, the drug binding rate $W(Q)$ of MEL and AMS calculated according to formulas (6) and (7) was 3.38%-1.88% (298K), 2.76%-1.67% (310K), 2.24%-1.46% (318K), protein binding rate $W(B)$ was 3.38%-47.03% (298K), 2.76%-41.79% (310K), 2.24%˜36.57% (318K). At three temperatures, the drug binding rate and protein binding rate of MEL to AMS decreased with the increase of temperature, and the content of free drugs and proteins increased with the increase of temperature, which indicated that the stability of the binding system decreased with the increase of temperature. The results were consistent with the experimental results of fluorescence quenching.

The ratios of $W(Q)$ and $W(B)$ to drug concentration and protein concentration were plotted, respectively, as shown in Figure 8. It could be seen from Figure 8 that the $W(Q)$ value decreased with the increased of temperature, while the $W(B)$ value was large and increased. Taking 310K data close to human body temperature as an example: The $W(Q)$ of MEL and AMS was 2.76%-1.67%, which indicated that the interaction between MEL and AMS had little effect on the efficacy of MEL as the

amount of MEL added increases. The $W(B)$ of MEL and AMS was 2.76%-41.79%, which indicated that the protein binding rate varies greatly with the increase of MEL addition. Combined with the results of 3.4, MEL might have an effect on the activity of AMS, which was not conducive to the digestion and absorption of starchy substances. Therefore, the intake of drugs should be strictly controlled when taking MEL, so as to reduce the adverse effects of drugs on the digestive system.

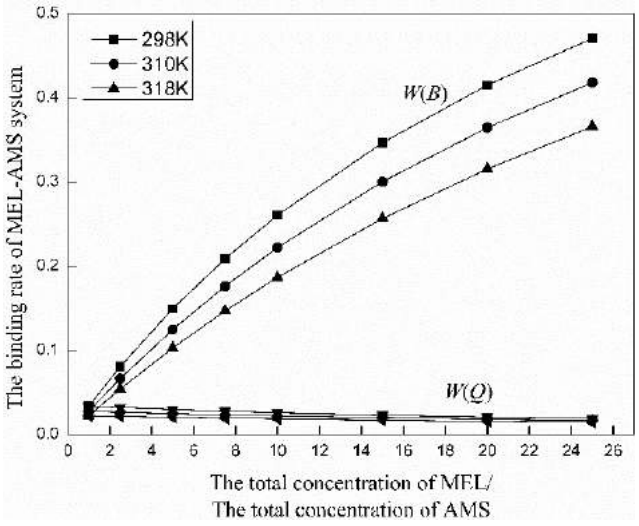

Figure 8. The binding rate of MEL to protein in different temperature and the binding rate of AMS to drug (λ_{ex}=280 nm)

4 Conclusion

In this paper, the interaction between MEL and AMS was studied by spectroscopic and theoretical modeling under simulated physiological conditions. The binding rate model of MEL and AMS was established. the interaction between MEL and AMS was used to treat drugs. The effects of AMS on the digestive function of starches were simply predicted. It provides a new idea to study the effect of the interaction between protein molecules and small drug molecules on the properties of proteins and the efficacy of drugs. The binding rate of ligand-protein system is studied by spectroscopy. Compared with other methods such as equilibrium dialysis, there will be some errors in the binding constant and the number of binding sites, but these commonly used binding rates are studied. The experimental equipment of the method is expensive, the experimental period is long and the concentration range of the experimental drug is narrow. However, the method of studying the binding rate by spectroscopy is simple, rapid and suitable for a wide range of applications, so this method is preferable.

References

[1] Franze JA, Carvalho TF, Galieri C, *et al*. Synthesis, characterization, thermal and spectroscopic studies and bioactivity of complexes of meloxicam with some bivalent transition metals. Journal of Thermal Analysis & Calorimetry, 2017, **127**(2): 1393-1405. http://doi.org/10.1007/s10973-016-6030-5

[2] Sayen S, Carlier A, Tarpin M, *et al*. A novel copper (II) mononuclear complex with the non-steroidal anti-inflammatory drug diclofenac: structural characterization and biological activity. Journal of Inorganic Biochemistry, 2013, **120**(3): 39-43. http://doi.org/10.1016/j.jinorgbio.2012.12.002

[3] Shantiaee Y, Javaheri S, Movahhedian A, *et al*. Efficacy of preoperative ibuprofen and meloxicam on the success rate of inferior alveolar nerve block for teeth with irreversible pulpitis. International Dental Journal, 2017, **67**(2): 85-90. http://doi.org/10.1111/idj.12272

[4] Ebrahimi M, Khayamian T, Hadadzadeh H, *et al*. Spectroscopic, biological, and molecular modeling studies on the interactions of [Fe (III)-meloxicam] with G-quadruplex DNA and investigation of its release from bovine serum albumin (BSA) nanoparticles. Journal of Biomolecular Structure and Dynamics, 2015, **33**(11): 2316-2329. http://doi.org/10.1080/07391102.2014.1003195

[5] Park KH, Kim TJ, Cheong TK, *et al*. Structure, specificity and function of cyclomaltodextrinase, a multispecific enzyme of the α-amylase family. Biochimica Et Biophysica Acta, 2000, **1478**(2): 165-185. http://doi.org/10.1016/S0167-4838(00)00041-8

[6] Pandey A, Nigam P, Soccol CR, *et al*. Advances in Microbial Amylases. Biotechnology and Applied Biochemistry, 2000, **31**(2): 135-152. http://doi.org/10.1042/BA19990073

[7] Gupta R, Gigras P, Mohapatra H, *et al*. Microbial α-amylases: a biotechnological perspective. Process Biochemistry, 2003, **38**(11): 1599-1616. http://doi.org/10.1016/S0032-9592(03)00053-0

[8] Omidyan R, Kazemi SH, Bordbar AK, *et al*. Spectroscopic study on the interaction of Bacillus subtilis α-amylase with cetyltrimethylammonium bromide. Journal of Luminescence, 2011, **131**(6): 1229-1233. http://doi.org/10.1016/j.jlumin.2011.02.001

[9] Lin FY and Qiang HE. Interaction between tannic acid and pancreatic α-amylase. Science & Technology of Food Industry, 2014, **35**(3): 63-66. http://doi.org/10.13386/j.issn1002-0306.2014.03.040

[10] Rakotoarivelo NV, Perio P, Najahi E, *et al*. Interaction between Antimalarial 2-Aryl-3H-indol-3-one Derivatives and Human Serum Albumin. The Journal of Physical Chemistry B, 2014, **118**: 13477-13485. http://doi.org/10.1021/jp507569e

[11] Elmas G and Esra Y. Fluorescence interaction and determination of sulfathiazole with trypsin. Journal of Fluorescence, 2014, **24**(5): 1439-1445. http://doi.org/10.1007/s10895-014-1427-7

[12] Zhang LH, Liu BS, Li ZY, *et al*. Comparative studies on the interaction of cefixime with bovine serum albumin by

fluorescence quenching spectroscopy and synchronous fluorescence spectroscopy. Asian Journal of Chemistry, 2015, **30**(5): 686-692.
http://doi.org/10.1002/bio.2805

[13] Mahaki H, Memarpoor-Yazdi M, Chamani J, *et al.* Interaction between ropinirole hydrochloride and aspirin with human serum albumin as binary and ternary systems by multi-spectroscopic, molecular modeling and zeta potential. Journal of Luminescence, 2013, **134**(3): 758-771.
http://doi.org/10.1016/j.jlumin.2012.06.051

[14] Safarnejad A, Shaghaghi M, Dehghan G, *et al.* Binding of carvedilol to serum albumins investigated by multi-spectroscopic and molecular modeling methods. Journal of Luminescence, 2016, **176**: 149-158.
http://doi.org/10.1016/j.jlumin.2016.02.001

[15] Moeiopour F, Mohseni-Shari FS, Malaekeh-Nikouei B, *et al*. Investigation into the interaction of losartan with human serum albumin and glycated human serum albumin by spectroscopic and molecular dynamics simulation techniques: acomparison study. Chemico-Biological Interactions, 2016, **257**: 4-13.
http://doi.org/10.1016/j.cbi.2016.07.025

[16] Cao SN, Liu BS, Li ZY, *et al.* A fluorescence spectroscopic study of the interaction between glipizide and bovine serum albumin and its analytical application. Journal of Luminescence,2014, **145**(31): 94-99.
http://doi.org/10.1016/j.jlumin.2013.07.026

[17] Amroabadi MK, Taheri-Kafrani A, Saremi LH, *et al*. Spectroscopic Studies of the interaction between alprazolam and apo-human serum transferrin as a drug carrier protein. International Journal of Biological Macromolecules, 2017, **108**: 263-271.
http://doi.org/10.1016/j.ijbiomac.2017.11.179

[18] Hu Y, Yang Y, Dai C, *et al*. Site-Selective Binding of human serum albumin by palmatine: spectroscopic approach. Biomacromolecules, 2010, **11**(1): 106-112.
http://doi.org/10.1021/bm900961e

[19] Abdus-Salam M, Rokonujjaman M, Rahman A, *et al.* Study of in Vitro Interaction of Sildenafil Citrate with Bovine Serum Albumin by Fluorescence Spectroscopy. Pharmacology & Pharmacy, 2015, **6**(2): 94-101.
http://doi.org/10.4236/pp.2015.62012

[20] Ross PD and Subramanian S. Thermodynamics of protein association reactions: forces contributing to stability. Biochemistry, 1981, **20**(11): 3096-3102.
http://doi.org/10.1021/bi00514a017

[21] Ma X, Song B, Xiao W, *et al*. Study on Interaction between Alliin and Bovine and Hunman Serum Albumin with Spectrometry. Spectroscopy and Spectral Analysis, 2017, **37**(6): 1826-1830.
http://doi.org/j.issn.1000-0593(2017)06-1826-05

[22] Zhou HF, Bi SY, Wang Y, *et al*. Characterization of the binding of paylean and DNA by fluorescence, UV spectroscopy and molecular docking techniques. Luminescence, 2016, **1**(4): 1013-1019.
http://doi.org/10.1002/bio.3066

[23] Buddanavar AT and Nandibewoor ST. Multi-spectroscopic characterization of bovine serum albumin upon interaction with atomoxetine. Journal of Pharmaceutical Analysis, 2017, **7**(3): 148-155.
http://dx.doi.org/10.1016/j.jpha.2016.10.001

[24] Xu CB, Gu JL, Ma XP, *et al*. Investigation on the interaction of pyrene with bovine serum albumin using spectroscopic methods. Pectrochimica Acta Part A-Molecular and Biomolecular Spectroscopy, 2014, **125**(9): 391-395.
http://doi.org/10.1016/j.saa.2014.01.132

[25] Chi ZX and Liu RT. Phenotypic Characterization of the Binding of Tetracycline to Human Serum Albumin. Biomacromolecules, 2011, **12**(1): 203-209.
http://doi.org/10.1021/bm1011568

[26] Hu XX, Yu ZH and Liu RT. Spectroscopic investigations on the interactions between isopropanol and trypsin at molecular level. Spectrochim Acta A Mol Biomol Spectrosc, 2013, **108**: 50-54.
http://doi.org/10.1016/j.saa.2013.01.072

[27] Najafian M, Ebrahim-Habibi A, Hezareh N, *et al*. Transchalcone: A novel small molecule inhibitor of mammalian alpha-amylase. Molecular Biology Reports, 2011, **38**(3): 1617-1620.
http://doi.org/10.1007/s11033-010-0271-3

[28] Jana S, Dalapati S, Ghosh S, *et al*. Study of microheterogeneous environment of protein human serum albumin by an extrinsic fluorescent reporter: a spectroscopic study in combination with molecular docking and molecular dynamics simulation. Journal of Photochemistry & Photobiology B Biology, 2012, **112**(231): 48-58.
http://doi.org/10.1016/j.jphotobiol.2012.04.007

[29] Ma LH, Liu BS, Wang CD, *et al*. The interaction mechanism of nifedipine and pepsin. Monatshefte für Chemie-Chemical Monthly, 2018, **149**(11): 2123-2130.
http://doi.org/10.1007/s00706-018-2269-9

J Pharm Biopharm Res, 2019, 1(1): 36-47
DOI: 10.25082/JPBR.2019.01.005

REVIEW

SeDeM Expert System: A review and new perspectives

Mingxian Gu[1] Tianbing Guan[1*] Shulin Wan[1] Han Zhang[1] Xuelian Li[1]
Songtao Kong[1] Jianbing Ren[1,3] Huimin Sun[2*] Chuanyun Dai[1*]

Abstract: The SeDeM Expert System was first known as a galenic pre-formulation system, which was based on the experimental research and quantitative determination of powdered substances. And the mathematical formula provided by the SeDeM Expert System has plays an important role in the study of powder properties. The system can be used not only to evaluate the powder direct compression (DC) of excipients and active pharmaceutical ingredients (API's), but also to predict the possible formulations, so it can reduce unnecessary research and trials, and shorten the time of development. In this paper, the research development and application of SeDeM Expert System in DC was summarized, and the results showed that with a few exceptions, the system was skilled in predicting acceptable tablet formulations. Finally, the new application prospect of the system is presented, including the application of the Internet traffic and content management (iTCM) database and the new co-processed excipients.

Keywords: SeDeM Expert System, radar graph, powder, direct compression, pre-formulation, co-processed

1 Introduction

Because of its simple process, convenience for the patient, accurate dose administration, and better stability than other dosage forms, tablet has become the most prevalent oral dosage forms in clinics. The primary manufacturing techniques of tablet are dry-granulation, wet-granulation and direct compression (DC) of dry powders. Over the past few decades, wet-granulation was widely used in pharmaceutical industry because of that the products of wet granulation have many advantages, such as beautiful appearance, good fluidity, strong wear resistance and good compression formability, even though it takes a long time and have high cost. Due to the emergence of various new excipients, the production of tablets is now changing to DC and high-speed production,[1] and compared with traditional wet-granulation process, DC can effectively avoid the granulation process, reduce the order of production, shorten the period of production and increase the rate of bioavailability.

There is no doubt that in the solid tablet manufacturing, DC is the best ones. However, DC is not applicable to all of the material tableting. Since DC is a process that does not pass through the granulation and the powder is directly mixed, it is possible to have a material that is not suitable for tableting, or the mixing is not uniform, which will seriously hinder the process of DC,[2] and what's more, it will make it difficult for the tablets to be produced. All of these are the basic reasons why DC is not widely used. In order for DC to be used more widely, the SeDeM Expert System was proposed in 2005 by Suñé Negre, *et al*.[3]

SeDeM Expert System known as "Sediment delivery model", it's an innovative tool developed by the University of Barcelona to characterize the powder, and it has been widely used in many preparation experiments and has proved to be powerful. The final result of the system is presented by SeDeM diagram. The dimension, compressibility, flow ability/powder flow, lubricity/stability, lubricity/dosage dose and so on, provided by SeDeM diagram, can be used to characterize the physical properties of the powder, including pressure, and the like.[4] According to the SeDeM diagram, it can intuitively indicate whether a substance is suitable for DC, and through the formula provided by SeDeM Expert System, it can get the minimum number of excipients needed for API's. SeDeM Expert System can be combined with prescription design effectively, which is of practical significance

Received: April 4, 2019 **Accepted:** April 22, 2019 **Published:** April 24, 2019

*Correspondence to: Chuanyun Dai, Chongqing University of Science and Technology, Chongqing 401331, China; Email: cydai@cqust.edu.cn; Huimin Sun, National Institutes for Food and Drug Control, Beijing 100050, China; Email: sunhm@126.com
[1] Chongqing University of Science and Technology, Chongqing 401331, China
[2] National Institutes for Food and Drug Control, Beijing 100050, China
[3] Chongqing LIYUN Nozzle Co., Ltd., Chongqing 401332, China

Citation: Gu M, Guan T, Wan S, *et al*. SeDeM Expert System: A review and new perspectives. *J Pharm Biopharm Res*, 2019, **1**(1): 36-47.

to reduce the cost of drug development and improve the final quality of the product.

As the summary of SeDeM Expert System in 2005 to 2019, most of them have reviewed the principle of SeDeM Diagram and SeDeM-ODT, but few have reviewed the research progress and application of SeDeM or SeDeM-ODT Expert System. In this paper, the research mainly development of SeDeM Expert System and its application in DC was summarized, and the new application prospect of SeDeM Expert System was presented, including the application of new co-processed excipients.

2 Development of SeDeM Expert System

The SeDeM Expert System was first proposed in 2005,[3] and it is mainly used to characterize the properties of powders to help pre-preparation determine the appropriate production process and whether it is suitable for direct pressing.[5] From the relevant literature, we can see that before 2012, SeDeM Expert System did not get much attention. However, with the maturation of DC technology, SeDeM Expert System has been widely used since 2012. With the development of SeDeM Expert System, it plays a more and more important role in the study of different powder properties and the design of direct tablet formulation. At the same time, improving and increasing the indicators of the system, make the results be more accurate and applicable.

2.1 Initial SeDeM Expert System

2.1.1 The main parameters

The initial SeDeM Expert System is mainly used to evaluate the direct compression properties of powders, and its main parameters are mostly related to the properties of powders. The system is consists of 5 primary indexes, and they are considered as the following:

- Dimension
- Compressibility
- Flow ability/Powder flow
- Lubricity/Stability
- Lubricity/Dosage

At the same time, the above 5 primary indexes are composed of 12 second-level indicators. Referring to the study of the European Pharmacopoeia and the research of Suñé Negre, *et al.*, the 12 second-level indicators were studied, and the results of these powder tests were treated with the equation shown in Table 1.[3] The results in Table 1 are standardized in accordance with the calculation method in Table 2, and the resulting data are used to draw the radar map (SeDeM Diagram), as shown in Figure 1. The SeDeM Diagram intuitively shows the 12 second-level indicators of the powder, and combines the calculation formula to determine whether the powder is suitable for DC. The 12 second-level indicators are considered as the following:

- Bulk density (Da)
- Tapped density (Dc)
- Carr index (IC)
- Inter-particle porosity (Ie)
- Cohesion index (Icd)
- Angle of repose (α)
- Hausner ratio (IH)
- Powder flow (t")
- Loss on drying (% HR)
- Hygroscopicity (%H)
- Homogeneity index (Iθ)
- Particle size (%Pf)

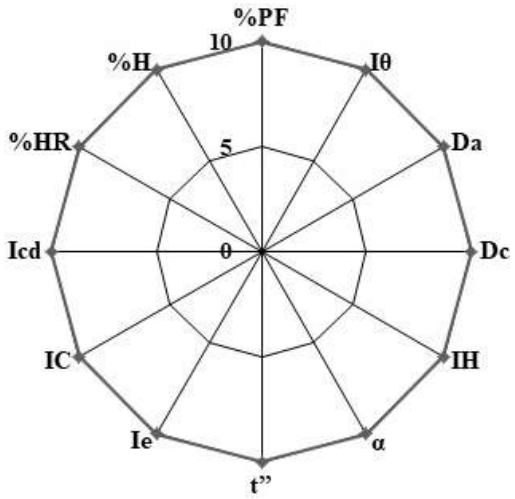

Figure 1. SeDeM Diagram

2.1.2 Powder compressibility evaluation

Based on the radius values of 12 second-level indicators of powder physical fingerprint spectrum in SeDeM Expert System, the parameter index (index of parameter, IP), parameter contour index (index of parametric profile, IPP) and the good compressibility index (the index of good compressibility, IGC), can be constructed respectively. It is used to judge the compressibility of powder and to speculate whether it is suitable for direct pressing of powder. The number of physical exponents defined as radius $\geq$ 5 is a percentage of the total number of physical indexes in the physical fingerprint spectrum, and the acceptable range is IP $\geq$ 0.5. The parameter contour index is defined as the average of the radius values of all physical indexes, and the acceptable range is IPP $\geq$ 5.The calculation method of good compressibility index: IGC = IPP $\times f$, and the acceptable range is IGC $\geq$ 5. For 12 second-level indicators f value =

Table 1. Parameter and equation used by SeDeM Expert System

Incidence factor	Parameter	Symbol	Unit	Equation
Lubricity / Dosage	Particles < 50 μm	%P*f*	%	Experimental
	Homogeneity index	Iθ	-	Iθ=Fm/100+ΔFmn
Dimension	Compressibility	Da	g/mL	Da=P/Va
	Tapped Density	Dc	g/mL	Dc=P/Vc
	Hausner Ratio	IH	-	IH=Dc/Da
Flowability / Powder flow	Angle of Repose	α	°	$\tan\alpha = h/r$
	Powder Flow	t"	s	Experimental
Compressibility	Interparticle porosity	Ie	-	Ie = Dc –Da/Dc*Da
	Carr Index	IC	%	IC = (Dc –Da/Dc)100
	Cohesion Index	Icd	N	Experimental
Lubricity/Stability	Loss on Drying	%HR	%	Experimental
	Hygroscopicity	%H	%	Experimental

Table 2. Limit values accepted for the SeDeM Diagram parameters and conversion factor to convert each parameter into radius values

Incidence factor	Parameter	Unit	Limit value (v)	Factor applied to v
Lubricity/Dosage	% P*f*	%	50~0	10−(v/5)
	Iθ	-	0~0.02	500v
Dimension	Da	g·mL-1	0~1	10v
	Dc	g·mL-1	0~1	10v
Flowability/Powder flow	IH	-	3~1	(30−10v)/2
	α	°	50~0	10−(v/5)
	t"	s	20~0	10−(v/2)
Compressibility	Ie	-	0~1.2	10v/1.2
	IC	%	0~50	v/5
	Icd	N	0~200	v/20
Lubricity/Stability	%HR	%	10~0	10−v
	%H	%	20~0	10−(v/2)

0.952.

The more the number of physical indexes in the physical fingerprint spectrum is, the larger the polygon area is, and the greater the reliability factor f is.

2.1.3 Powder compressibility correction

When the compactness of powder is poor (IGC<5), the 5 primary indexes (piling, homogeneity, fluidity, compressibility and stability) can be corrected by adding appropriate kinds and proportion of excipients. To make it meet the requirements of compressibility. The correction method is to calculate simultaneously the minimum amount of excipients needed to meet the minimum radius value of each index of the API. The formula is as follows:

$$\mathrm{CP} = 100 - \frac{\mathrm{RE} - \mathrm{R}}{\mathrm{RE} - \mathrm{RP}} \times 100 \qquad (1)$$

CP indicates the percentage of adjuvants used for correction, RE denotes the mean radius of physical indexes of auxiliary materials for correction, R represents the expected physical index radius (5 is the minimum expected correction), RP represents the average radius of the physical index of the Chinese herbal extract powder to be corrected.

If the compressibility index of the API powder IGC is less than 5, it is optional to mix it with an excipient with a good quality attribute (first-order index average > 5), According to Equation 1, the amount of correction excipients needed to be added in theory can be obtained by calculation of re and RP which are expected to reach to R=5 and are calculated with radius value.

2.2 Optimization of the parameters

2.2.1 Optimization of IH

It can be seen from the formula in Table 1 that Da = P/Va, Dc = P/Vc, and IH = Dc/Da, so we can prove that IH = Va/Vc (Where Va, initial volume and Vc, final volume). In general, the compacted powder (V_c) is lower than bulk volume (V_a). However, due to some factors such as the interaction between particles affecting the spatial distribution of particles, the V_c value may also be higher than V_a.

By using SeDeM Expert System, 22 kinds of excipients were experimentally studied. Ans the results show that the limit range of IH of these excipients is 1.1 to 2.46. Considering the possibility of appearing outside the range of the interval and making the calculation easier, the interval of IH is adjusted to 1 to 3, and an exception value less than 1 shall be treated as a non-current or almost non-current product with a radius of 0, as shown in Table 3.[6]

Table 3. Parameter and equation used by SeDeM radius

Values and conversions	Function or incidence	Parameter	Limit values	Conversion to radii (r)
Current	Flowability/powder flow	Flowability	3–0	0–10
Proposed	Flowability/powder flow	Flowability	3–1	0–10
	Flowability/powder flow	Flowability	<1	0

2.2.2 Optimization of %HR

%HR is get by doing experiments, and in order to make the standardization conversion more convenient, some researchers characterized 22 kinds of excipients by SeDeM Expert System and simplified them by two methods. The first is to convert it by different calculation methods, and the second is to divide the range of %HR according to the experimental results. By comparison, the second method is better. According to the experimental results, the relative humidity parameters are divided into three regions. Humidity less than 1% indicates that the powder is very dry and easy to produce static electricity to hinder the flow of the powder. Humidity above 3% indicates that the powder is too wet, which easily leads to agglomeration and makes the fluidity worse, and also makes it stick to the punching plate and the template. Therefore, 1% to 3% is the best range for%HR.

2.2.3 Optimization of the Icd

In the established SeDeM Expert System (Table 1), Icd is the only parameter to measure the cohesion of powder.[6]The general method of Icd measurement is to use eccentric press to make 5 elliptical convex pieces of 1 gram (g) with a 19×10 mm punch format with an eccentric press.[7] The average hardness of these 5 tablets is the final value of Icd.[8] From this, we can see that the Icd value is related to hardness.[9] When the final plate weight is fixed at 1 (±0.05) g, the size and thickness of the tablet are the main variables. The main factors affecting these two variables are the physical properties of the powder, such as elastic recovery and bulk density.

Because the physical properties of the powder are different and the bulk density of the different powder is different, there will be a big deviation in the calculation of the Icd with the final slice weight of 1 g. To make the results more accurate, Nofrerias, *et al.*[10] performed SeDeM characterization experiments on several different powders. The Icd is used as the unique variable (the variable experiment of varying the weight of the sheet at different levels is carried out to obtain different Icd values). Compared with the final set of SeDeM Diagrams, they proposed a new Icd determination method. According to different volume densities, different tablet weights are required, for example, high density excipients require

the production of heavier tablets. Otherwise, the production of lighter tablets is required.

2.3 SeDeM-ODT with a new factor: Disgregability

Because of the widespread use of tablets, in order to make the study of pre-formulation more convenient and rapid, the SeDeM Expert System has been further developed. In 2012, Aguilar-Díaz, *et al.*[11] aimed at ODT drugs based on five factors of the SeDeM system. A new factor is added and the concept of SeDeM-ODT is proposed for the first time.

The SeDeM-ODT methodology is composed of 6 primary indexes, which come from 15 second-level indicators. Based on the SeDeM method, it adds an incidence factor index and 2 tests or parameters. The new primary indexe is Disgregability, and it is affected by Effervescence (DE), Disintegration Time with disc (DCD) and Disintegration Time without disc (DSD). The newly added indicators and calculation formulas are shown in Table 4, and the newly added acceptable range of physical quality indicators and standardized conversion methods are shown in Table 5. And the radar image of powder characterization is shown in Figure 2. And in the end, the calculation method of Powder compressibility evaluation and Powder compressibility correction is the same as that of SeDeM.

Table 4. SeDeM-ODT characterizing powder index and calculating formula

Incidence factor	Parameter	Symbol	Unit	Equation
Disgregability	Effervescence	DE	minutes	Experimental
	Disintegration Time with disc	DCD	minutes	Experimental
	Disintegration Time without disc	DSD	minutes	Experimental

Table 5. Acceptable range of physical quality indicators and standardized conversion

Incidence factor	Parameter	Unit	Limit value (v)	Factor applied to v
Disgregability	DE	minutes	0~5	10v
	DCD	minutes	0~3	10v
	DSD	minutes	0~3	10v

2.4 Specific surface area and true density

The SeDeM Expert System depends on the powder properties of the materials, and the results of the materials with different powder properties are different. In order to make the SeDeM results more accurate, some experts proposed a new parameter value.[12] In addition to the 12 secondary indicators that have been proposed, Zhang, *et al.*[13] have proposed two properties: specific surface area and true density. The specific surface area and true density are one of the basic properties of the powder, which has an important effect on the experimental results, such as absorbance. With the addition of two new parameters, the SeDeM Diagram forms a 14-sided polygon, and its accepted reliability (reliability factor = 0.967) is also improved (shown in Figure 3).

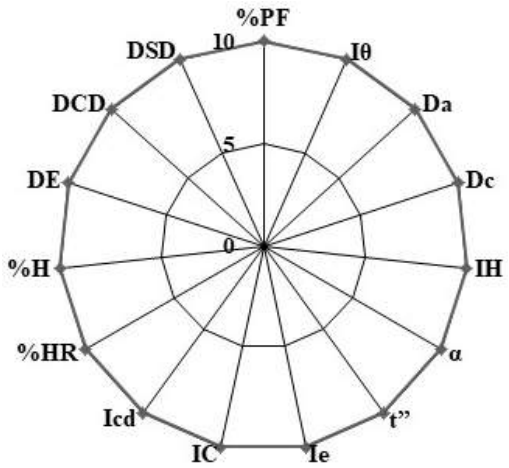

Figure 2. SeDeM ODT Diagram

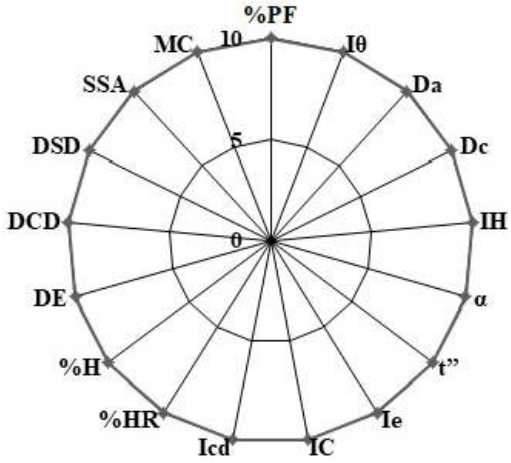

Figure 3. New SeDeM ODT Diagram

3 The application of Expert System

At present, the SeDeM Expert System is mainly used in the research of the DC performance of APIs and excipients, Pre-formulation study and proportion of APIs and auxiliary materials in prescription.

3.1 Evaluation of the suitability of a material for DC

In the study of preparation, the powder properties of APIs and excipients are very important. Different manufacturers, different batches, different types, and different chemical groups of APIs or excipients have different powder properties. So, it is necessary to conduct a comprehensive study of their powder properties.

3.1.1 Research on different batches of material

SeDeM Expert System can be used to prove the acceptability of the straight pressure properties of the materials and to characterize the physical properties of the related powders. Three batches of glucosamine salt F0130 (an API material) were characterized by SeDeM Expert System in order to study the consistency of powder properties of different batches of glucosamine salt F0130.[14] The results show that although the API is not suitable for DC, the materials of different batches have good reproducibility, which shows that the reproducibility of different batches of API is good.

3.1.2 Research on different chemical groups of material

Aguilar-Díaz, *et al.* use the new SeDeM Expert System to analyze the suitability of 43 excipients for DC with separation properties from eight chemical families. Characteristics of the chemical family of the excipients and the analyzed Analysis by chemical family of the value obtained for the 5 SeDeM factors are shown in Table 6 and Table 7.[15]

3.1.3 Research on different types of material

The physical properties of different materials are different, and the SeDeM Diagram can show the difference intuitively. The SeDeM Expert System has practical significance in studying the straightness and the improvement of the straightness of different materials. Suñé Negre, *et al.* performed SeDeM Expert System characterization tests on an API (Glucosamine salt API F0357) and 6 diluents (such as Avicel PH 101 and Kleptose), respectively. The results showed that the API had poor straightness.[16] However, when a small quantity (29.09%) of the excipient Plasdone S630 is added, it can be compressed directly. This experiment shows for the first time that SeDeM Expert System can not only prove the straightness of the material, but also correct the API with a certain dose and kind of excipient. Recently Wan et al corrected the DC properties of rhodiola extract with a certain dose and variety of excipients.[17]

Different materials have different properties of DC. In order to know more intuitively the range of direct pressure of all kinds of materials, Su-Negre et al have characterized 51 kinds of DC excipients through the sSeDeM Expert System.[18] The maximum and optimum values of DC diluents, as well as the parameters, functions and mathematical limits of the direct compressibility level are determined, and their properties are sorted out to form the periodic table of classification of excipients (shown in Figure 4[18]).

3.2 Determination of the amount of excipient in formulation development

In many cases, a single drug or excipient can't be pressed directly, so it is necessary to mix the powder with a certain amount of excipient to improve the poor properties of the single drug. Combined with the modified equation provided by SeDeM Expert System, we can calculate the minimum amount of excipient which can make up for the deficiency of API's directness. Negre et al used SeDeM to characterize an API and 5 kinds of excipients (Avicel ph102, avicel 2000 and others), and finally selected the best excipient. However, the modified equations of SeDeM Expert System are not all valid. Schooltz, *et al.*[19] have studied the ability of SeDeM Expert System to predict the combination of API and excipient concentration according to equation 12. However, considering the fragility of tablets, some of the APIs cannot be pressed directly. At present, SeDeM Expert System is mainly tested on binary powder system. The research of multicomponent powder system is still in progress, and the research method of SeDeM Expert System is also under further study.

3.3 Application of SeDeM Expert System in pre-formulation

With the emergence of the first SeDeM Expert System related literature in 2005, the influence of SeDeM Expert System has grown rapidly. Before 2012, the SeDeM system is not particularly mature, so the application literature is less, mostly the research on its related properties. After 2012, the application of SeDeM Expert System has been growing rapidly.

3.3.1 Pre-formulation study of convention Oral tablets

Oral tablet is the most common dosage form, and DC is the most convenient table pressing technology. With the development of SeDeM Expert System and the maturation of DC, Many researchers have studied the preformulation of oral tablets directly pressed by SeDeM Expert System. SeDeM Expert System can avoid unnecessary experimental formulations and shorten the preparation time for the development of oral tablets suitable for DC.

In 2012, inderbir singh and pradeep kumar used the

Table 6. Characteristics of the chemical family of the excipients analysed

Chemical family	%Commonly used	Solubility	Humidity	Mechanism of disintegration
Microcrystalline cellulose	5%–15%	Slightly soluble in 5% w/v sodium hydroxide solution; practically insoluble in water, dilute acids, and most organic solvents	Typically less than 5% w/w	Swelling
Alginic acid	1%–5%	Soluble in alkali hydroxides, producing viscous solutions; very slightly soluble or practically insoluble in ethanol (95%) and other organic solvents	7.01%	Swelling
Starch	3%–15%	Practically insoluble in cold ethanol (95%) and in cold water	Commercially available grades of corn starch usually contain 10–14%	Swelling Deformation
Sodium starch glycolate	2%–8%	Sparingly soluble in ethanol (95%); Practically insoluble in water. At a concentration of 2% w/v sodium starch glycolate disperses in cold water	Not more than 10.0%	Rapid and extensive swelling with minimal gelling
Sodium starch glycolate	0.5%–5%	Practically insoluble in acetone, ethanol (95%), ether, and toluene. Easily dispersed in water at all temperatures. Forming clear, colloidal solutions	Typically contains less than 10% water	Wicking due to fibrous structure, swelling with minimal gelling
Crospovidone	2%–5%	Practically insoluble in water and most common organic solvents	Maximum moisture sorption is approximately 60%	Water wicking, swelling and possibly some deformation recovery
Calcium silicate		Practically insoluble in alcohols, water and organic solvents	1%	Swelling but it is used as synergic with other excipient
Magnesium aluminium silicate		Practically insoluble in alcohols, water, and organic solvents	6.0%–9.98%	Swelling but it is used as synergic with other excipient

SeDeM Expert System to study the pre-formulation of cefuroxime axetil and paracetamol.[20] The results show that SeDeM Expert System can directly show the relevant data of the DC performance of axetil and paracetamol. In 2013, Aguilar-Díaz, *et al.* used the SeDeM Expert System to study ibuprofen prescriptions and obtained 8 prescriptions, which proved the reference value of sedem prescription research on ODT.[21] In 2016, Campiez, *et al.*[22] used the SeDeM Expert System to study the DC ability of carbamazepine. The results showed that carbamazepine had proper direct compression ability.

Here are some related studies combined with SeDeM-ODT: In 2017, Dasankoppa, *et al.*[23] used SeDeM-ODT Expert System to characterize excipients and developed rosuvastatin calcium dispersible tablets. And in the same year, SIPOS, *et al.*[24] used SeDeM and SeDeM-ODT Expert System to study ibuprofen ODT tablets in children. And Campiñez, *et al.*[25] used the SeDeM Expert System to test the prescription design of polyurethane, and found that this biodegradable polymer had good fluidity and could be used in direct pressing tablets. Unnecessary excipient screening is reduced.

3.3.2 Pre-formulation study of sustained-release and controlled release preparations

The sustained-release preparation is a kind of preparation which can continuously release the drug for a long period of time. The release of the drug is mainly a first order rate process. Controlled release preparation is a preparation in which a drug can be automatically released at a predetermined rate within a predetermined period of time, so that the blood drug concentration is kept within the effective concentration range for a long time. Drug release is mainly at zero or near zero within a predetermined period of time.

In 2014, Saurí, *et al.*[26] studied the DC formula of captopril skeleton tablets by SeDeM Expert System, and obtained good results. In 2016, Ofori-Kwakye, *et*

Table 7. Analysis by chemical family of the value obtained for the 5 SeDeM factors

Chemical family	Dimension	Compressi-bility	Flowability/powder flow	Flowability/powder flow	Lubricity/dosage
Microcrystalline cellulose	+++++	+++++++	+++	++++++	+++++
Alginic acid	+++++	+++	++	++++	+++++
Starch	+++++++	++++	+++	+++++	++++
Sodium starch glycolate	++++++++++	+	++++	++++	++++++
Sodium carboxymethylcellulose	++++++	++++++	++	+++	++++++[a]
Crospovidone/copovidone	++++[b]	++++++	++++	+++	+++++[c]
Calcium silicate/magnesium aluminium silicate	++++++	+++	++	+++++	+++++++

al.[27] developed and evaluated two kinds of natural gelatine sustained-release matrix tablets, and they used SeDeM Expert System for the two different water-soluble drugs. Results from the study have shown that light grade cashew gum powder can be used for DC of tablets. And in 2018, Tadwee, *et al.* used SeDeM Expert System to develop losartan potassium sustained-release tablets. The results showed that losartan API was not suitable for direct compression.

3.3.3 Pre-formulation study of other style tablets

The SeDeM Expert System is used not only in the pre-prescription research of oral solid preparations and sustained-release or controlled release preparations, but also in other formulations, such as effervescent tablets, and it is found that the SeDeM Expert System is not only suitable for pre-formulation research of western medicine, it is also applicable to the pre-formulation study of traditional Chinese medicine.

In 2014, Khan, *et al.*[28] studied the development of effervescent tablets with SeDeM Expert System, and explained the applicability of SeDeM Expert System to effervescent tablets. In 2015, Khan, *et al.*[29] used SeDeM Expert System to predict the effects of taste masking on the disintegrating behavior, mechanical strength and rheological properties of highly water-soluble drugs. And In the same year, Campiez, *et al.*[30] studied the DC of a new biodegradable polythiourea controlled release matrix polymer using SeDeM Expert System. The results show that the new synthesized polythiourea has sufficient rheological properties. Borges, *et al.*[31] used SeDeM Expert System to characterizing the active substance and polyvinyilpyrrolidone eliminating metastable forms in an oral lyophilizate, and the use of SeDeM Diagram provided valuable data regarding the stability behavior of CTZ in its solid form.

The following is a study of traditional Chinese medicine and pellets: In 2016, Zhang, *et al.*[32] used SeDeM Expert System to characterize the extract powder of traditional Chinese medicine. The results showed that the establishment of physical fingerprint spectrum of extract powder of traditional Chinese medicine was helpful to the application of QbD in the research and production of traditional Chinese medicine preparation. In 2017, Hamman, *et al.* developed pellets of different sizes based on SeDeM Expert System, and the study have shown that the SeDeM EDS was successfully applied to pellets of different sizes ranging from 0.5 mm to 2.5 mm to identify potential inadequacies for compression into MUPS tablets,and the incidence factor that was identified as a potential shortcoming for compression into MUPS tablets of all the pellet sizes was compressibility.[33] And in the second year, Hamman, *et al.* developed pellets containing different active drug components based on SeDeM Expert System, and the results of this study showed that the SeDeM EDS was successfully applied to pellets containing different active pharmaceutical ingredients for prediction of formulations for preparation of MUPS tablets with acceptable properties.[34]

4 New perspectives

With the improvement of SeDeM Expert System, the data of SeDeM expert system is more and more accurate, and the scope of SeDeM expert system is more extensive.

4.1 The internet traffic and content management (iTCM) database

Since the SeDeM Expert System was put forward, Researchers have used it to characterize a variety of APIs and excipients, and a lot of relevant data have been obtained. The related data of powder properties were summarized and the iTCM database was obtained. The iTCM database is the largest and the solely one at present based on the SeDeM Expert System, and it laid the foundation of the knowledge space under the framework of

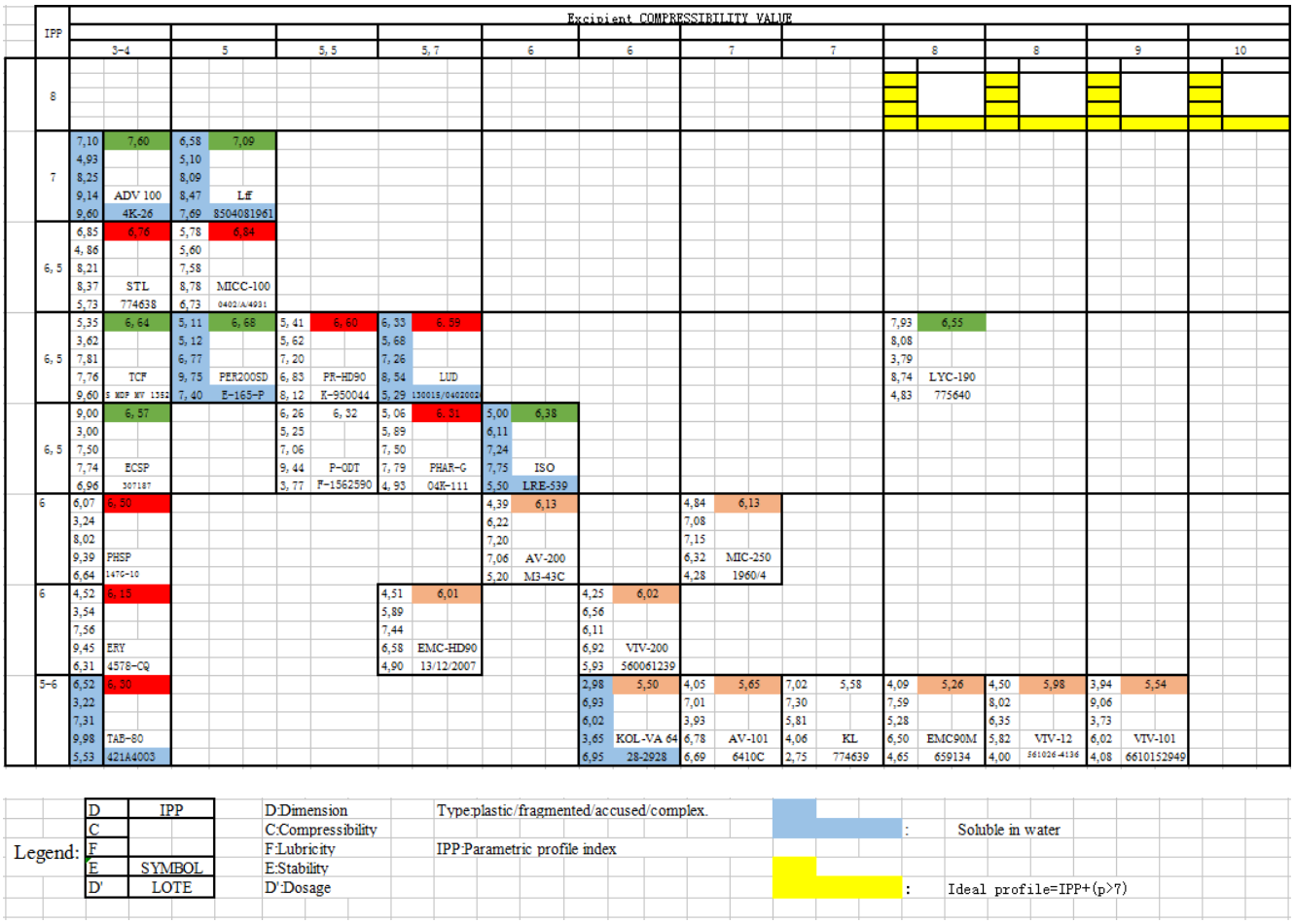

Figure 4. Periodic table of excipients for direct compression

pharmaceutical Quality by design (QbD), and could ideally continue to be perfected.[35]

Except for the 12 basic parameters, there are still other indexes to be developed. As an important disease prevention and control product, the drug efficacy is the most important evaluation standard, and the performance of powder is one of the important factors affecting the bioavailability and efficacy of the drug. The properties of the powder include the mixture uniformity, fluidity of the powder and Disintegration, *etc*.

• The more uniform the mixture, the more uniform the bioavailability, the more stable the curative effect is and the more stable the treatment is. The factors that affect the uniformity of mixing are: particle size, Particle size difference and density difference, Electrostatics and surface energy, *etc*.

• The fluidity of powder is the key factor in the development of solid preparation.

• Disintegration is the most important condition for drug dissolution and therapeutic effect, and the premise of disintegration is that pharmaceutical preparation must be wetted by aqueous solution. And the disintegration of solid preparations is affected by the following factors: porosity, Compression process, Wettability.

4.2 Design of co-processed excipient

Co-processing excipient is a new type of excipient which is different from ordinary single excipient, it is obtained by two or more kinds of excipients through a certain processing procedure.[36] Because there is no chemical reaction in the process, the new co-processing accessory does not have to carry out strict safety tests.[37] Compared with the general physical direct mixture, the co-processing excipient is a kind of functional material with better physical properties, and its various physical indexes are better than the single material or ordinary mixture, which greatly improves the cost effectiveness. At present, excipient co-processing technology mainly includes melting granulation, spray drying and so on.[38,39] However, the use of co-processing excipient is limited by its fixed proportion, and the fixed proportion of excipient is not the best proportion in preprepara-

tion.[40]

The SeDeM Expert System provides an intuitive spectrum of powder properties. The excipients were characterized by SeDeM Expert System, and the defects of the excipients, such as poor fluidity, were studied according to the characterization atlas. The related treatment schemes, such as airflow crushing, were designed, and then the processed excipients were re-characterized by SeDeM Expert System. Study the changes after processing. For the design of co-processing excipients, the complementary excipients can be selected as co-processed excipients according to SeDeM Diagram. After processing and mixing, the co-processing excipients can be characterized by SeDeM Expert System and verified by direct pressure experiments. Combined with SeDeM to design co-processing accessories can reduce unnecessary work and time. According to the SeDeM Expert System, several kinds of co-processed excipients are designed, and the database of co-processing excipients is established so as to select the proportion of excipients needed by different prescriptions.

5 Conclusions

With the wide use of DC technology in pharmaceutical industry, it is important to use a more convenient method to analyze API and excipients and their mixtures which can be compressed directly. Through the summary and analysis above, SeDeM Expert System can be used to analyze and correct the direct compressibility of various kinds of drug powder, and it can be used in the study of different formulations, which can directly reflect the properties of powder science.

At present, the API and excipients of different batches or different kinds, different manufacturers, different chemical family excipients have been characterized by SeDeM Expert System, and the differences of powder properties between them have been analyzed. However, the SeDeM system is not particularly complete. With the continuous emergence of problems encountered in the experiment, the SeDeM Expert System should be improved accordingly.

6 Conflict of interests

The Authors declare they have no conflict of interest.

Acknowledgements

This work was supported by National Science & Technology Major Project Key New Drug Creation and Manufacturing Program (2015ZX093001002007), R & D platform project of Chongqing science & Technology Commission (cstc2015yfpt-zdsys0042) and Industrial key research and development project of Chongqing science & Technology Commission (cstc2017zdcy-cdyf193), the Postgraduate Science and Technology Innovation Program of Chongqing University of Science and Technology (YKJCX1820505).

References

[1] Chun-Sheng G. Direct compression technique:a promoter of pharmaceutical industrial development. Journal of International Pharmaceutical Research, 2009, **36**(1): 1-5.

[2] Li Z, Zhao L, Lin X, *et al*. Direct compaction: An update of materials, trouble-shooting, and application. International Journal of Pharmaceutics, 2017, **529**(1-2):5 43. https://doi.org/10.1016/j.ijpharm.2017.07.035

[3] JM SN, Carreras R, Garca F, *et al*. Nueva metodología de preformulación galénica para la caracterización de sustancias en relación a su viabilidad para la compresión: Diagrama SeDeM. Cienc Tecnol Pharm, 2005, **15**(3): 125-136.

[4] Negre JMS, Carreras MR, García RF, *et al*. SeDeM Diagram: an expert system for preformation, characterization and optimization of tablets obtained by direct compression. Formulation Tools for Pharmaceutical Development. Elsevier, **2013**: 109-135. https://doi.org/10.1533/9781908818508.109

[5] Rowe RC, Sheskey PJ, Cook WG, *et al*. Handbook of Pharmaceutical Excipients Pharmaceutical development and technology. 2006, **18**(2): 544. https://doi.org/10.3109/10837450.2012.751408

[6] Josep M. Suñ-Negre, Pilar Pérez-Lozano, Roig M , *et al*. Optimization of parameters of the SeDeM Diagram Expert System: Hausner index (IH) and relative humidity (%RH). European Journal of Pharmaceutics & Biopharmaceutics, 2011, **79**(2): 0-472. https://doi.org/10.1016/j.ejpb.2011.04.002

[7] Negre JMS, Montoya EG, Lozano PPr, **et al**. SeDeM diagram: a new expert system for the formulation of drugs in solid form. Expert systems for human, materials and automation. InTech, **2011**: 392.

[8] RC M. United States Pharmacopeia-National Formulary. JExcipients and Food Chem. 2015, **6**(3): 61-64.

[9] Reynolds GK, Campbell JI and Roberts RJ. A compressibility based model for predicting the tensile strength of directly compressed pharmaceutical powder mixtures. International Journal of Pharmaceutics, 2017, **531**(1): 215-224. https://doi.org/10.1016/j.ijpharm.2017.08.075

[10] Nofrerias I, Nardi A, Sune-Pou M, *et al*. Optimization of the Cohesion Index in the SeDeM Diagram Expert System and application of SeDeM Diagram: An improved methodology to determine the Cohesion Index. PLoS One, 2018, **13**(9): e0203846. https://doi.org/10.1371/journal.pone.0203846

[11] Aguilar-Diaz JE, Garcia-Montoya E, Sune-Negre JM, *et al*. Predicting orally disintegrating tablets formulations of ibuprophen tablets: an application of the new SeDeM-ODT expert system. European journal of pharmaceutics and biopharmaceutics, 2012; **80**(3): 638-648. https://doi.org/10.1016/j.ejpb.2011.12.012

[12] Zhang Y, Che E, Zhang M, *et al*. Increasing the dissolution rate and oral bioavailability of the poorly water-soluble drug valsartan using novel hierarchical porous carbon monoliths. International Journal of Pharmaceutics, 2014, **473**(1-2): 375-383.
https://doi.org/10.1016/j.ijpharm.2014.07.024

[13] Zhang Y, Xu B, Wang X, *et al*. Setting up multivariate specifications on critical raw material attributes to ensure consistent drug dissolution from high drug-load sustained-release matrix tablet. Drug development and industrial pharmacy, 2018, **44**(11): 1733-1743.
https://doi.org/10.1080/03639045.2018.1492608

[14] Perez P, Sune-Negre JM, Minarro M, *et al*. A new expert systems (SeDeM diagram) for control batch powder formulation and preformulation drug products. European journal of pharmaceutics and biopharmaceutics, 2006, **64**(3): 351-359.
https://doi.org/10.1016/j.ejpb.2006.06.008

[15] Aguilar-Diaz JE, Garcia-Montoya E, Perez-Lozano P, *et al*. The use of the SeDeM Diagram expert system to determine the suitability of diluents-disintegrants for direct compression and their use in formulation of ODT. European journal of pharmaceutics and biopharmaceutics , 2009, **73**(3): 414-423.
https://doi.org/10.1016/j.ejpb.2009.07.001

[16] Joseph MSN, Perez-Lozano P, Minarro M, *et al*. Application of the SeDeM Diagram and a new mathematical equation in the design of direct compression tablet formulation. European journal of pharmaceutics and biopharmaceutics, 2008, **69**(3): 1029-1039.
https://doi.org/10.1016/j.ejpb.2008.01.020

[17] Sulin Wan, Rui Yang, Han Zhang, *et al*. Application of the SeDeM Expert System in Studies for Direct Compression Suitability on Mixture of Rhodiola Extract and an Excipient. AAPS PharmSciTech, 2019, **20**(3): 105.
https://doi.org/10.1208/s12249-019-1320-4

[18] Sune-Negre JM, Roig M, Fuster R, *et al*. New classification of directly compressible (DC) excipients in function of the SeDeM Diagarm Expert System. International Journal of Pharmaceutics. 2014, **470**(1-2): 15-27.
https://doi.org/10.1016/j.ijpharm.2014.04.068

[19] Scholtz JC, Steenekamp JH, Hamman JH, *et al*. The SeDeM Expert Diagram System: Its performance and predictability in direct compressible formulations containing novel excipients and different types of active ingredients. Powder Technology, 2017, **312**: 222-236.
https://doi.org/10.1016/j.powtec.2017.02.019

[20] Singh I and Kumar P. Preformulation studies for direct compression suitability of cefuroxime axetil and paracetamol: a graphical representation using SeDeM diagram. Acta poloniae pharmaceutica, 2012, **69**(1): 87-93.

[21] Aguilar JE, Montoya EG, Lozano PP, *et al*. New SeDeM-ODT expert system: an expert system for formulation of orodispersible tablets obtained by direct compression. Formulation tools for pharmaceutical development, **2013**: 137-154.
https://doi.org/10.1533/9781908818508.137

[22] Campiñez MD, Casas M, Caraballo I. Characterisation of the Ability of Carbamazepine for Processing It through Direct Compression Applying the New Expert System SeDeM. International Journal of Clinical Pharmacology & Pharmacotherapy, 2016, **1**(1): 105.
https://doi.org/10.15344/2456-3501/2016/105

[23] Dasankoppa FS, Sajjanar VM, Sholapur H, *et al*. Application of SeDeM ODT Expert System in Formulation Development of Orodispersible Tablets of Antihyperlipidemic Agent. Journal of Young Pharmacists, 2017, **9**(2): 203-208.
https://doi.org/10.5530/jyp.2017.9.40

[24] Sipos E, Oltean AR, Szabó ZI, *et al*. Application of SeDeM expert systems in preformulation studies of pediatric ibuprofen ODT tablets. Acta pharmaceutica. 2017, **67**(2): 237-246.
https://doi.org/10.1515/acph-2017-0017

[25] Campinez MD, Benito E, Romero-Azogil L, *et al*. Development and characterization of new functionalized polyurethanes for sustained and site-specific drug release in the gastrointestinal tract. European journal of pharmaceutical sciences, 2017, **100**: 285-295.
https://doi.org/10.1016/j.ejps.2017.01.017

[26] Sauri J, Millan D, Sune-Negre JM, *et al*. The use of the SeDeM diagram expert system for the formulation of Captopril SR matrix tablets by direct compression. International Journal of Pharmaceutics, 2014, **461**(1-2): 38-45.
https://doi.org/10.1016/j.ijpharm.2013.11.029

[27] Ofori-Kwakye K, Mfoafo KA, Kipo SL, *et al*. Development and evaluation of natural gum-based extended release matrix tablets of two model drugs of different water solubilities by direct compression. Saudi Pharmaceutical Journal, 2016, **24**(1): 82-91.
https://doi.org/10.1016/j.jsps.2015.03.005

[28] Khan A, Iqbal Z, Rehman Z, *et al*. Application of SeDeM Expert system in formulation development of effervescent tablets by direct compression. Saudi Pharmaceutical Journal, 2014, **22**(5): 433-444.
https://doi.org/10.1016/j.jsps.2013.07.002

[29] Khan A, Iqbal Z, Ibrahim M, *et al*. Prediction of the effect of taste masking on disintegration behavior, mechanical strength and rheological characteristics of highly water soluble drug (itopride HCl); an application of SeDeM-ODT expert system. Powder Technology, 2015, **284**: 411-417.
https://doi.org/10.1016/j.powtec.2015.06.062

[30] Campinez MD, Ferris C, de Paz MV, *et al*. A new biodegradable polythiourethane as controlled release matrix polymer. International Journal of Pharmaceutics, 2015, **480**(1-2): 63-72.
https://doi.org/10.1016/j.ijpharm.2015.01.011

[31] Florez Borges P, Garcia-Montoya E, Perez-Lozano P, *et al*. The role of SeDeM for characterizing the active substance and polyvinyilpyrrolidone eliminating metastable forms in an oral lyophilizate-A preformulation study. PLoS One, 2018, **13**(4): e0196049.
https://doi.org/10.1371/journal.pone.0196049

[32] Zhang Y, Xu B, Sun F, *et al*. Physical fingerprint for quality control of traditional Chinese medicine extract powders. China Journal of Chinese Materia Medica, 2016, **41**(12): 2221-2227.

[33] Hamman H, Hamman J, Wessels A, *et al*. Development of multiple-unit pellet system tablets by employing the SeDeM expert diagram system I: pellets with different sizes. Pharmaceutical development and technology, 2018, **23**(7): 706-714.
https://doi.org/10.1080/10837450.2017.1342657

[34] Hamman H, Hamman J, Wessels A, *et al*. Development of multiple-unit pellet system tablets by employing the SeDeM expert diagram system II: pellets containing different active pharmaceutical ingredients. Pharmaceutical development and technology, 2019, **24**(2): 145-156. https://doi.org/10.1080/10837450.2018.1435691

[35] Wen C, Zhang J, Zhang H, **et al**. Advances in ultrasound assisted extraction of bioactive compounds from cash crops-A review. Ultrason Sonochem, 2018, **48**: 538-549. https://doi.org/10.1016/j.ultsonch.2018.07.018

[36] Reimerdes D. The near future of tablet excipients. Manufacturing chemist, 1993, **64**(7): 14-15.

[37] Russell R. Synthetic excipients challenge all-natural organics: Offer advantages. Pharmaceutical technology, 2004, **28**(4): 38-50.

[38] Garg N, Pandey P, Kaushik D, *et al*. Development of novel multifunction directly compressible co-processed excipient by melt granulation technique. International Journal of Pharmaceutical Investigation, 2015, **5**(4): 266-274. https://doi.org/10.4103/2230-973X.167692

[39] Chauhan SI, Nathwani SV, Soniwala MM, *et al*. Development and Characterization of Multifunctional Directly Compressible Co-processed Excipient by Spray Drying Method. AAPS PharmSciTech, 2017, **18**(4): 1293-1301. https://doi.org/10.1208/s12249-016-0598-8

[40] Gohel MC and Jogani PD. A review of co-processed directly compressible excipients. Journal of Pharmacy & Pharmaceutical Sciences, 2004, **8**(1): 76-93.

Journal of Pharmaceutical and Biopharmaceutical Research is an independent open access journal published by Syncsci Publishing. Pte. Ltd.

SyncSci Publishing Pte. Ltd.
50 Chin Swee Road
#09-04 Thong Chai Bldg
Singapore 169874
Tel : (+65) 68264112; (+65)98107233
Email : editorial@syncsci.com
Website: www.syncsci.com

ISSN 2630-533X

Print Version USD 75.00